Development and Analysis of Synthetic Composite Materials Emulating Patient AAA Wall Material Properties

A thesis

submitted by

Christa M. Margossian

In partial fulfillment of the requirements

for the degree of

Master of Science

in

Biomedical Engineering

TUFTS UNIVERSITY

February 2013

Adviser: Robert A. Peattie, PhD

Abstract

Abdominal Aortic Aneurysm (AAA) rupture accounts for 14,000 deaths a year in the United States. Since the number of ruptures has not decreased significantly in recent years despite improvements in imaging and surgical procedures, there is a need for an accurate, noninvasive technique capable of establishing rupture risk for specific patients and discriminating lesions at high risk. In this project, synthetic composite materials replicating patient-specific wall stiffness and strength were developed and their material properties evaluated. Composites utilizing various fibers were developed to give a range of stiffness from 1825.75 kPa up through 8187.64 kPa with one base material, Sylgard 170. A range of strength from 631.12 kPa to 1083 kPa with the same base material was also found. By evaluating various base materials and various reinforcing fibers, a catalogue of stiffnesses and strengths was started to allow for adaptation to specific patient properties.

Three specific patient properties were well-matched with two composites fabricated: silk thread-reinforced Sylgard 170 and silk thread-reinforced Dragon Skin 20. The composites showed similar stiffnesses to the specific patients while reaching target stresses at particular strains. Not all patients were matched with composites as of yet, but recommendations for future matches are able to be determined. These composites will allow for the future evaluation of flow-induced wall stresses in models replicating patient material properties and geometries.

Acknowledgements

I would like to thank my adviser, Dr. Robert Peattie, for his guidance over the course of this project. I would also like to thank Dr. Luis Dorfmann and Dr. David Kaplan for their guidance and willingness to serve on my committee. Additionally, I am extremely grateful to Dr. Mark Iafrati of Tufts Medical Center and Mr. Francesco Pancheri for access to the patient samples and the data from which this project is based.

I would also like to thank those at Tufts University for their support and friendship throughout this experience. I would like to thank Milva Ricci for all that she does in the front office as she helps us all to get to our goals. To the other members of the Peattie Lab, I am grateful for everything we learned along the way. Roberto Elia and Rodrigo Jose, you were never too busy to help discuss test setups, solidworks, or play some pool. To Ethan Golden, thank you for providing distractions when they were absolutely necessary as well as never saying no to yet another crazy request for a tweak to moulds. Other than maybe Kelvin Perez, no one else may ever know how difficult it is to simply cast a simple tube.

I would like to thank Katie Martinick and Shannon Smith for providing "encouragement" while I ran mechanical test, after mechanical test, after mechanical test for weeks straight. Becky Scholl Hayden, Thomas Dabrowski, and Lisa Bartlett- your friendship is greatly appreciated. To Lee Tien, Amanda Baryshyan, Alex Mitropoulous, and Andrew Reeves, for always

answering a simple question and reminding me to ask “Why?” I was doing what I was doing. And to those at 200 in general, just for trying to remind me that there was life outside of this project and the sudden increase in my taste for Starbucks.

Lastly, I would like to thank my friends and family for all of their encouragement during this project. Without their love and support, this project never would have been completed, but this is nothing new as their support has been with me every step of the way.

Table of Contents

List of Tables

List of Figures

List of Abbreviations

Abbreviation	Definition	Fiber Orientation [#]	Mould	Protocol
+2x	Double-stranded external reinforcement of Sylgard 170	*//*	**C**	Cyclic Uniaxial
DS10	Dragon Skin 10 Slow	n/a	**B**	Pre-cycled Uniaxial
DS20	Dragon Skin 20	n/a	**B**	Pre-cycled Uniaxial
			C	Pre-cycled Uniaxial
DS20 +Ext	External silk thread reinforcement of Dragon Skin 20	*//*	**C**	Cyclic Uniaxial
DS20 +Ext (⊥)	Reinforced Dragon Skin 20 by external silk thread perpendicular to test axis	⊥	**C**	Cyclic Uniaxial
+Ext	External silk thread reinforcement of Sylgard 170	*//*	**C**	Cyclic Uniaxial
+Ext (⊥)	Reinforced Sylgard 170 by external silk thread perpendicular to test axis	⊥	**C**	Cyclic Uniaxial
+GzDB	Embedded dog-bone cut gauze reinforcement of Sylgard 170	*//*	**B**	Pre-cycled Uniaxial
+GzGL	Embedded gauze in gauge region reinforcement of Sylgard 170	*//*	**B**	Pre-cycled Uniaxial
+Int	Internal silk thread reinforcement of Sylgard 170	*//*	**C**	Cyclic Uniaxial
+Int (⊥)	Reinforced Sylgard 170 by internal silk thread perpendicular to test axis	⊥	**C**	Cyclic Uniaxial
Mould A	Sylgard 170	n/a	**A**	Pre-cycled Uniaxial

Abbreviation	Definition	Fiber Orientation [#]	Mould	Protocol
+Sutures	Embedded silk suture reinforcement of Sylgard 170	//	**B**	Pre-cycled Uniaxial
S160	Sylgard 160	n/a	**A**	Uniaxial
S170 / Sylg170	Sylgard 170	n/a	**A**	Uniaxial
			B*	Pre-cycled Uniaxial
			C	Cyclic Uniaxial
S184	Sylgard 184	n/a	**A**	Uniaxial
+Thread	Embedded 100% pure silk thread reinforcement of Sylgard 170	//	**B**	Pre-cycled Uniaxial
Wash160	Wire-washer reinforced (WWR) Sylgard 160	//	**A**	Uniaxial
Wash170	Wire-washer reinforced (WWR) Sylgard 170	//	**A**	Uniaxial
Wash184	Wire-washer reinforced (WWR) Sylgard 184	//	**A**	Uniaxial
+Woven	Embedded cotton woven dressing reinforcement of Sylgard 170	//	**B**	Pre-cycled Uniaxial
WWR	Wire-washer reinforced samples	//	**A**	Uniaxial

[#]Fiber Orientation defines the direction of fibers compared to the direction of tensile testing

*****MouldB is another name for the Sylgard 170 cast in Type B moulds when compared directly to Mould A-cast samples tested with Pre-cycled Uniaxial testing protocol.

Development and Analysis of Synthetic Composite Materials Emulating Patient AAA Wall Material Properties

Chapter 1 – Problem Statement

Abdominal Aortic Aneurysms (AAAs) are permanent dilations of the portion of aorta between the renal arteries and iliac bifurcation. Aortic Aneurysm rupture accounts for 15,000 deaths annually in the United States with approximately half specifically labeled due to AAA[1]. Generally, an enlargement of the aorta is considered to be an AAA when the minimum anteroposterior diameter is at least 3.0 cm[2]. As the aneurysm continues to grow, surgical intervention may be suggested to prevent rupture. The current standard for surgical intervention is the maximum diameter criterion, that is, if the maximum diameter is larger than 5.5 cm, elective surgical repair is recommended. However, this is not mechanically sound because bursting will occur when the internal wall stress is greater than the wall strength to resist the pressure. The aortic tissue of each individual has a different tensile strength and the individual's lifestyle choices, for example smoking, also influence the degradation of the wall[2,3].

The overall goal of this project is to gain insight into AAAs by fabricating models that replicate both the exact shape and the mechanical properties of specific patient lesions and to use those models in hemodynamic studies. In particular, as a first step towards that goal, in this project a set of synthetic reinforced materials emulating patient material properties were developed. A crucial aspect of this was to emulate the nonlinear nature of tissue due to

the combined presence of collagen and elastin fibers. This work specifically focused on the following areas:

- Show the ability to modify the properties of polymers by reinforcing the base material.
- Determine an appropriate base material through uniaxial tensile testing.
- Select fibers to modify the determined base material properties through uniaxial tensile testing.
- Develop selected composites in a repeatable manner such that characterization through uniaxial tensile testing can be completed.
- Develop a 3-D ideal tube of the synthetic analogue and determine changes in burst pressure as a result of reinforcement.

By achieving these goals, 3-D analogues to patient AAAs can be fabricated. Models fabricated from these materials can then be used for testing purposes that are not feasible *in vivo*.

Chapter 2 – Background

2.1 Aneurysm Definition and Statistics

Aneurysms, from the Greek ανευρυσμα (aneurusma), meaning widening[4] can occur in various locations in the body and are defined as a permanent dilation of a vessel. The aorta is the largest blood vessel in the body, and dilations of its diameter to approximately 150% are qualified as aortic aneurysms[2,3]. The description of an aortic aneurysm, depicted in Fig. 1, relies on the location of the aneurysm: thoracic, abdominal, or expanding over both locations, thoracoadominal. Additionally, the aneurysm can be classified by its shape: saccular, when only part of the circumference of the aorta is affected, or fusiform, when the entire artery is affected[4]. Thoracic Abdominal Aneurysms (TAAs) occur between the aortic arch and the aortic hiatus within the diaphragm. AAAs refer to those of the Infrarenal aorta. TAAs tend to occur less frequently than AAAs (one third the frequency)[3,5]. The abdominal aorta is more susceptible to the deposition of plaque as compared to the rest of the aorta, and this was thought to cause the weakening of the wall leading to AAA formation and the higher frequency of localization here[6]. An alternative theory revolves around elastin degradation, as Baxter et al. showed a significant ($p < 0.001$) decrease in insoluble elastin content in AAA patients (1.3% ± 0.04%), as compared to healthy samples (12% ± 2.8%)[7]. The expansion of part of the aorta to create a bulge region has been looked

at, but a common reason for development is not yet universally agreed upon. These expanded regions continue to grow toward rupture, and most often death, if left untreated[8].

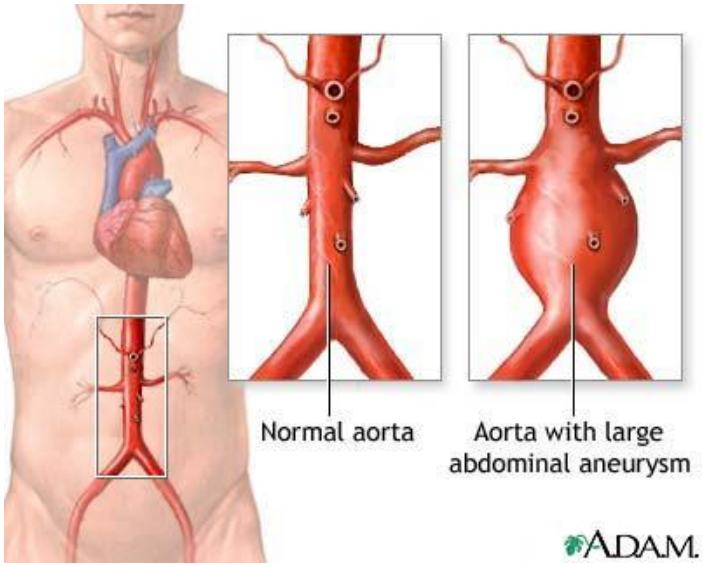

Figure 1. Visual representation of AAAs and their location[9].

Though generally a male-specific disease, over time more women have been diagnosed with AAAs[10]. The general female population has a lower prevalence rate than in men, but subgroups with history of smoking and heart disease are at higher risk of having an AAA[10]. Currently the National Institute of Health's Organization of Rare Diseases (ORD) lists AAAs as a rare disease, and by definition affects no more than 200,000 Americans each year[11]. The CDC reports show a high rate of deaths reportedly caused by AAA (some specifically mentioned rupture, while some did not) in males over

the age of 65 with incidence increasing as age increases beyond 75 for 1968-1978[12]. Crude death rates from AAA rupture for various age groups are tabulated for comparison for 1968-2009[1,12,13] in Table 1.

Crude Rate, reported as AAA related deaths per 100,000, also increases in women as age increased during the 1970s, albeit the initial rate is much lower. Unlike their male counterparts, there are differences in incidence for women aged 74-85 and 85+ (16.1 as compared to 34.5). Over the course of 1968-2009, the occurrence of death due to a AAA has decreased from approximately 34 per 100,000 down to 13 per 100000 in males aged 65-74.

In more recent years, the reported data may specify death related to AAA rupture, while other deaths are caused by AAA without specific mention. The data reported here includes both specifically- and non-specifically-mentioned rupture due to AAAs. However, the data does not include those deaths characterized as a result of aortic aneurysms (not specifically AAAs). In doing so, there is a small chance that mischaracterized deaths were not included. The data for all AAA-caused deaths is shown in Fig. 2. In the last decade, at most 75% of the AAA caused deaths were reported specifically as burst aneurysms (males aged 65-74). For this reason, the CDC search consisted of death by AAA sorted by reason, if available. From 1979-1998, occurrence rose in males 85+ from 67 per 100,000 to 90+, but more interestingly, in the last ten years, incidence has decreased below the 1968-1978 rate to 39.7.

The incidence for females remained consistent across age groups from 1968-1998 with a decrease across the board in the last ten years, as was the case with men. Unfortunately, these numbers are not indicative of whether the disease is declining, or surgeries are getting better. According to Heller et al., the number of surgeries performed has not decreased, leading to the conclusion that screening has improved and earlier intervention is helpful[14–16]. Though, according to Sakalihsan and sources, incidence has risen over the past two decades to approximately 8,000 deaths per year in the United Kingdom and 15,000 in the United States[4].

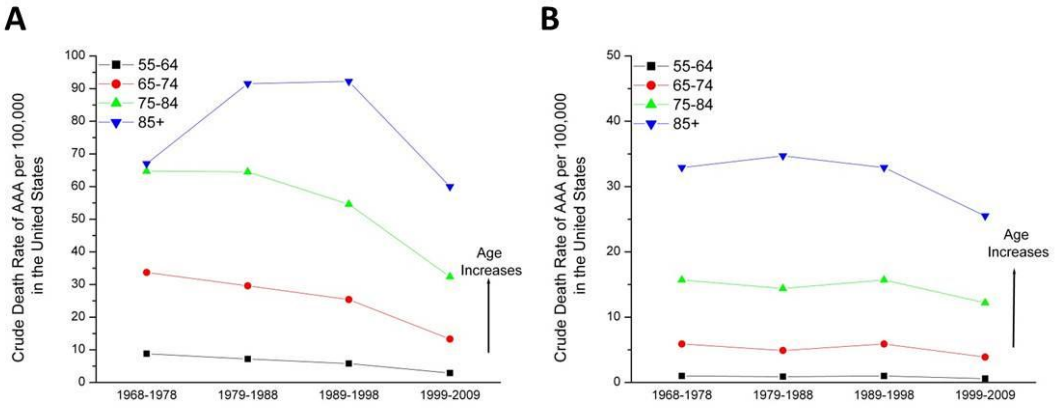

Figure 2. Changes in crude rate of AAA from 1968-2009. Take from the CDC Compressed Mortality Data from 1968-2009 for (A) men and (B) women. Using Wonder online database with a search for Abdominal Aortic Aneurysm (ruptured and without mention of rupture) for 1978-2009[1,12,13].

Table 1. Crude death rate in the United States for AAA per 100000 persons organized by decades for years as well as age and split by gender. The CDC reports these as deaths as a result of abdominal aortic aneurysms and where applicable both by documented rupture and undocumented rupture [1,12,13].

Crude Death Rate in the United States per 100000 persons				
Year Range	**55-64**	**65-74**	**75-84**	**85+**
		Men		
1968-1978	8.8	33.7	64.7	67.0
1979-1988	7.2	29.6	64.5	91.5
1989-1998	5.8	25.4	54.6	92.2
1999-2009	2.9	13.3	32.4	60.0
		Women		
1968-1978	1.0	5.9	15.7	32.9
1979-1988	0.9	4.9	14.4	34.7
1989-1998	1.0	5.9	15.7	32.9
1999-2009	0.6	3.9	12.2	25.5

CDC archives suggest a decrease in male deaths related to AAA rupture from the late 1960s through today. Male deaths for those 65-74 and 75-84 experienced a relative decrease, shown in Fig. 2, as technology and disease prevention has improved. Males aged over 85 saw a spike in incidence during the 1980s and 1990s, but the incidence rate has since returned to the level of the 1960s. One of the major decreases in incidence seen is in that of the 75-84 age population as an initial incidence of 65 per 100,000 has been cut in half. The incidence rate in women has remained consistent for those 65-74 and 75-84, but the incidence in those 85 and older has decreased by half.

The normal diameter of the aorta differs due to various factors such as age, gender, and weight, and the diameter decreases as the abdomen is approached[4]. AAAs initially grow gradually over a few years ranging from rates of 0.25 to 0.75 cm per year, though 75% of the disease population does not have rates exceeding 0.5 cm per year. As the aneurysm grows, the expansion rate then increases dramatically [3,17]. Both environmental factors, such as smoking, and a predisposition contribute to this disease[2,3,18–22]. Brady et al. have reported a higher expansion rate (0.283 cm per year) in men who smoke as opposed to 0.253 cm per year for non-smokers[23]. Ogata et al. reported the occurrence of AAAs in brothers of patients ranging between 8.9% and 28.6% in specific populations[24]. Though the development of AAA is thought to be inherited genetically, the exact pathway is not yet

determined, highlighted by both an autosomal dominant and autosomal recessive pattern describing the development[3,25–27].

2.2 Wall Histology

The aorta has typical inner diameter of 2.5 cm and a 2 mm wall thickness where it connects to the left ventricle[28]. The aortic wall consists of three layers: the intima, the media, and the adventitia. The intima, the inner-most layer, consists of a single layer of endothelial cells and resists the shear forces of blood flow. The media, the middle layer, houses the elastin, extracellular matrix and smooth muscle cells. The media is responsible for the extensibility of the wall as the blood flow changes. The outer layer, the adventitia, is comprised mostly of fibroblasts and collagen, providing the tensile strength of the wall[3].

All three layers of the aortic wall are affected by the development of true AAAs. The intima is affected by atherosclerosis, whereas the media experiences changes in the extra-cellular-matrix. This occurs as elastic fibers are degraded[7,29] by metallomatrix proteases (MMPs). The adventitia is altered by collagen degradation. Collagen types I and III are crucial to providing the aortic wall with strength, but the increased turnover cannot compete with the level of degradation eventually leading to wall weakening and ultimately rupture[4].

2.3 Clinical Considerations

Most AAAs are diagnosed as doctors search for other problems using an ultrasound or a physical abdominal exam. Ultrasound is generally used to gauge the aneurysm, as both specificity and sensitivity approach 100%[30]. Prior to rupture, most AAAs are asymptomatic, though back, abdominal, or groin pain may be signs of an AAA, along with hypotension and urinary retention. Once an AAA is ruptured, immediate care is necessary. Ruptured AAAs release large amounts of blood into the abdomen rendering ultrasound images useless and thus requiring the use of computer tomography (CT) or CT-angiograms[3]. Ease of screening today permits preventative measures to take place. Currently when an aneurysm reaches a maximum diameter of 5.5 cm, surgical repair is suggested. However, this criterion does not take into account that the aneurysm will burst when the internal pressure is greater than the wall strength. There are two methods of surgical repair: open-abdomen repair and endovascular repair. The maximum diameter criterion was determined as such that the risk of rupture and thereby death was greater than the risk of repercussions from the surgery itself. In an open abdomen procedure, a prosthesis is implanted to replace the aneurysmal portion of the aorta. Dissimilarly, with the endovascular approach, an endograft is locked into place after traveling through the transfemoral or the transiliac arteries. Grafts introduce their own set of complications including endoleaks, which themselves require more surgeries[3].

2.4 Hemodynamics of AAA

Flow fields and wall stresses have been evaluated by Edgar[31] and Dorfmann et al.[32] using a series of patient-based rigid models. Initially these models, designed based on patient CT scans, were rigid with one entrance and one exit for flow[31,32]. The pressure and flow was evaluated at various Reynolds numbers corresponding to rest and working conditions of the heart. In recent years, these rigid models were adapted to include both renal and iliac arteries to better simulate *in vivo* conditions.

The hemodynamic results from physical testing are compared with computational results by Dorfmann et al. as well[32]. Using the patient data made available for this work, fellow students have been computationally modeling the material properties of the patient samples. Additionally, complex wall distribution stresses of 660 kPa have been shown on the inner surface of the aneurysm bulge[32].

2.5 Aortic Wall Properties

The diameter of a healthy aorta decreased as it extends toward the iliac arteries. A healthy aorta is typically 2 cm in diameter for the Ascending Aorta (where connected to the left ventricle)[28], with Kahraman et al. reporting as large as 3.26 ± 0.33 cm for that portion and 2.89 ± 0.35 cm for the Descending Aorta[33]. The study by Kahraman et al. divided the abdominal aorta into three sections: the Suprarenal Abdominal Aorta, the

Infrarenal Abdominal Aorta, and the Suprailiac Abdominal Aorta, and reported a decrease in diameter from 1.90 ± 0.25 cm to 1.57 ± 0.28 cm to 1.42 ± 0.24 cm, respectively[33].

Average aneurysmal diameter has been calculated numerous times, but the results rely heavily on the sampling pool. For example, Van't Veer et al. calculated an average maximum aneurysmal diameters of 5.8 ± 0.6 cm for ten male patients[34]. Hirsh et al. reported diameters as large as 7 cm, and women were found to have smaller aneurysmal diameters than men[2]. The gender difference stems back to the differences in healthy aorta diameter. According to the American College of Cardiology/American Heart Association (ACC/AHA) Guidelines, the female Infrarenal Abdominal Aorta has a diameter ranging between 1.19 and 2.16 cm, whereas males have diameters in the range of 1.41 cm to 2.39 cm.[2]

Anisotropic properties were shown by testing the mechanical properties of the aortic wall[35,36]. Vorp et al. and Raghavan et al. showed significant differences in peak wall stress and wall strength between aneurysmal and nonaneurysmal tissue. The wall strength of a healthy aorta, 1210 kPa, was significantly decreased in AAA patients whose strength was reduced to 650 kPa (longitudinal) or 680 kPa (circumferential)[35]. Additional research also showed that the AAA wall strength of rupture AAAs was significantly lower than that of electively repaired AAAs (542 kPa versus 823 kPa respectively)[36]. Raghavan et al. showed ultimate stress values for healthy

aortas averaged to 2014 kPa, whereas AAA samples tested longitudinally reached an ultimate stress of 864 kPa, and those oriented circumferentially reached 1019 kPa[37]. Di Martino et al. found that AAA specimens from electively repaired aneurysms had average UTS of 820 kPa, significantly higher than that of ruptured samples at 540 kPa[36].

An additional property of aortic tissue is the non-linear stress-strain behavior observed[37–39]. A *J*-shaped tensile stress-strain curve having three regions of stiffness has been observed for aortic tissue, as well as other soft tissues. Aortic tissue is comprised of two load bearing fibers: elastin and collagen. In the initial region of the stress-strain curve, collagen fibers are relaxed, and elastin is primarily responsible for bearing the load. As the load increases, the collagen fibers begin to assemble and aid in the load bearing, causing a change in the stiffness of the response. At high stress, the collagen fibers have aligned and begin to elongate to resist the load, introducing a third region with its own stiffness.

2.6 Elastomeric Analogues

Silicone is a synthetic polymer comprised of alternating silicon and oxygen atoms that have the capacity to recover from large deformations. As a result, it is often seen as suitable as an analogue to soft tissue and vessels[40,41]. Silicones are water-resistant and do not change properties as a result of salt or wind[42]. Silicones are found in a wide range of products in airbags,

cosmetics, baby care products, medicine, sealants, toys, lubricants, and polishes[42].

Various types of silicones exist, but the industry has accepted that the term refers to one common siloxane polymer: polydimethylsiloxane (PDMS)[43]. PDMS is used in many devices and areas as an encapsulant due to its inexpensive nature and sealant properties. Additional benefits include its optical transparency, biocompatibility, and flexibility[44–46]. PDMS is used to embed and encapsulate electronic components in these devices. For example, in actuators, PDMS is used to conceal ferrofluid and in microvalves the elastic nature is valuable to help movement. It is also used as a sealant in the microvalves as well as in adaptive lenses in microoptics[45]. An additional benefit is the ability to tune the mechanical properties to those desired by altering the ratio of base material to curing agent[40,44]. Gordan et al. were able to change the elastic modulus of Sylgard 184 (PDMS) in a range of 11 kPa up to 1.6 MPa[47]. The stiffer versions are a result of ratios closer to 10:1, with the limiting factor the amount of curing agent. At a ratio of 6:1 and greater, the system is oversaturated causing the curing process to slow down and produce softer samples[48]. Additional information available suggests batch to batch variation is approximately 20%[49] and all reported values should be considered an estimation. Commercially available forms of PDMS include Sylgard 170 (Dow Corning, USA), Sylgard 184 (Dow Corning, USA), Silicon II

(GE, USA), Cosmesil HC (Principality Medical, UK), and MED-4920 (Nusil, USA) to name a few[50,51].

Though the material properties and other benefits of silicones were desirable, the lack of strength of these rubbers is often an issue. As a result, these materials are often reinforced with fibers to stiffen mechanical properties, in turn creating composites. The definition of composite is generally understood as a matrix material reinforced with fibers. Fiber-reinforced plastic (FRP) controls the commercial market as a thermosetting polymer matrix containing glass fibers. The fibers are impregnated by the matrix, which protects the fibers and aids in transferring the load to the fibers. As a result of directionally orienting fibers, anisotropy can be achieved with different material properties in different directions.

2.7 Principles of Mechanics

The engineering stress-strain curve provides useful information for characterizing the mechanical properties of a material. The information from a two-dimensional load-elongation curve, recorded by a tensile tester, provides the information to calculate engineering stress and engineering strain. It is customary to normalize the force by dividing by cross-sectional area when reporting information about tensile testing. The engineering stress, σ, is defined as the applied force, F, per unit initial area, A_o:

$$\sigma = \frac{F}{A_o}, \tag{1}$$

and the engineering strain, ε, is defined as

$$\varepsilon = \frac{l - l_o}{l_o} = \frac{\Delta l}{l_o}, \tag{2}$$

where l_o refers to the initial length, l the current length, and Δl the change in length[52]. Strain infers a third material property, referred to as the stretch ratio, λ, calculated as

$$\lambda = \frac{l}{l_o}, \tag{3}$$

where l and l_o are defined in the previous sentence[52]. Most curves are represented as stress-stretch in the following work. The values can easily be converted from strain to stretch with the following relation[52]

$$\lambda = 1 + \varepsilon. \tag{4}$$

The engineering stress and engineering strain are used instead of the true stress and true strain because the engineering values are independent of geometry. True stress and true strain are determined by the use of the final area with the presumption of non-constant area. The use of the engineering curves is valid because there is no difference between true and engineering curves until after the specimen's cross-sectional area changes indicating more than elongation. Since the polymers are not expected to experience necking as a metal would, there is no need to correct their stress-stretch curves for area changes.

An additional material property determinable from the stress-strain curve is the traditional elastic modulus (E). This modulus measures the force necessary to produce a small elongation and for the linear region of a stress-strain curve, it is calculated as [52]

$$E = \frac{\sigma}{\varepsilon}. \quad (5)$$

At larger elongations, the slope of the stress-strain curve is indicated by a tangent modulus. The lower the elastic modulus the easier it is to stretch a sample, as indicated by the difference in moduli between rubber, 0.83 MPa, and steel, 206 MPa. Additional sample elastic modulus values for common materials can be found in Table 2.

Table 2. Various elastic moduli of materials adapted from Mechanics of Materials[52].

Sample Elastic Modulus Values	
Material	**E (MPa)**
Rubber	0.83
Nylon	4.14
Bone	12.82
Concrete	31.72
Glass	68.95
Steel	206

There are multiple moduli, in addition to E, that can be defined, especially for non-linear materials. For example, a non-linear stress-strain response can be characterized by a maximum segmented modulus in an attempt to comment on the linearity of the response. This modulus is determined by finding the maximum of a series of elastic moduli calculated for one curve.

Though geometry does not affect the stress or moduli, the strain rate during testing is known to have an impact on stress and moduli[48]. Higher strain rates result in a steeper load-elongation curve. This requires the reporting of strain rate when discussing information retrieved from a stress-stretch curve.

Various stress points are also used to characterize the material. The yield stress, σ_y, is the stress at which permanent or plastic deformation occurs. The ultimate tensile stress (UTS, σ_u) is the maximum stress reached prior to failure, indicated in Fig. 3. At this stress, the stretch is referred to as the Ultimate Stretch, or λ_{ULT}. After this peak stress, the stress will decrease as the strain increases. This occurs until mechanical failure of the sample, or the breaking strength (σ_f). It is important to note that strength and stiffness are not equivalent. They represent two additional mechanical properties of a material. Strength is the resistance of a material to failure whereas stiffness is a measure of the load required to induce a specific deformation.

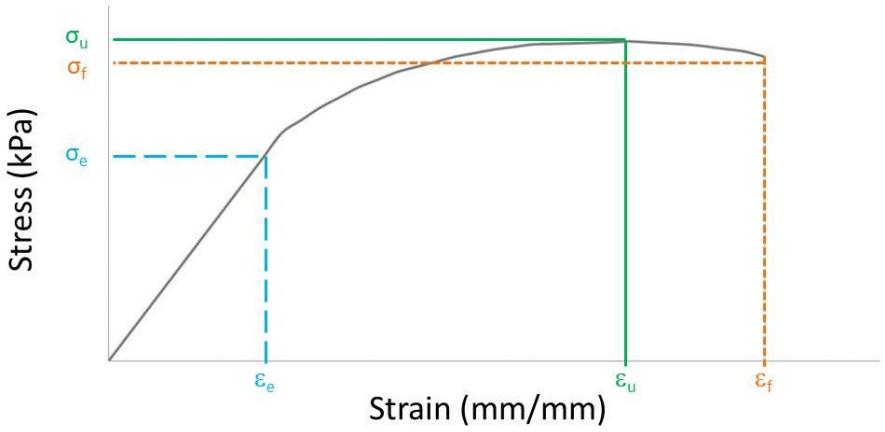

Figure 3. Generalization of stress-strain curve depicting multiple properties such as the ultimate tensile stress (σ_u) and the strain at which it occurs (ε_u), the failure stress (σ_f) and the strain at which failure (ε_f) occurs, as well as the elastic limit of the material (ε_e, σ_e).

The UTS is reported as the engineering stress but could easily be converted to true UTS by multiplying the ratio of the final area to the initial area,

$$\sigma_{true,UTS} = \frac{A}{A_o}\sigma_{UTS}, \qquad (6)$$

and correspondingly the true strain is the natural logarithm of the ratio of true UTS to engineering UTS[52]. With polymers, the maximum engineering UTS occurs when polymer backbones are aligned and about to break.

Different hardness scales are used to quantify hardness, defined as the resistance of a material to permanent indentation. A shore hardness value of zero is the softest and the closer it is to zero on any scale represents the softer materials. Three such scales are the Shore 00, Shore A, and Shore D scales and they have approximations to convert between themselves and

well as to Young's modulus. Extremely soft objects, such as gummy bears, register 10 on the Shore 00 hardness scale but are too soft to register on both the A and D scales, as shown in Fig. 4. Rubber bands are approximately 20 on the Shore A scale, while Shore D is used for harder materials such as tire treads and hard hats.

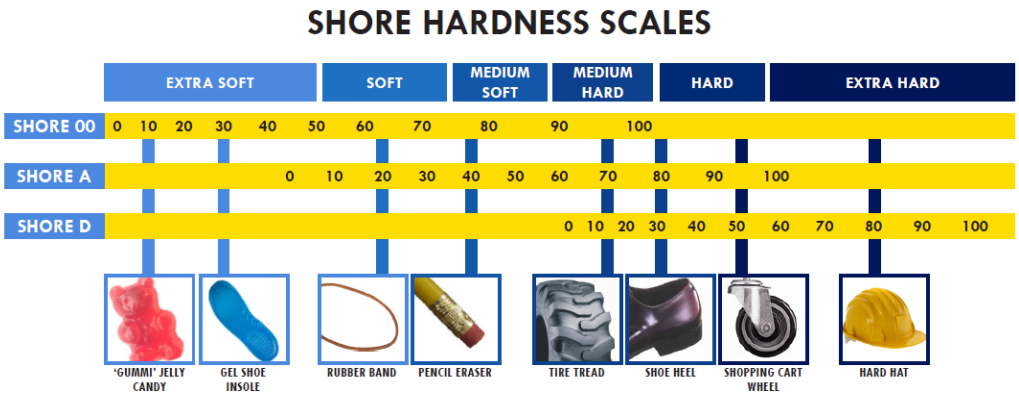

Figure 4. Comparison of materials on various shore hardness scales as provided by Smooth-On Inc.[53]

Chapter 3 – Methods and Materials

AAAs are permanent localized expansions of the aorta that occur where the diseased and weakened artery expands under the influence of blood pressure. In this project, a set of synthetic materials replicating patient material behaviors were developed. All procedures were carried out with full approval of the Tufts University Institutional Review Board.

3.1 Patient Data Acquisition

In a separate experiment conducted by another student, the mechanical behavior of patient tissue samples was evaluated. AAA wall specimens were harvested from patients undergoing elective open-abdomen repair at the Tufts Medical Center. Only excess human tissues, which would otherwise be discarded in the normal course of surgical procedures, were utilized in these experiments. Tissue samples were collected at the time of surgery recording gender, age, and pertinent medial details such as medications and cholesterol levels. Clinical observations regarding the aorta were made by the operating surgeon.

The samples were placed on ice, but not frozen, before transfer to the Tufts University Advanced Technologies Labs (ATL) in Medford, MA. Following approved IRB protocol, the samples were placed in three layers of protection for transportation. The primary layer consisted of a leak-proof histology sample container with 0.9% saline solution. This container was surrounded

by a layer of absorbent cotton wadding, and the two made up the first layer. This primary layer was placed inside a Ziploc bag filled with ice to keep the sample chilled. The ice-filled bag with the primary layer was placed in an additional Ziploc bag, which was then placed in a box for transportation.

Material properties were measured within 48 hours of collection. These specimens were tested with a protocol developed by Francisco Pancheri to best emulate *in situ* tissue behavior during systole. Both uniaxial and biaxial testing were performed using a custom-designed 2-D tensile tester (Zwick/Roell Inc., Model Z2.0, Germany) dependent on the physical dimensions of the sample. The samples were tested at 37 °C with a control area 6.5 mm by 6.5 mm, unless the sample provided had physical limitations, and as such that area was diminished. Five loading and unloading cycles (non-contact strain control) to predefined stretch levels were tested with strain rate 0.0037 s^{-1}. The protocol set uniaxial stretch aim to 1.1 for five cycles and increased in 0.025 increments toward 1.2 stretch until specimen failure. Data was automatically recorded via software compliant with Zwick/Roell tensile tester. The raw data collected was then analyzed by the author in the same manner as self-gathered data strictly for comparative purposes.

3.2 Planar Casting Moulds

For testing of planar samples, three sets of moulds were used. These moulds varied and are summarized in Table 3. All three moulds, post processing, result in samples advantageous for one-dimensional tensile testing. Each sample consisted of two wider width tab regions joined by a smaller width, but longer region known as the gauge region. This shape is referred to as a dog-bone and results in dog-bone shaped samples. This specific shape was chosen to encourage failure within the gauge region of the material as opposed to a uniform width sample where failure often occurs due to clamp pressure.

Table 3. Reference table for the various mould types. Information included is to serve as a reminder for the differences between them.

Mould Type Comparisons

Type	Product	Mould Material	Gauge Length	Schematic Location
Type A	Single Sample	3-D Printed	45 mm	Figure 5
Type B	Single Sample	3-D Printed	60 mm	Figure 6
Type C	Multi-sample sheet	Assay Tray [#]	35 mm	Figure 7

[#] A single sheet from which individual samples are die cut from (ASTM-D638 Die D).

3.2.1 Type A Moulds

Type A moulds were fabricated with a 3-D printer (Dimension SST 1200, MN, USA). Figure 5 shows a schematic of Type A moulds used to cast individual samples with gauge region dimensions 7 mm wide and 45 mm long. The tab regions, 27 mm wide and 35 mm long, were used to install the specimen in the tensile tester. These regions are wider to spread the load of the clamps. The total length of each sample was 115 mm with uniform thickness 6 mm.

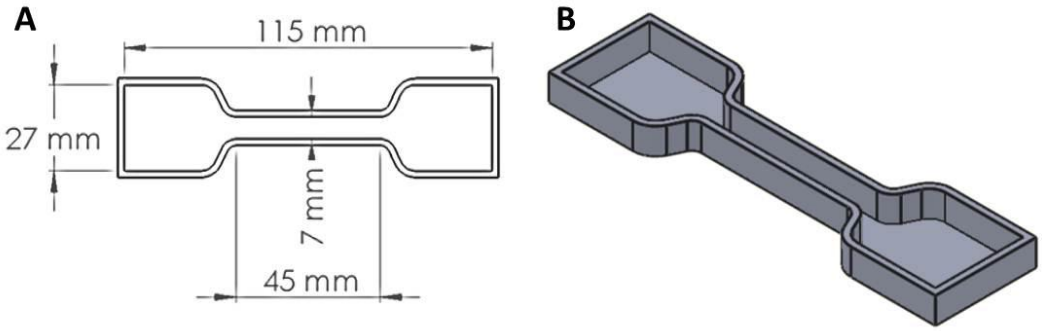

Figure 5. Schematic of Type A moulds used for uniaxial tensile testing. A) This mould has two tab regions connected by a rectangular gauge region (width 7 mm, length 45 mm). B) 3-D depiction of one mould used to cast Sylgard 160, Sylgard 170, and Sylgard 184 base samples and their wire-washer reinforced samples.

Type A moulds were used to cast unreinforced samples of Sylgard 160, Sylgard 170, Sylgard 184, and Wire-Washer Reinforced samples, subjected to the Uniaxial Loading Protocol (Section 3.8.1). Type A moulds were also used to compare the effects of mould dimensions on mechanical properties. These samples were made of Sylgard 170 and subjected to the Cyclic Loading

Uniaxial Testing Protocol (Section 3.8.2). They served as direct comparisons to Type B casts of the same base material and same testing protocol.

All moulds, including those of Type A, were lightly coated in mould release (Mann Ease 200) thirty minutes prior to casting. 15 mL of mixed, degassed base filled one mould and created one test sample.

3.2.2 Type B Moulds

Type B moulds were also fabricated with a 3-D printer (Dimension SST 1200). These moulds were created to better distinguish the tab regions from the gauge region within test samples. Type B moulds, shown in Fig. 6, have the same basic structure as Type A moulds. There are two tab regions, 35 mm wide with length 40 mm each, connected by a rectangular gauge region, 60 mm in length and 8 mm in width. The total length of the samples was 140 mm with uniform thickness 6 mm.

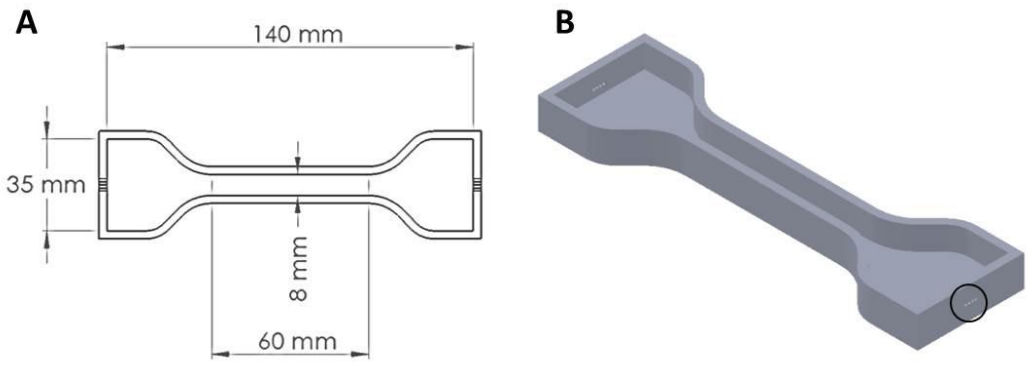

Figure 6. Schematic of Type B moulds used for pre-cycled uniaxial testing. Mould B casts have two tab regions connected by a rectangular gauge length region. This gauge region (A) is 8 mm by 60 mm long. The entire sample has a uniform thickness of 7 mm. B) 3-D model of one Type B mould with emphasis on the built-in holes used to guide reinforcement.

Type B moulds had additional built-in features that were not in Type A moulds, shown in Fig. 6B. On the outer face of the tabbed regions, small holes were built into the moulds. There were two or four holes on each edge, with the outermost holes 6 mm apart. These holes were included to aid alignment of embedded fibers, when appropriate. With all samples cast in Type B moulds, generic rubber bands were snuggly fit around the exterior of the mould. The rubber bands either held the fibers taut or were used to prevent material from seeping out unused holes in the unreinforced or gauze-reinforced cases.

3.2.3 Type C Moulds

A single cast made in one Type C mould produced a set of samples that required the use of additional tools to create individual testing samples. Both A and B moulds produced individual samples per cast, but Type C moulds produced sheet casts. Type C moulds were not 3-D printed as Type A and Type B moulds were. Instead, square bioassay trays (Nalgene® or Corning® BioAssay Dish, 245 mm x 245 mm x 25 mm), as shown in Fig. 7A were purchased (Fisher-Scientific). A plastic insert was created to help align embedded fibers. Four interlocking pieces of plastic had holes laser cut every 3 mm across the width of the pieces at a height of 1.5 mm. The insert was set in place regardless of whether fibers were to be embedded or not to provide consistency. After the properly mixed and poured silicone set, the cured silicone was removed from the oven and separated from the plastic jig and the assay tray. The resultant cured silicone sheet was then cut into samples using an ASTM-D639 Type 4 Die D Cutter (ODCTooling.com). Use of the die cutter produced on average ten samples per cured sheet. Thicknesses of cured sheets were 3.69 ± 1.38 mm.

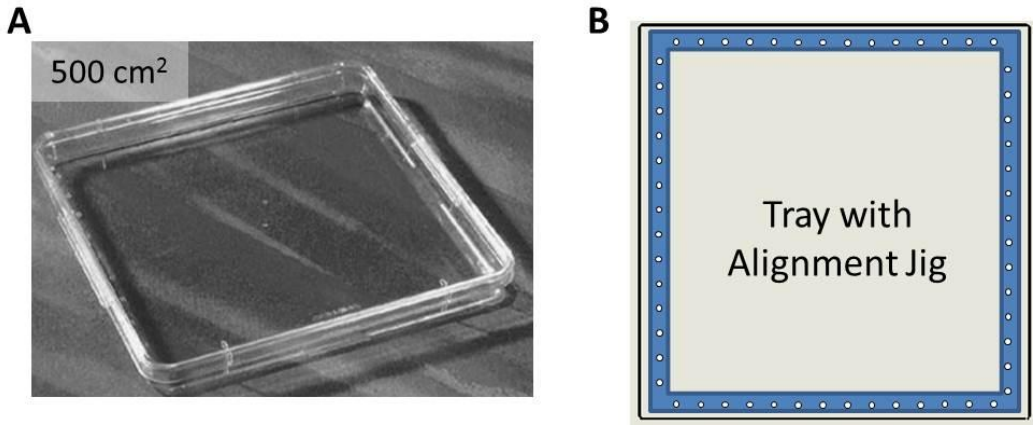

Figure 7. Type C mould depiction of (A) the mould purchased (Fisher-Scientific), a clear square assay tray with 500 cm^2 filling area. All casts in Type C moulds were made by inserting the plastic alignment jig (B). These interlocking plastic pieces were fabricated with laser cut holes every 3 mm across the jig for alignment help with internally reinforced Sylgard 170 composites.

3.3 Base Materials

To replicate the patients' material properties, a set of materials was developed consisting of base polymer in which reinforcing fibers were embedded. Determination of an appropriate base material took into account different factors such as tensile strength, viscosity, and pot life to choose the base material pool, among other properties summarized in Table 4. Sylgard 160, Sylgard 170, and Sylgard 184 (Dow Corning Inc.) were initially chosen due to their use in other labs[40,54,55] as starting points for characterization. The tear strengths of these three materials (Table 4) are low compared to others, and as a result, typical elongation does not exceed 150%. (Elongation associated with polymers approaches 1000%[53].) Though ultimate elongation is not a determining factor, base materials with the ability to easily extend to large strains were desired to round out the sampling pool. Additionally,

upon tactile analysis of the three Sylgards, in addition to initial tests, a softer, more easily stretched material closer to that of healthy human tissue was desired. Dragon Skin 10 and Dragon Skin 20 (Smooth-on Inc.) were chosen to complete the lower range. Some of the base materials differed in their casting protocols, and therefore each is individually described below.

Table 4. Material property comparison of potential base materials from literature. All of the materials are two-part elastomers varying in viscosity, hardness, tear strength, and ultimate tensile strength[53,56–58]. Units are indicated in parentheses unless otherwise noted.

Material Properties of Potential Base Materials

Name	Mix Ratio	Demold time at RT (h)	Demold time at 60 °C (h)	Elongation at Break	Initial Mixed Viscosity (cps)	Pot Life Viscosity (cps)	Pot Life (m)	Shore A Hardness	Tear Strength (kN/m)	Ultimate Tensile Strength (MPa)
Dragon Skin® 10 Medium	1:1	5	1	1000%	23000	n/a	20	10	17.9	3.3
Dragon Skin® 20	1:1	4	1	620%	20000	n/a	25	20	21.0	3.8
Sylgard® 160	1:1	24	28 m	105%	8775	17500 *	20	56	5.3	4.2
Sylgard® 170	1:1	24	1	150%	2900	11000 *	30	41	3.5	2.4
Sylgard® 184	1:10	24	3+	140%	3900	7800 *	2 h	50	2.6	7.1

n/a refers to an unpublished parameter
* refers to calculated value based on the definition of pot life

3.3.1 Sylgard® 160

Sylgard® 160 is a dark grey, two part (1:1) silicone elastomer (Dow Corning, USA). Sylgard 160, referred to as S160, has the highest Shore A Hardness value, 56, of the five potential base materials. Sylgard 160 is created by mixing equal volumes of its two parts, Sylgard160A and Sylgard160B. Sylgard160A and Sylgard160B are sold as one kit, and each part comes in a separate container. Per manufacturer's instructions, each distinct canister was thoroughly mixed by hand to homogenize the material, as over time filler may settle on the bottom[57]. Equal volumes of Sylgard 160A and Sylgard 160B were measured and mixed together. Mixing continued until a uniform color was observed. The mixture, uncured Sylgard 160, was then placed in a vacuum dome connected to house vacuum for approximately five minutes to eliminate air bubbles. The degassed material was cautiously poured into Type A moulds. These uncured samples were then oven-cured at 60 °C for one hour, demoulded, and left to assimilate to room temperature before undergoing uniaxial tensile testing.

3.3.2 Sylgard® 170

Sylgard® 170 is a black, two-part (1:1) silicone elastomer. Sylgard® 170, also referred to as S170, has a Shore A durometer value equal to 41. Sylgard 170 is purchased as a kit containing two separate containers labeled Sylgard 170A and Sylgard 170B. Per manufacturer's instructions, each individual container, Sylgard 170A and Sylgard 170B, was thoroughly mixed by hand to

homogenize the material as overtime filler may settle on the bottom[56]. Sylgard 170 is fabricated by combining Sylgard 170A and Sylgard 170B in equal parts by either volume or weight. Samples that underwent the Uniaxial Loading protocol were created by mixing equal volume parts of Sylgard 170A and Sylgard 170B. Samples that underwent the Cyclic Preloaded Uniaxial Loading and Cyclic Uniaxial Loading protocols were created by mixing equal weight parts Sylgard 170A and Sylgard 170B. Tubular samples created for burst pressure tests were also created by mixing equal weight parts of Sylgard170A and Sylgard 170B. Equal parts (by weight or volume) were measured and mixed together until a uniform color was achieved. The mixed, but uncured Sylgard 170, was placed into a vacuum for approximately five minutes to remove all air bubbles from the mixture. Sylgard 170 was then carefully poured into the mould used for casting and the mould moved to the 60 °C oven for curing. After curing, the Sylgard 170 samples were removed from the oven and demoulded.

3.3.3 Sylgard® 184

Sylgard® 184 is a transparent, two part (10:1) silicone elastomer commonly known as PDMS. Sylgard 184 has the second highest Shore A durometer value, 48, of the potential base materials. Sylgard 184 is purchased as a set with two containers labeled base and catalyst. Per advisory of Dow Corning, each individual container was thoroughly mixed by hand to homogenize the material, as over time filler may settle on the bottom[58]. Sylgard 184 is

produced by mixing the base and catalyst in a 10:1 ratio by volume. The mixture was blended until a uniform color was observed. The mixture was placed in vacuum casting system for a minimum of ten minutes to degas. Caution was taken to provide room for Sylgard 184 to expand as it degassed and not overflow in the vacuum. After sufficient degassing, the uncured Sylgard 184 is then carefully poured into Type A moulds. These filled moulds were then oven-cured at 60 °C for 3.5 hours, demoulded, and assimilated to room temperature before uniaxial tensile testing.

3.3.4 Dragon Skin® 10 Slow

Dragon Skin® 10 Slow (DS10) was used for base material selection and cast in Type B moulds. DS10 is a commercially available platinum cure silicone elastomer mixed in 1:1 ratio (by weight or volume) and cures at room temperature in five hours. DS10 is purchased as a kit with two containers labeled Dragon Skin 10A and Dragon Skin 10B. Equal weights of parts Dragon Skin 10A and Dragon Skin 10B were measured and then mixed together for homogenization. The blend was then degassed in a vacuum chamber for a minimum of ten minutes with caution taken as the material expands as it is degassed. The mixture was then poured into pre-mould released Type B moulds and oven-cured at 60 °C for one hour. Samples were removed from the oven, separated from the moulds, and left to assimilate to room temperature prior to tensile testing.

3.3.5 Dragon Skin® 20

Dragon Skin® 20 (DS20) is a highly extensible material that is mixed in a 1:1 (by weight or volume) ratio and cures in room temperature in four hours. DS20 is sold as a kit comprised of two containers labeled Dragon Skin 20A and Dragon Skin 20B. Equal weight portions from each individual container were measured, combined to create a homogenous mixture, and degassed in a vacuum chamber (minimum ten minutes) until visible air bubbles were no longer present. The uncured Dragon Skin 20 was then poured slowly into its mould (either Type B or Type C) and set to oven-cure at 60 °C for one hour. After time elapsed, the cured Dragon Skin 20 and its moulds were removed from the oven and separated.

3.4 Wire-Washer Reinforcement Technique

To display the base materials' ability to exhibit different mechanical behavior with the addition of reinforcements, Type A moulds were used (Fig. 5). To increase the tensile strength of Sylgard® 160, Sylgard® 170, and Sylgard® 184, 24 gauge wire with 0.51 mm diameter was embedded in the base material. The wire was coiled three times in the gauge region, as shown in Fig. 8A, to allow for extension of the base material before the reinforcement engaged in an attempt to both control and predict behavior. The wire was wrapped ten times around each two washers to secure its position within the mould. The washers were each placed in a tab region of the sample aligned the coiled wire with the gauge region.

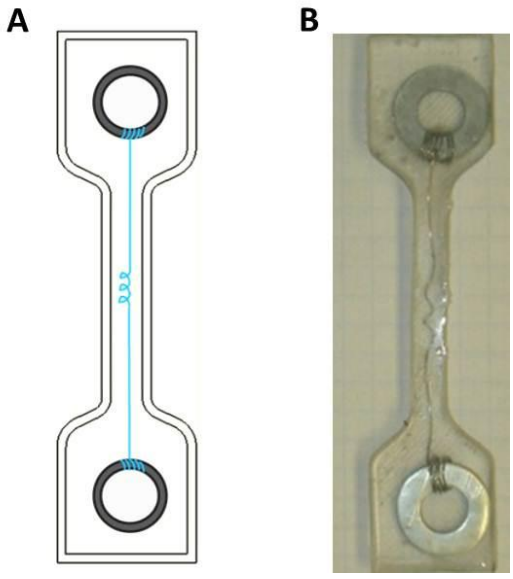

Figure 8. WWR technique schematic (A) and example of WWR-Sylgard 184 sample (B). 24 gauge wire was wrapped around one washer 10 times, then coiled three times within the gauge region of the sample, and then wrapped round a second washer 10 times. This washer-wire-washer system was placed into the mould, and the Sylgard poured around it to create WWR samples.

Type A moulds were filled halfway with prepared base material (as described in Section 3.3) as they would be for unreinforced samples. The washers were placed 6.45 cm apart along the length of each sample to ensure the pneumatic grips of the tensile tester would grab the wire and pull the reinforced sample as one. Each mould was then filled with base material to cure as one unit. The samples were moved to the 60 °C oven to be cured for the appropriate time for each base material outlined in Table 4. Cast samples, e.g., the WWR Sylgard 184 sample shown in Fig. 8B, were one solid silicone unit, with the washers and wire embedded within, and were referred

to as wire-washer reinforced (WWR). These WWR samples for each base (Sylgard 160, Sylgard 170, and Sylgard 184), along with corresponding unreinforced samples, underwent uniaxial tensile loading using the protocol defined in Section 3.8.1.

3.5 Reinforcement Techniques for Fiber Selection

All samples were cast in the Type B moulds (Fig. 6). Ideally samples would have gauge region 8 mm wide and 6.5 mm thick with length of 60 mm. On average, these samples were 8.11 ± 0.48 mm wide and 6.42 ± 0.48 mm thick measured with a Mitutoyo Pocket Thickness Gauge with accuracy ± 20 μm (Mitutoyo 7309 10 mm gauge in 0.01 mm gradations). Four types of reinforcements were used: silk sutures, gauze, woven cotton dressing, and 100% pure silk thread.

3.5.1 Silk Suture Reinforcements

Samples of Sylgard 170 reinforced with silk sutures (+Suture) utilized the holes printed into Type B moulds to aid alignment. Moulds were sprayed with mould-release prior to inserting the sutures. Ethicon C012D black braided silk 2-0 sutures were passed through one of the outermost holes on the front face of the mould and pulled across the sample through the corresponding outer hole, as shown in Fig. 9. The suture was then looped along the outer back face to the opposite outermost hole, and pulled back the length of the sample through the remaining empty outer hole. Rubber bands

were used to secure the sutures in place and prevent seeping through any, if any, empty holes. Sylgard 170 was prepared accordingly (Section 3.3.2) to fill the moulds which were then oven-cured at 60 °C for a minimum of one hour. The rubber bands were then removed, and the samples continued to oven-cure for at least three more hours. This reinforcement method results in a sample with two lengths of suture along the gauge length embedded in Sylgard 170.

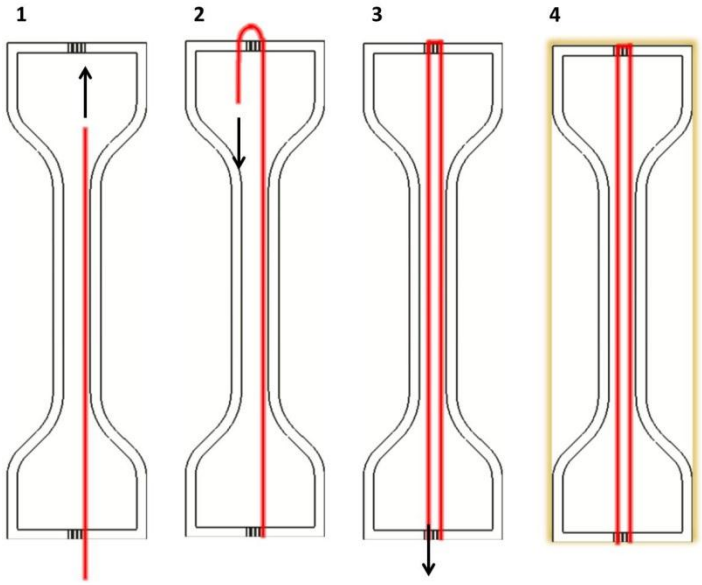

Figure 9. Suture and Thread reinforcement method depiction. The fiber was passed through one outer edge hole and run the length of the sample (**1**). The fiber was looped around the opposite outer edge and run back down the length of the sample (**2**). The fiber was passed through the remaining outer hole and held taut (**3**). The fibers were then secured in place using a generic rubber band (**4**). The base material was cast, and the entire mould placed in the oven to cure.

3.5.2 Gauze Reinforcement Techniques

Gauze reinforced samples were fabricated by one of two methods. Both techniques incorporated Dukal Corp 1212 Sterile Gauze Pad 2x2" (12 ply). The first technique, resulting in samples referred to as Gauze Dog-bone (+GzDB), reduced the gauze to one single layer. The single layer was then cut into the shape of Type B moulds. The shape of the cut gauze (and mould) resembles a dog-bone and is referred to as such. Sylgard 170 was prepared according to Section 3.3.2 and poured into pre-mould released, rubber banded moulds. The cut gauze dog-bone was then placed with tweezers in the mould and pushed down such that it was submerged by the silicone (Fig. 10a). These samples were then oven-cured at 60 °C for one hour at which point the rubber band was removed and then allowed to oven-cure for at least three additional hours. The samples were removed completely from the oven, permitted to return to room temperature, and then demoulded.

The second method produced samples referred to as Gauze Gauge Length (+GzGL). For this method, all twelve layers of the sterile gauze pad were cut in a rectangular shape, 8 mm wide by 60 mm long, matching the gauge length region of the Type B moulds, as shown in Fig. 10b. The pre-sprayed moulds with the band around the exterior were filled with Sylgard® 170, followed by the submergence of the gauze to the gauge length region only. After one hour, the rubber bands were removed from the exterior of all samples, and the samples were returned to the oven for a minimum of three more hours.

The samples were removed and permitted to return to room temperature before the demoulding process.

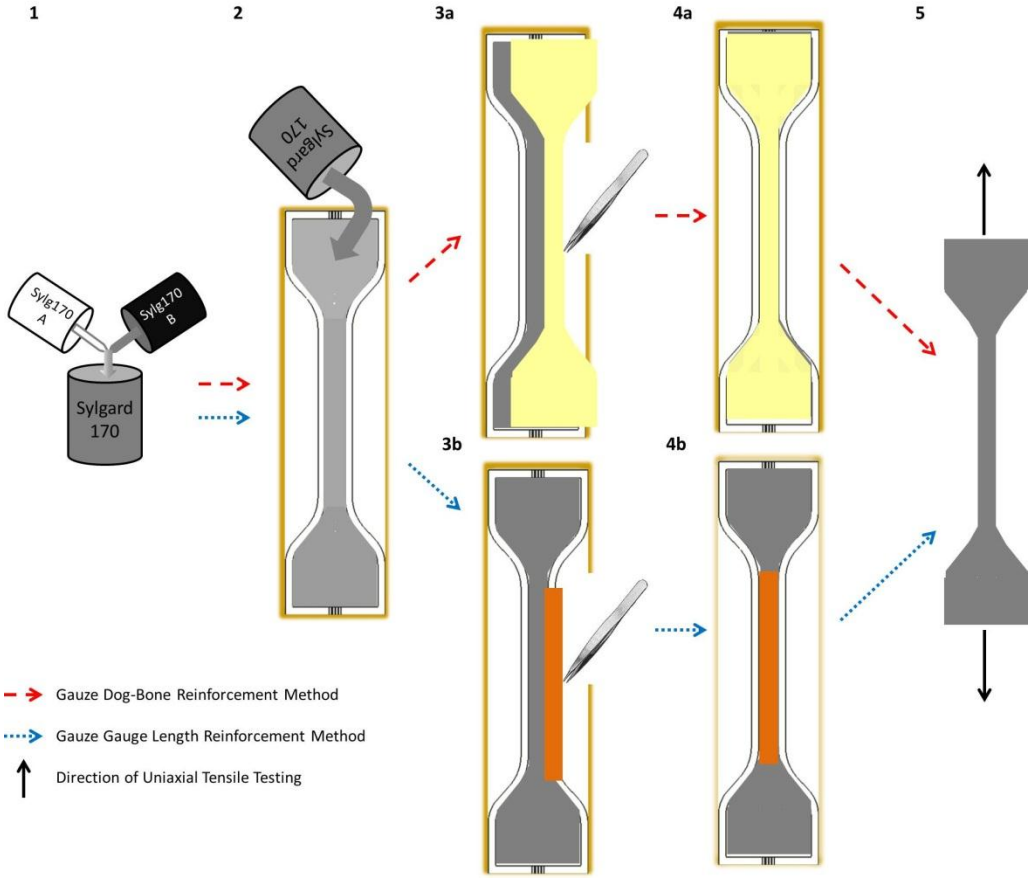

Figure 10. Schematic of gauze reinforcements for Gauze Dog-Bone samples (path A in red), where a single-layer of gauze is cut into the shape of the mould, and Gauze Gauge Length samples (path B in blue), where the twelve-ply gauze is cut to fill the gauge region only. S170 was prepared (**1**) and poured into the moulds (**2**). The appropriate gauze either dog-bone shaped (in yellow, **3a**) or gauge-length cut (in orange, **3b**) were placed into the S170-filled mould (**4ab**). The samples were oven-cured at 60 °C and then demoulded to produce samples for uniaxial testing (**5**).

3.5.3 Woven Dressing Reinforcements

Sylgard 170 reinforced with woven dressing samples, +Woven, were fabricated with rayon polyester blend CVS Gauze Pads (2x2", 12 ply). One gauze pad was unfolded such that a single layer would be embedded per sample. The single layer was then cut into the shape of Type B moulds, a dog-bone shape, to embed in the base material. Sylgard 170 was prepared as defined above in Section 3.3.2 as a thin layer of mould release sprayed on the mould dried. After partially filling the mould with Sylgard 170, the dog-bone shaped gauze was placed atop the layer of material with tweezers and then covered with the remaining material to fill the mould. The samples were oven-cured at 60 °C for one hour. At this point, the rubber band was removed from the outer surface of the moulds and the samples left to oven-cure for an additional three hours. The cured samples were removed from the oven and permitted to return to room temperature prior to removal from the mould and tensile testing.

3.5.4 Silk Thread Reinforcements for Mould B Samples

The reinforcement process for embedding silk thread into the base material used commercially available 100% pure silk thread (Gutermann 100% pure silk S303 Sewing Thread). After the moulds were sprayed with mould release and a minimum of thirty minutes passed, a needle was used to string the thread such that two lengths were embedded in the gauge region. Starting with one of the outermost holes on the forward face of the mould,

the thread was passed through and along the length of the mould through the corresponding hole. The thread was looped around the outer edge, and pushed through the hole diagonally opposite the starting hole. The thread was then pulled back down the mould to the corresponding hole on the starting side, as shown in Fig. 9. Pulled taut, the thread was secured with a rubber band, and the mould filled with the prepared base material. The samples were placed in the 60 °C oven for one hour, after which the rubber bands were detached, and the samples were left to oven-cure for an additional three hours. Samples were removed and allowed to acclimate to room temperature before demoulding.

3.6 Reinforcement Techniques for Patient Matching

All samples were tested using the cyclic loading protocol defined in Section 3.8.3 and cast in Type C moulds: square assay trays (Nalgene® or Corning® BioAssay Dish, 245 mm x 245 mm x 25 mm) available from Fisher-Scientific (Fig. 7). Due to the introduction of new moulds and protocol, reinforcement techniques required adjustment for Type C-cast composites as opposed to those cast individually in Type A or Type B moulds (Table 3). Sheets of material casts in Type C moulds were cut into individual samples using an ASTM-D638 Type 4 die D cutter with the procedure outlined in Fig. 11.

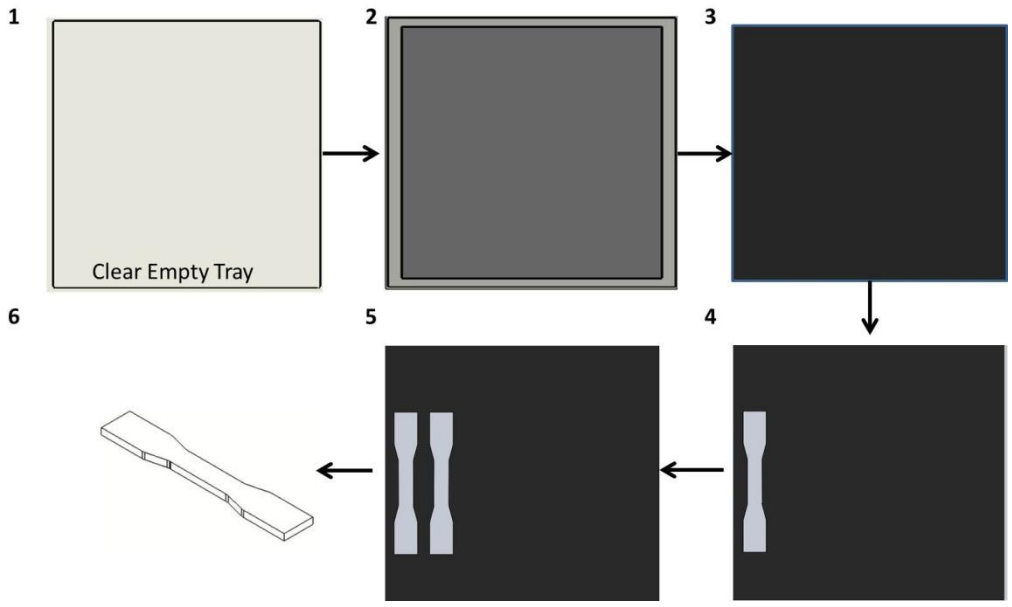

Figure 11. Converting Mould C-casts to samples of Sylgard 170. One single assay tray (Type C mould) was sprayed with mould-release (**1**). Sylgard 170 was then prepared and poured into the mould (**2**). The silicone-filled mould was moved to the 60 °C oven to cure. After removal from the oven, the cast sheet was removed from the mould (**3**). To obtain samples for testing, a die D cutter was used (**4**). Samples were gathered by cutting from left to right unless otherwise noted (**5**) and the resultant samples were single specimens available for tensile testing (**6**).

3.6.1 Internal Reinforcements

For internal reinforcement of base material samples (+Int), Dow Corning Sylgard® 170 was prepared. The jig allowed for thread to be held taut while enveloped by the material cast in the tray. 100% Silk Thread (used in Section 3.5.4) was secured on the left-hand top side of the jig and then woven through every other hole. When the opposite end of the jig was reached, the thread was pulled taut and secured. The jig with thread was inserted into the square assay tray, and prepared Sylgard® 170 was poured atop. The tray was shifted from side to side to achieve uniform thickness. Minimal material

seeped into the four corners but this was not seen as an issue because all four corners retained material and the samples were cut from the middle of the tray, unless otherwise noted. The material was oven-cured at 60 °C for a minimum of four hours. After removal from the oven, the cured tray was allowed to return to room temperature before cutting the thread at the jig-material interface. The sheet of material with embedded silk thread was then removed from the casting tray and samples were cut using ASTM standard die D cutter, as depicted in Fig. 12.

Samples were cut from the middle of the cast sheet accumulating on average seven samples per cast, unless otherwise noted. Sample size altered based on visible edge effects due to open-air casting. Samples were cut with the die cutter to obtain one fiber in the gauge region (more than one fiber would alter the properties).

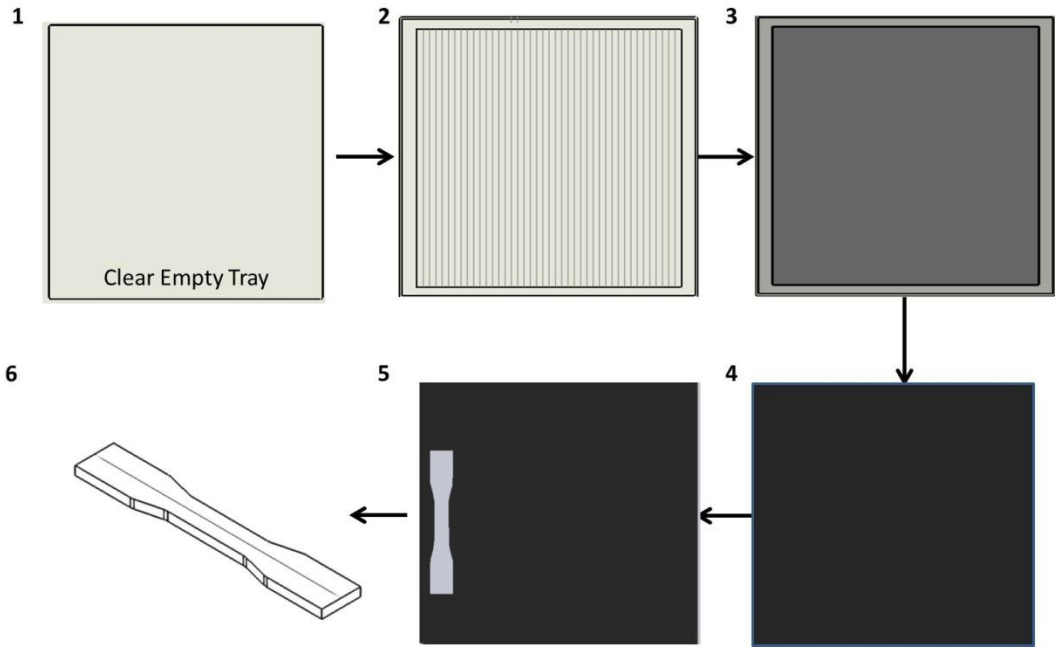

Figure 12. Reinforced Sylgard 170 sample fabrication. One single assay tray (Type C mould) was sprayed with mould-release (**1**). One thread was placed every 6 mm across the sample utilizing the plastic jig for alignment (**2**). Sylgard 170 was then prepared and poured into the mould (**3**) covering the threads, and in turn embedding the fibers. The silicone-filled mould was moved to the 60 °C oven to cure. After removal from the oven, the sheet was demoulded by cutting the threads at the thread-plastic interface (**4**). To obtain samples for testing, a die D cutter was used (**5**). Samples were gathered by cutting from left to right unless otherwise noted and the resultant samples were single specimens available for tensile testing (**6**).

3.6.2 External and Double-Stranded External Reinforcements

Sylgard 170 or Dragon Skin 20 was prepared as described above in Sections 3.3.2 and 3.3.5, respectively. The base material was poured into the pre-mould-released Type C moulds and oven-cured at 60 °C oven for a minimum of four hours. After removal from the oven, the tray of material was allowed to return to room temperature before demoulding. Forty strands of 100% pure silk thread, approximately 40 mm in length, were laid out 5 mm apart

across the material sheet, as depicted in Fig. 13. A secondary batch of the base material was prepared to attach the fibers to the sheet to completely cover the thread without adding much thickness. Each individual strand of thread was pulled taut, coated with the appropriate base to create one cohesive sheet, and secured in place. All strands were weighted down at their ends to keep fibers taut. The additional layer of material cured at room temperature for greater than forty-eight hours, providing one solid, coherent sheet of silicone. Similar to the internal embedded composites that were cut at the thread-jig interface, the excess thread attached to the tabletop was cut from the sheet. With ASTM-D638 Type 4 die D cutter, samples were cut from the center of the sheet (as shown in Fig. 13). On average, seven samples per mould were cut and measured using a micrometer. Sample size altered depending upon the edge effects seen from casting in an open-air tray.

To qualify as a single-stranded external reinforced sample (+Ext), there must have been only one thread along the gauge length of the cut sample. Samples that would have been excluded for double the quantity of fibers in the gauge region created their own test group, Double-stranded Externally Reinforced (+2x) samples. The gauge width of all Mould C-die-cut samples was 6 mm, so the occurrence of two threads that are placed 5 mm apart within that 6 mm is not uncommon.

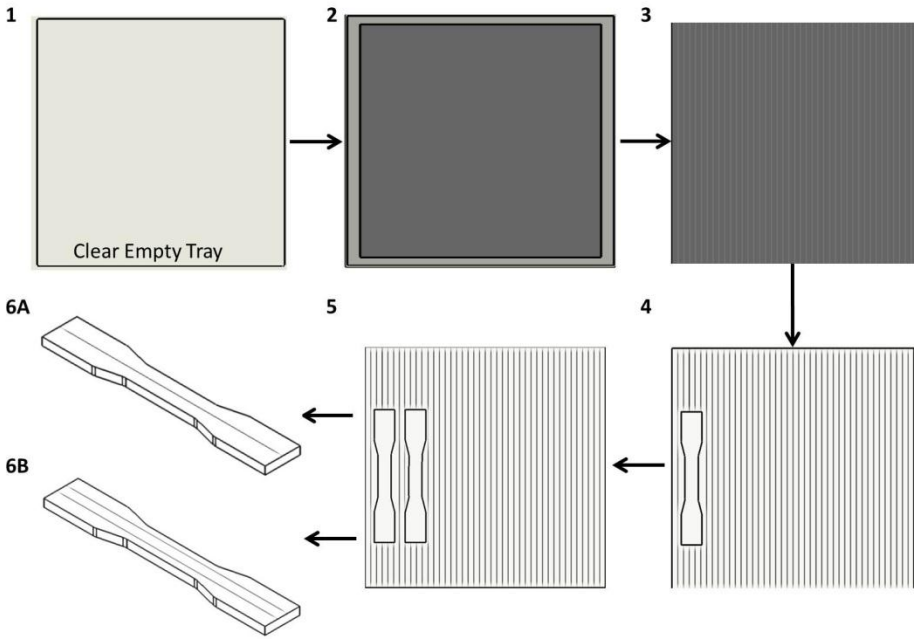

Figure 13. External and Double-stranded external reinforcement of Sylgard 170. One single assay tray (Type C mould) was sprayed with mould-release (**1**). Sylgard 170 was then prepared and poured into the mould (**2**). The silicone-filled mould was moved to the 60 °C oven to cure. After removal from the oven, the cast sheet was removed from the mould. 100% pure silk thread was aligned once every 5 mm across the width of the sheet. The thread was adhered to the cured sheet by an additional batch of uncured base material (**3**). After 24 hours a die D cutter was used to obtain samples for testing (**4**). Samples were gathered by cutting from left to right unless otherwise noted (**5**) and the resultant samples were single specimens available for tensile testing reinforced by either one single fiber (**6a**) or were double-stranded, with twice the density of thread within the gauge region of the single-fiber samples (**6b**).

3.6.3 Perpendicular Reinforcement Samples

For all reinforced Mould C-cast samples, the fibers were aligned with the direction of uniaxial testing when samples were die-cut. Two Sylgard 170 samples, one sample each for the internal and external reinforced samples, are referred to as perpendicular samples and denoted with ⊥. These samples were cut with the fibers perpendicular to the direction of stretch. The

samples were cut from underneath the sample set used for testing, as shown in Fig. 14A with the fibers colored blue for clarity. Figure 14B shows the perpendicular sample from the externally reinforced set (+Ext ⊥). Two externally reinforced Dragon Skin 20 samples were cut in the same manner (DS20 +Ext ⊥) as well.

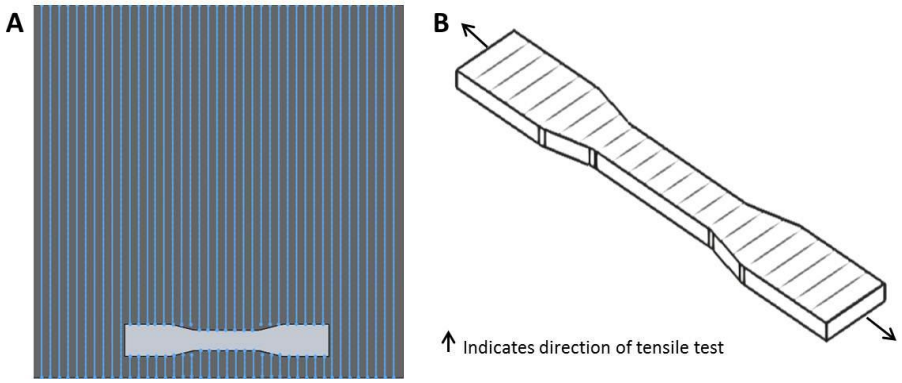

Figure 14. Perpendicular (⊥) samples cut for reinforced Sylgard 170. A) These samples were cut from the bottom of the sheet with the fibers oriented perpendicular to the stretch direction. B) The resulting sample had many, shorter fibers, but none aligned with the direction of testing. Both internal and external reinforcements of Sylgard 170 and Dragon Skin 20 had samples cut to evaluate.

Material properties for both the internal perpendicular (+Int ⊥) and external perpendicular (+Ext ⊥) samples should resemble unreinforced Sylgard 170. Similarly, material properties for the externally reinforced Dragon Skin 20 sample cut with fibers perpendicular to the axis of direction (DS20 +Ext ⊥) should mimic unreinforced Dragon Skin 20. The fibers were not required to elongate as the sample stretched as a result of the perpendicular orientation

to the axis of stretch. They should therefore render useless in altering the stress. The results from the tensile testing of these samples are included for visual comparison only and not statistical testing.

3.7 Hollow Tube Technique

Cylindrical tubes of Sylgard 170 were fabricated using loss-wax casting techniques to further evaluate the effects of reinforcements. Both thick-walled (3.79 ± 0.18 mm) and thin-walled (1.59 ± 0.16 mm) samples were created, with half the samples reinforced generating four test groups. All samples were then measured and subjected to burst pressure testing as described in Section 3.8.5.

3.7.1 Thick Unreinforced Tubular Samples

The core for thick-walled samples was made with red machinable casting wax (McMaster-Carr, 93955K74). This wax has softening temperature 62.2 – 68.9 °C. It was liquefied and then poured into 0.53" diameter tubes held in place by a custom-printed endcap. The wax was poured around a wire rod included to help the wax keep form while oven-curing. This plastic-wax setup was then placed in a refrigerator to cool the wax before it could deform the plastic tube, aiding to produce a straight core. After the wax set, the plastic was removed leaving the wax core intact. A second set of custom endcaps was used to secure the wax, the embedded rod, and the 0.79" diameter outer shell to produce a uniform hollow tube.

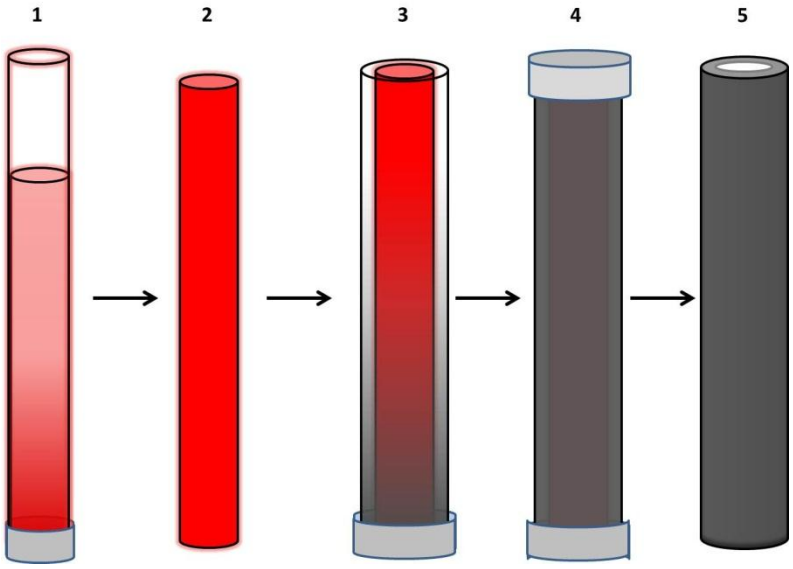

Figure 15. Schematic of 3-D samples created using wax cores. Plastic tubes (ID=0.53") were secured in an endcap and filled with heated casting wax (**1**). The wax was set to cool in a refrigerator or ice bucket. Once set, the plastic sheath was removed (**2**). The wax core and outer plastic shell (ID=0.79") were placed in an endcap. The gap created between the two was filled with prepared Sylgard 170 (**3**). The second endcap was attached and extra material added via a syringe port (**4**). The samples were oven-cured at 60 °C and once cured, the endcaps removed. The wax-Sylgard-plastic sheath samples were placed in a beaker of boiling water to melt the wax and aid the removal of the plastic sheath. This method resulted in a hollow 3-D structure (**5**).

The endcaps, wax, and outer shell were lightly coated in mould release. The shells were not pre-scored as that led to the production of seams in the hollow tubes. During the thirty minutes suggested drying time, Sylgard 170 was prepared accordingly and degassed. The cores were then positioned in the end caps followed by the positioning of the outer shells. The Sylgard 170 was positioned into the gap created between the wax core and the shell via syringe. Once filled to the top, the upper end cap was positioned to help the wax remain aligned. Extra material was added via a syringe port on the

upper end cap to compensate for settling material. The shell-material-core was moved to the 60 °C oven for one hour. At this point the Sylgard 170 should be cured, but a longer cure time was preferred to ensure full cure. The red wax began to liquefy after one hour. The endcaps were removed, and a bin placed beneath the tubular sample to catch the wax. After a second hour of oven-curing, the tubes were removed from the oven and the excess wax placed aside. These tubes were then placed in a beaker of boiling water (enough water to submerge the entire tube) to melt the remainder of the wax. A secondary benefit was the deformation of the plastic shell for ease of removal. This method produced thick-walled hollow tubes.

3.7.2 Thick Reinforced Tubular Samples

Reinforced thick-walled samples were made similarly to thick walled reinforced samples with the exception of casting in an ice bucket. Red machinable wax was cast in 0.53" diameter tubes inside an ice bucket. Moving the system to the refrigerator after the liquid wax was poured resulted in non-straight cores more times than naught. By surrounding the plastic tubes and endcaps in an ice-chest, ice was added as necessary to cool the wax and fabricate straight cores. Due to the ice, the plastic tubes were unaffected by the addition of hot wax, and the resulting tubes were observed to be more uniform. After casting and removing the outer shell (0.79" diameter), 100% pure silk thread (Gutermann 100% pure silk S303 Sewing Thread) was wrapped circumferentially around the tube at 5 mm intervals

Fig. 16). The thread was secured to a separate tube placed through the hollow sample to allow for rotation to provide a uniform coating. After the thread was held in place, mixed-and-degassed Sylgard 170 was used as a glue to hold the thread to the cured Sylgard 170 tube, similar to the method described for external reinforced planar samples. The reinforced tubes were moved to the 60 °C oven for one hour to cure, and moved to a bench top for 24 h to acclimate to room temperature. Afterwards, the extra rod was removed.

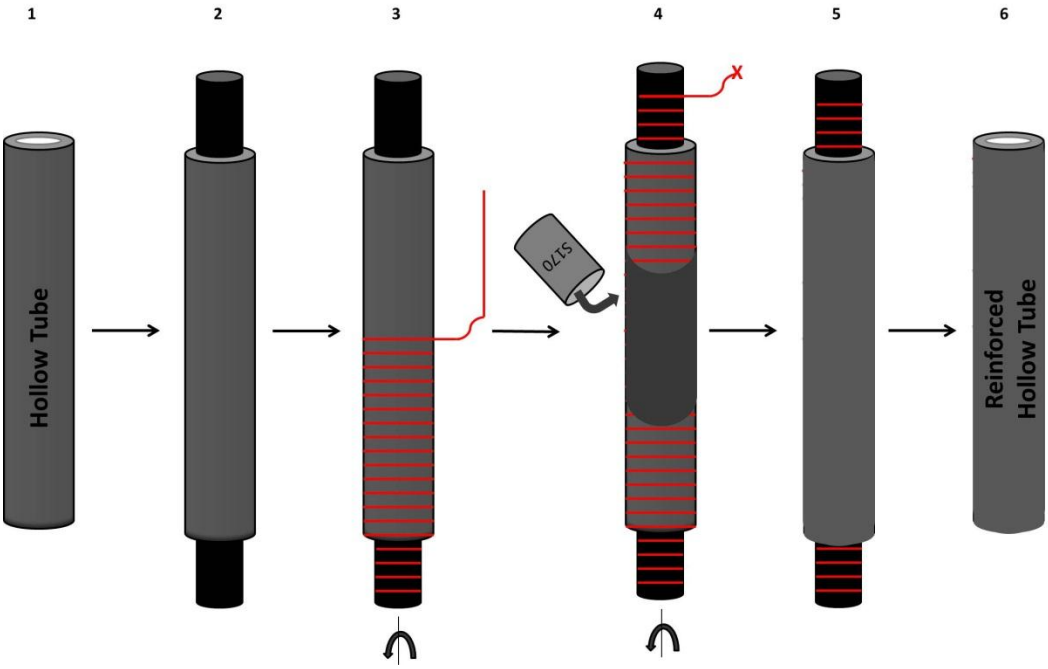

Figure 16. Schematic of reinforced tubular samples fabrication. Hollow samples created (**1**) were reinforced by placing a rod through the center (**2**) of the tube to give support. 100% pure silk thread was attached to the rod and placed 5 mm apart down the length of the tube aligned circumferentially (**3**) by rotating the rod. Once in place, the fibers were adhered to the tube using uncured Sylgard 170 (**4**) until the tube was covered. The reinforced tubes were moved to the 60 °C oven for one hour and then left at room temperature for 24 h (**5**) at which point the rod was removed. This method resulted in reinforced hollow tubes (**6**) for pressure tests.

3.7.3 Thin Unreinforced Tubular Samples

Thin-walled tubes were made following the thick-walled protocol with different wax and a different inner tube. To make thin walled samples, thicker wax cores were required. The red wax used previously was found too brittle, and was replaced with Brown Victory Sculpture Wax (Compleat Sculptor, 83103S). 0.7" plastic tubes were secured in endcaps and surrounded by ice in a bucket. The brown wax, with softening temperature 74 °C, was heated and poured into cores. As the liquid wax was added, the ice melted surrounding the tubes, and more ice was added to help speed the process of the wax solidification. After the wax set, the plastic shell was removed providing an inner core slightly less than the anticipated 0.70" diameter. The wax core, outer plastic shell (0.79" ID), and a second of endcaps were lightly coated in mould release while a batch of Sylgard 170 was prepared. The core and shell were secured in the bottom endcap, and Sylgard 170 was syringed into the narrow gap until filled. The upper end cap was positioned, and the shell-Sylgard170-wax group was moved to the 60 °C for curing. After two hours, the Sylgard 170 was fully cured, and the entire group was removed from the oven. The end caps were detached and the remaining parts were submerged in a beaker of boiling water. The brown wax did not liquefy as the red did in the 60 °C oven, so the boiling water served to remove the wax from the silicone tube, as well as to aid in the removal of the outer plastic sheath.

3.7.4 Thin Reinforced Tubular Samples

Reinforced thin-walled samples were randomly selected from the unreinforced thin tubular samples and made similarly to thick reinforced tubular samples (Fig. 16). The 100% silk thread (Gutermann) was wrapped circumferentially around the tube at 5 mm intervals. The thread was secured at both ends to a separate rod that had been placed in through the middle of the hollow Sylgard 170 tube. The rod allowed for rotation of the sample for an even second coating as well as a place to secure the thread. Mixed, degassed Sylgard 170 was then used to cover the tube and thread to adhere the thread in its position. The sample was placed in the 60 °C oven for two hours. After time elapsed, the sample was moved to a bench top and left to acclimate to room temperature for 24 hours, at which point the secondary tube was removed. This method resulted in the reinforced thin-walled samples.

3.8 Protocols for Data Acquisition

3.8.1 Uniaxial Loading Protocol

The initial protocol was developed with the intention to show differences between potential base materials and their reinforced counterparts. Three unreinforced test samples cast in Type A moulds provided control cases for S160, S170, and S184. Three reinforced test samples for each base provided experimental cases for S160, S170, and S184. Each specimen's dimensions

were measured three times with calipers along the gauge length, and the average was input into Blue Hill Software (Instron, Norwood, MA) that digitally recorded the test load and extension. The sample was loaded into a uniaxial test machine (Instron Inc., Model 3366) using pneumatic grips. The sample was moved to obtain zero load resulting in a gauge length between 68 and 90 mm. Samples were loaded uniaxially at a strain rate of 1.50 mm/min. These tests concluded at the failure of each individual sample. In the case of reinforced samples, the rubber failed before the wire causing the test to be terminated before computer-registered failure. The failure of the Sylgard surrounding the wire was considered to be a complete test to failure. Reported data corresponds to the initial experience at each strain.

3.8.2 Cyclic Preloaded Uniaxial Loading Protocol

All samples, unless otherwise specified, were made using one of six 3-D printed Type B moulds. The thickness and width of each sample were measured three times along the gauge length, and the average value used to calculate the cross-sectional area (product of width and thickness). The samples were loaded into a uniaxial tension tester with consistent gauge length, 60 mm. Cyclic preloading was applied from 0.0 mm to 5.0% strain at a rate of 5.0% strain/min (Fig. 17), for five loading-unloading cycles. The sample was then pulled to failure at a rate of 5.0 mm/min, with both extension and loading force automatically captured every 100 ms. Both Dragon Skin 10 and Dragon Skin 20 samples stretched to more than twice

their original length without signs of failure and tests stopped at 200 mm extension were deemed conclusive. Reported data corresponds to the initial experienced strain outside the pre-cycling maximum, unless otherwise noted.

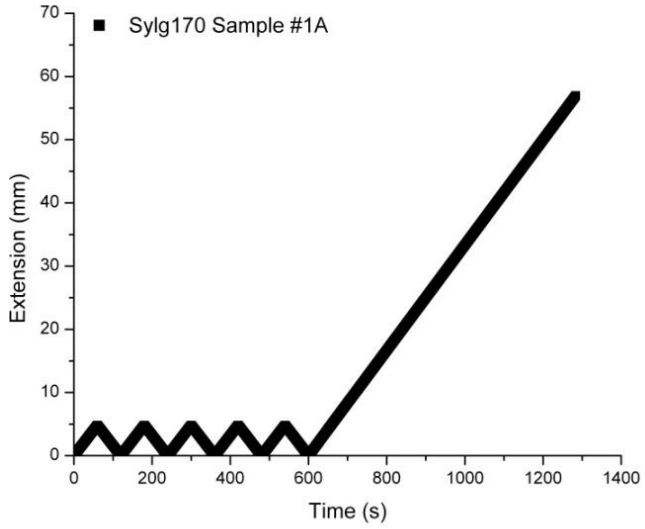

Figure 17. Cyclic preloaded uniaxial testing protocol: each sample was pre-cycled five times at 5% strain/min to 5% strain before pulling to failure at 5.00 mm/min.

3.8.3 Cyclic Uniaxial Loading Protocol

Each sample cast in Type C moulds followed an identical test protocol (Fig. 7). All samples were cut from a square sheet cast of material with an ASTM die D cutter. Each sample's dimensions were measured three times along the gauge length and the median value determined in order to calculate cross-sectional areas. Each sample was loaded in the uniaxial tensile tester with a gauge length of 35 mm and preloaded to 0.1N at a strain rate of 0.10 mm/s.

Cyclic uniaxial loading was applied as follows: five levels of maximum deformation were performed to target stretches beginning at λ= 1.1 through 1.2 increasing by 0.025 steps (equivalent to 2.5% strain increase). Each level (λ= 1.1, 1.125, 1.15, 1.175, and 1.20) was cycled five times at 0.1295 mm/s. After the fifth unloading cycle from 10% strain, the sample proceeded to 12.5% strain and 5 cycles followed. At the completion of the test, each sample underwent twenty-five loading-unloading cycles, with extension and loading force automatically captured every 100 ms by software designed to work with the uniaxial tensile tester by the manufacturer, BlueHill testing Software.

3.8.4 Sylgard®170 Longevity Protocol

Untested samples were set aside from casts made in Type C moulds for longevity testing. One sample each for unreinforced Sylgard 170, internally reinforced Sylgard 170, and externally reinforced Sylgard 170 were tested in the following manner. The samples were preloaded to 0.1N at a strain rate of 0.10 mm/s. Five hundred loading and unloading cycles began from 0.1N to 15% strain at a rate of 0.1295 mm/s. Loading force and extension were captured automatically via Blue Hill Software (Instron Norwood, MA) for the uniaxial tensile tester every 100 ms. This data was converted to engineering stress, engineering strain, and stretch ratio.

It was previously noted that by the fifth cycle to a particular strain, the stress response of the materials was stable. After the fifth cycle, changes in stress as cycle number increased were minimal.

3.8.5 Wall Strength and Burst Pressure Protocol

Cylindrical hollow samples were tested to establish the two-dimensional response to internal pressure and the changes to the response that reinforcement would provide. Tests were setup according to Fig. 18, utilizing a pressure transducer (PX219-060A10V, Omegadyne, Ohio). The set-up remained the same for all tubular samples tested with appropriate couplings adjusted for the differences in wall-thickness.

Lines connected the house air to the pressure transducer, with multiple necessary to account for the different diameter ports for which no one coupling was available. The pressure transducer was connected to the tubular test sample, and an exit line was added to the outlet side of the sample. This exit line was then occluded, as indicated by the "X" in Fig. 18, to close the system.

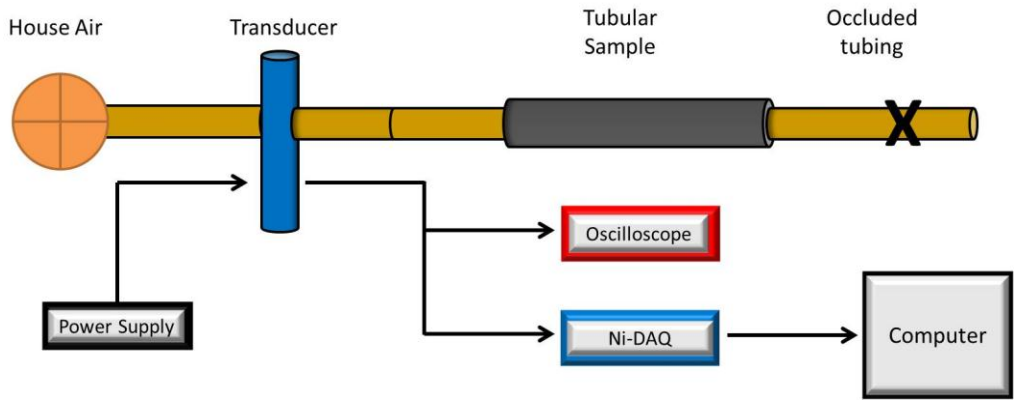

Figure 18. Schematic of the laboratory setup for burst measurements. The pressure transducer, powered by a lab power supply, was connected to both the house air and the tubular sample. An exit line from the sample was occluded to produce a closed system. The transducer was attached to both an oscilloscope and data acquisition unit (Ni-DAQ), with the latter attached to a computer for data capture.

Powered by a general lab power supply, the transducer's output was connected to both an oscilloscope and a data acquisition unit (NI-DAQ, National Instruments). The Ni-DAQ was connected via USB to a lab computer with labVIEW software loaded (National Instruments). labVIEW software was used to automatically record the time and voltage data from the transducer every 100 ms. The duration of the labVIEW protocol was set for eight minutes for thick-walled samples (five minutes for thin-walled) before it would generate a text file. This text file was then imported into Microsoft Excel for conversion to pressure measurements using the daily standard calibration curve.

Each day of testing, a new standard calibration curve was generated to transform the voltage readings to pressure for measurements. For these

curves, a pressure gauge was added to the system in place of the silicone tube to be tested. The pressure-voltage data was captured both manually by visually reading the voltage off the oscilloscope, and digitally as the computer recorded data. Both sets were imported into excel as a check that labVIEW was recording the appropriate voltage. This also served to give confidence that the oscilloscope could be used in later steps for target pressure steps. The computer generated data was then plotted with a linear trend line defined to best describe the relation.

The maximum voltage allowed by the NI-DAQ was 10.5 V and thus may limit the maximum pressure reported by the system. There were five standard curves used to generate burst pressure data. From these standard curves, the maximum pressure to be reported was 57.85 psi. Throughout testing, no tube withstood 50 psi, and therefore, the maximum of the system never reached.

After setup, if applicable, a digital camera (Olympus Stylus 1010) was turned on to record changes in diameter. Fifteen seconds later (all times were recorded and kept track of with a timer) the labVIEW software began to acquire data. An additional fifteen seconds later (thirty from the camera recording) house air was turned on no higher than 5 psi (3.10 ± 1.17 psi). Readings off the oscilloscope were recorded to ensure the validity of the data reported by the software in the event of a glitch. The pressure was increased every thirty seconds until failure. The labVIEW generated text file was

imported into Excel and converted to pressure values using the appropriate standard curve.

Wall strength analysis was performed under the assumption of constant, uniform wall thickness. Increases in wall stress were approximated by the law of Laplace,

$$\sigma = \frac{P * r}{t}, \tag{7}$$

where P is the internal pressure, r is maximum outer radius, and t is the undeformed wall thickness. The outer radius was used as an approximation due to the inability to accurately determine the inner radius with the camera placement.

The burst pressure reported was the maximum pressure before failure. Several samples failed at a lower pressure as a direct result of nicks in the tube from clamping to the adapters. These samples were not included as they did not contribute to the mechanical integrity of the samples, but rather attest to the ease at which a puncture can perpetuate early failure.

3.9 Data Collection and Analysis

Planar mechanical testing data was recorded digitally by the software accompanying the uniaxial tensile tester. Data was exported as a comma separated values (CSV) file and imported into excel for analysis.

For data acquired by the uniaxial loading protocol or the pre-cycled uniaxial loading protocol, each individual sample's representative stress-stretch response was calculated. For the pre-cycled uniaxial loading protocol, data was only used after pre-cycling had completed. The data was sectioned into λ=0.001 segments with an average calculated. This average stress was considered the representative response for these stretches. A characteristic stress-stretch curve for each test group was then calculated by averaging the representative points at each λ and reporting both average and standard deviation. Two types of moduli were calculated. For uniaxial testing protocol samples, the tangential modulus was calculated at five strain points along the single curve. Using the twelve surrounding data points, inclusive of the strain, the slope was calculated and reported as the tangential modulus. A second modulus, the maximum segmented modulus, was calculated to further examine the linearity of the stress-stretch curves. For each individual sample's response curve, the data was split into sections and the slope of each calculated. The maximum of these slopes was classified as the maximum segmented modulus for each individual sample. The average and standard deviation of the maximum segmented modulus for each test group was found and reported.

For data acquired by the cyclic uniaxial loading protocol and for patient data, all twenty-five test cycles were treated individually for each sample. For each individual cycle, the stress was binned into λ=0.001 segments with an

average stress calculated. This resulted in twenty-five stress-stretch responses per sample. The data reported is the average and standard deviation of a specific cycle across specimens in one test group.

Two types of moduli were calculated for each of the individual specimen's responses. The tangential modulus for each of the five target strains was calculated from the fifth and final cycle to that particular strain for each specimen. The tangential modulus for 15% strain was not calculated while the specimen was stretched to 20%, but rather the fifth cycle to 15%. As a result, the tangential modulus could not be calculated with the target strain comprising the middle of the data selection, but rather it was the end point. The twelve points closest to the target strain were used and the slope of these points calculated. The maximum segmented modulus was also calculated for each of the twenty-five stress-strain cycles. For each individual curve, the data was split into twelve point sections and the slope calculated. The maximum of these slopes was classified as the maximum segmented modulus for each individual sample. The average and standard deviation of the maximum segmented modulus for each test group was found and reported.

The significance of reinforcement types was determined by Student's *t*-test ($p < 0.05$) and analysis of variance (ANOVA, $p < 0.05$), where appropriate. The statistical tests were run with StatView Software (SAS Institute Inc.).

Chapter 4 – Results and Discussion for Base Material Selection

By embedding a variety of materials with varying properties of their own, it was anticipated that different response curves would be produced. In practice, successful reinforcement was limited by the ability of silicone to adhere to the reinforcements. For example, the embedment of vinyl mesh was attempted, but ultimately failed due to the incompatibility between silicone and vinyl.

4.1 Sylgard Bases and Wire-Washer Reinforced Samples

Testing of the three base materials in Type A moulds was performed as a control, to quantitatively analyze the effect of reinforcing the intrinsic properties of silicone. The three Sylgard materials (Sylgard160, Sylgard 170, and Sylgard 184) were cast in Type A moulds (Table 3). Reinforced samples were created using the wire-washer method described above in Section 3.4. The stress-stretch curves for each of the unreinforced cases showed little sample-to-sample variability compared to their respective reinforced versions. Up through 20% strain, the average Sylgard 160 response indicates linear relationship between stress and stretch (Fig. 19A), as does Sylgard 170's (Fig. 19B) and Sylgard 184's (Fig. 19C).

The reinforced Sylgard 160 replicates were less consistent once strained beyond 7.3% as the range of values within the region of interest (up through 20% strain) was greater than 50 kPa (Fig. 19A). Although the samples were thought to be made identically, human error would account for these differences as the wire may have been tauter or even placed in a different location throughout the gauge length despite efforts for repeatability. Reinforced Sylgard 170 samples were consistent through 10% strain, and similarly, reinforced Sylgard 184 samples showed consistency through 11% strain, shown in Figs. 19B and 19C.

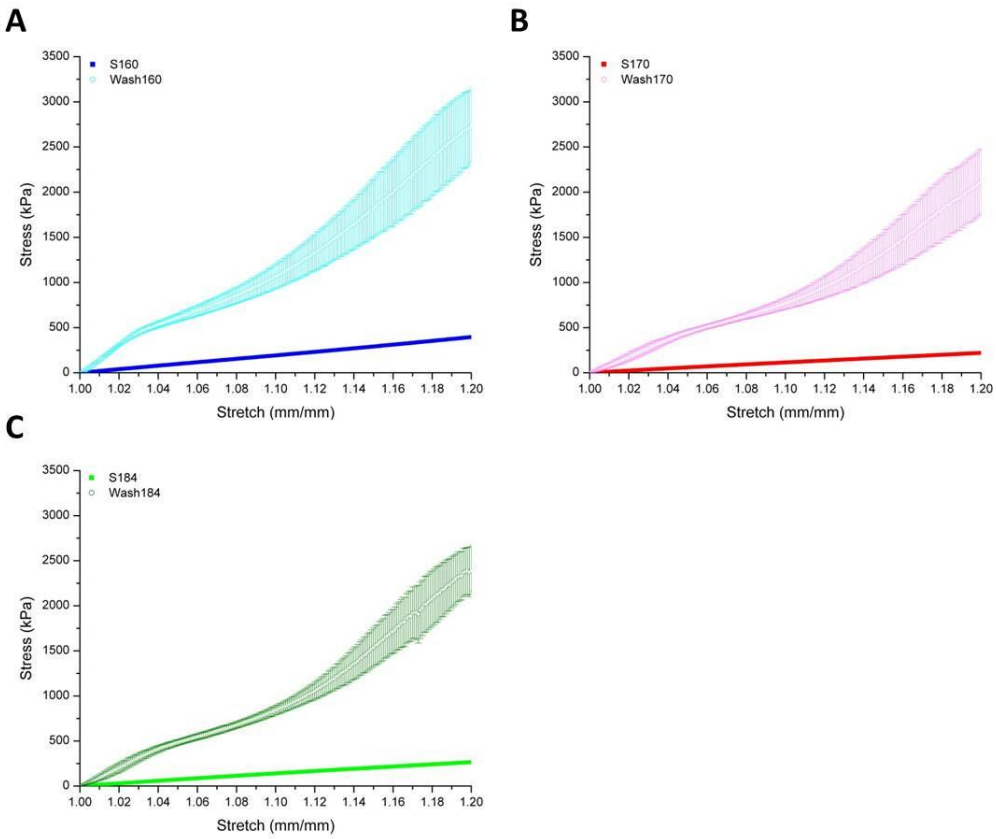

Figure 19. Stress-stretch curves for WWR tests. Comparison of the average (n=3) tensile stress-stretch curves of Sylgard base materials A) Sylgard 160, B) Sylgard 170 and C) Sylgard 184 to their respective wire-washer counterparts up to a stretch of 1.2 mm/mm.

The intrinsic material properties of these base materials were altered significantly with the inclusion of wire. By embedding a stronger material, changes in tensile stress were relevant at early strains. The instantaneous stress is quantified in Table 5 for the six groups at strains from 10% to 20% strain in 2.5% intervals. At 10% strain, the average instantaneous stress for Sylgard 160 was 192.13 ± 2.32 kPa, but with the embedded wire the stress increased significantly to 1065.28 ± 163.84 kPa, 5.5 times greater (Student's

t-test, $p < 0.05$). Reinforced Sylgard 170 recorded a significant increase in stress, reporting more than six times that of the unreinforced average's 113.05 ± 3.37 kPa. Similarly, the stress experienced at 10% by reinforced Sylgard 184 was, sixfold greater, a statistically significant difference, from its unreinforced average: 840.74 ± 63.55 as compared to 140.06 ± 5.17 kPa (Student's *t*-test, $p < 0.05$).

Table 5. Average instantaneous stress for WWR tests. The stress was calculated for the Sylgard 160, Sylgard 170, and Sylgard 184 samples and the reinforced versions of each at 10%, 12.5%, 15%, 17.5%, and 20% strain, with sample size indicated in parentheses. Each unreinforced base showed a statistical significant difference from its reinforced version at all five strain points (Student's *t*-test, $p < 0.05$).

	Instantaneous Stress (kPa)				
Type	**10%**	**12.50%**	**15%**	**17.50%**	**20%**
Sylgard 160 (3)	192.13 ± 2.32	240.89 ± 3.38	290.74 ± 4.70	342.03 ± 6.07	395.07 ± 7.67
Reinforced Sylgard 160 (3)	1065.28 ± 163.84	1404.80 ± 265.39	1823.51 ± 391.44	2286.11 ± 503.80	2730.32 ± 496.74
Sylgard 170 (3)	113.05 ± 3.37	139.10 ± 4.54	164.97 ± 6.03	190.33 ± 7.73	215.54 ± 9.68
Reinforced Sylgard 170 (3)	769.35 ± 79.78	1000.76 ± 164.68	1323.91 ± 282.71	1726.43 ± 399.97	2110.54 ± 445.37
Sylgard 184 (3)	140.06 ± 5.17	172.48 ± 6.36	203.79 ± 7.83	234.42 ± 9.01	264.47 ± 10.12
Reinforced Sylgard 184 (3)	840.74 ± 63.55	1123.78 ± 137.11	1537.73 ± 260.01	1982.68 ± 373.56	2391.26 ± 322.31

As a result of the nonlinear response to the inclusion of wire, the values of stress reported and their significance were only valid for the particular strain for the calculation. For example, at 10% strain, there was a 973 kPa difference in stress between unreinforced and reinforced Sylgard 160 (192.13 kPa as compared to 1065.28 kPa). By 20% strain, reinforced Sylgard 160 has stress seven times the value for the unreinforced material, 2730.32 kPa and 395.07 kPa, respectively (Table 5, Fig. 20). As strain increased, the difference between the unreinforced and the reinforced versions continued to increase. At 17.5% strain, the average instantaneous stress for Sylgard 160 was increased by 1944 kPa to 2286.11 kPa, by reinforcement via the wire-washer method. At 20% strain, the difference in stress between Sylgard 160 unreinforced samples and WWR samples was 2335 kPa. This nonlinear increase in strain by samples reinforced by this technique was exhibited in all three Sylgard bases. Due to this non-linear behavior, the specification of strain level, in addition to strain rate, is important when reporting data.

Overall for each of the three Sylgards, the wire-washer reinforcement method significantly altered the intrinsic mechanical properties (Student's *t*-test, $p < 0.05$). Direct comparison of average instantaneous stress, tabulated in Table 5 and depicted in Fig. 20, showed minimal differences between the three bases materials when compared with the effects of the reinforcement. S160, S170, and S184 report less than 500 kPa of stress at 20% strain, whereas Wash160, Wash170, and Wash184 well exceed that stress by 10%

strain, and approach that level of variation by 20% strain. Generalizations can be made from analyzing Fig. 20 regarding the relationships between base materials. Sylgard 170 reached the lowest stress of the three Sylgard bases at all five strains examined, and continued to have the lowest stress when reinforced. Similarly, Sylgard 160 and WWR-Sylgard 160 reached the highest stress at each of the five strains within their respective groupings.

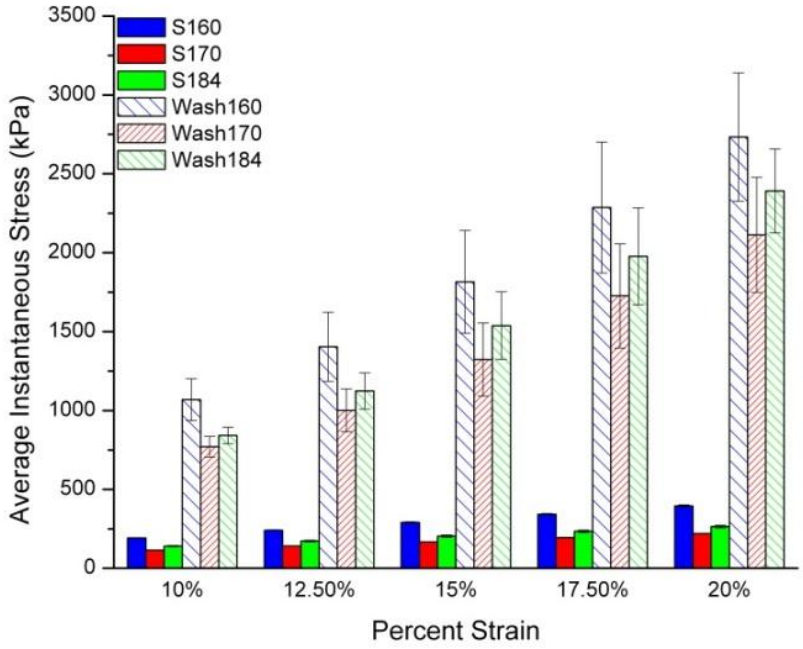

Figure 20. Average instantaneous stress comparison for WWR tests. Visual comparison of the average instantaneous tensile stress (n=3) at 10%, 12.5%, 15%, 17.5%, and 20% strain of the base materials and the wire-washer reinforcements reported in Table 5. At all five strains, unreinforced Sylgard 160 was significantly different from reinforced Sylgard 160, unreinforced Sylgard 170 different from reinforced Sylgard 170, and unreinforced Sylgard 184 different from reinforced Sylgard 184 (Student's *t*-test, $p < 0.05$).

In an attempt to quantify the linearity of the stress-strain relationships, both the tangential modulus (Table 6) and the maximum segmented modulus (Table 7) were calculated. The tangential modulus of Sylgard 170, calculated at five points on the stress-strain curve, did not change as the sample continued to be stretched. This indicated a rough linear nature for this base material. As the samples were stretched from 0-20% strain, the increase in stress for a 5% increase in strain remained consistent (between 1048 and 1086 kPa). This pattern was also seen for Sylgard 184, albeit higher moduli were found (1213-1316 kPa). Due to the larger stresses at 10%, 12.5%, 15%, 17.5%, and 20% strain, and the apparent linearity of the stress-strain response, higher tangential moduli were expected for Sylgard 184 when compared to Sylgard 170. The response curve was steeper, and this is indicated by larger tangential moduli. By the same logic, Sylgard 160 should have an even larger modulus at each of the five strain points. Unreinforced Sylgard 160 had tangential moduli values closer to 2000 kPa.

The tangential modulus was also calculated at each of the five strain points (10%, 12.5%, 15%, 17.5%, and 20%) for the WWR samples. The responses shown in Fig. 19 show a clear non-linear relationship between stress and strain for each of the WWR samples. As strain increased, the tangential modulus should change. Additionally, it is anticipated that the WWR tangential moduli would be significantly higher than those of their corresponding bases due to the significant increase in stress at each strain.

The tangential modulus for WWR-Sylgard 160 increased as strain increased up through 17.5% strain. The tangential modulus at 10% strain, 10796 kPa, increased as strain reached 15% to 17698 kPa. The different tangential modulus values for WWR 160 (Table 6) suggest that the curve has multiple regions of stiffness, as would be expected. The tangential modulus at 10% strain for reinforced Sylgard 170 is 7065 kPa, as compared to the tangential modulus at 10% strain for unreinforced Sylgard 170, 1086 kPa. By reinforcing the base material, a significant increase in stress was required to deform the material. The tangential modulus of WWR Sylgard 170 increased as strain increased also indicating changes in the linearity of the stress-strain response. By 17.5% strain, the tangential modulus of WWR Sylgard 170 was 16682 kPa. Reinforcement of Sylgard 184 raised the tangential modulus of Sylgard 184 at 10%, 12.5%, 15%, 17.5%, and 20% strain. Unlike the other two bases that saw the steepest part of their curve at 17.5% strain, WWR Sylgard 184 peaked at 15% strain. After this strain, WWR Sylgard 184 continued to increase in stress, but did so at a slower rate.

Table 6. Tangential modulus for WWR samples. The average and one standard deviation are reported with sample size indicated in parentheses. Each unreinforced base was statistically significant from its reinforced version at the specific strains (Student's *t*-test, $p < 0.05$).

Tangential Modulus (kPa)					
Type	**10%**	**12.5%**	**15%**	**17.5%**	**20%**
Sylgard 160 (3)	1899.18 ± 37.43	1967.21 ± 43.27	2023.56 ± 57.66	2068.19 ± 65.75	2089.07 ± 56.85
Reinforced Sylgard 160 (3)	10795.73 ± 3104.44	14511.91 ± 4407.86	17698.24 ± 5725.79	19258.70 ± 3843.95	18983.02 ± 3073.74
Sylgard 170 (3)	1086.03 ± 8.12	1062.88 ± 14.72	1061.31 ± 7.59	1047.04 ± 18.38	1055.48 ± 11.09
Reinforced Sylgard 170 (3)	7064.97 ± 1961.96	10154.55 ± 3792.93	13690.12 ± 4727.20	16882.83 ± 5479.04	16791.64 ± 5201.66
Sylgard 184 (3)	1316.01 ± 57.83	1285.57 ± 40.23	1255.55 ± 57.84	1214.53 ± 57.69	1213.05 ± 54.30
Reinforced Sylgard 184 (3)	8532.51 ± 1622.40	12576.72 ± 4217.64	18153.61 ± 5134.19	14941.43 ± 8637.46	16866.12 ± 5683.29

The maximum segmented modulus is used to compare the magnitudes of the stress-strain response (Table 7). Each stress-strain response was segmented and the slope calculated. The maximum slope was then averaged for the test group and reported. As anticipated, the maximum segmented moduli for reinforced samples were significantly greater than for unreinforced samples. By using the wire-washer reinforcement technique, the maximum segmented modulus of Sylgard 160 was increased by 18443 kPa. Similarly,

reinforcement of Sylgard 170 this way increased this modulus by 16002 kPa, and for Sylgard 184 it increased by 18611 kPa. This information indicates distinct differences in the magnitude of linearity of the responses.

Table 7. Maximum segmented modulus for Sylgard and WWR samples. Each sample is divided into segments, the elastic modulus calculated, and the maximum per sample averaged for a representative modulus. Average (n=3) and standard deviation are reported. Each unreinforced base was statistically significant from its reinforced counterpart (Student's *t*-test, $p < 0.05$).

Maximum Segmented Modulus (kPa)		
Base	**Unreinforced**	**Reinforced**
Sylgard 160	2124.69 ± 62.86	20568.38 ± 2253.32
Sylgard 170	1241.70 ± 13.52	17243.79 ± 4501.46
Sylgard 184	1500.72 ± 48.95	20111.16 ± 3077.96

The effect of the wire-washer reinforcement technique on ultimate values of stress and stretch were also examined and are shown in Fig. 21. The ultimate tensile strength of unreinforced Sylgard 160, 1307.25 ± 270.47 kPa, was increased to 4700.17 ± 195.82 kPa by the WWR technique. Though reinforcing in this manner increased the ultimate stress of the material, it did not affect the stretch at which failure occurred. Failure for WWR samples

was taken at the point of the mechanical failure of the rubber. This was due to the rubber tearing around the intact wire. Similarly, Sylgard 170 saw a significant increase in UTS from 780.15 ± 302.52 kPa to 3879.87 ± 548.30 kPa, and saw no significant change in ultimate stretch. Reinforcement of Sylgard 184 significantly altered the UTS and the ultimate stretch. The UTS for Sylgard 184 increased from 1406.37 ± 423.46 kPa to 4173.41 ± 133.55 kPa. The λ_{ULT} was significantly decreased by reinforcing the material from 1.93 ± 0.20 down to 1.48 ± 0.01.

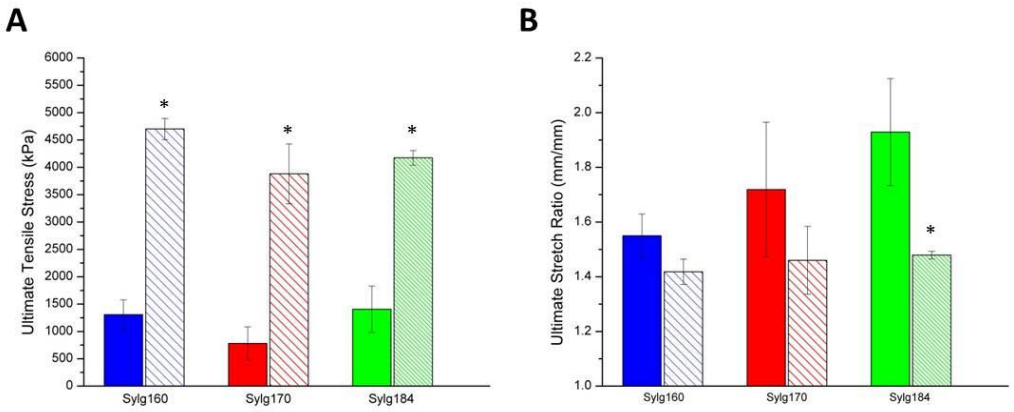

Figure 21. Ultimate values for WWR samples with A) ultimate tensile stress (kPa) and B) the stretch ratio at UTS (mm/mm) reported. A * represents significance between unreinforced and reinforced samples with the same base material (Student *t*-test, $p < 0.05$).

Based on the shore hardness values, it was predicted that S160 would be the material with the highest E value and the steepest slope, leading to higher stresses at comparative strains. S184 was thought to be the middle of the

three Sylgards with S170 having the least stress per strain. As the six groups were undergoing identical testing protocols, it was predicted that Wash160 would have the steepest slope of the three reinforced versions, producing a larger stress at the five examined strains, followed by Wash184. Figure 19 showed these overall patterns with Sylgard 160 experiencing the highest stresses, at all five strains examined, for the three base materials and its reinforced version reporting the highest stresses of all six test groups. Stresses reported for Sylgard 184 were between the other two unreinforced samples, and the WWR Sylgard 184 between the other reinforced averages.

4.2 Material Property Dependence on Mould Size

A non-linear stress-stretch relationship was achieved for Sylgard 160, Sylgard 170, and Sylgard 184. Although reinforcing the material with wire poses problems moving forward (e.g., repeatable positioning of the wire), a sixfold difference in stress was not expected to be necessary to match patient data. Valuable information regarding the relative locations of the stress-stretch curves was determined from these tests, which called for the testing of less stiff materials (Dragon Skins 10 and 20).

After the initial tests for base material selection with Sylgard 160, Sylgard 170, and Sylgard 184, the test procedure was modified to improve the significance of data generated. Both the moulds and the protocol were redesigned. Dragon Skins 10 and 20 had yet to be tested, and as a result,

S170 was chosen to compare directly to the lower bound materials based on the WWR test results, in addition to the consistency with which S170 could be cast. Before testing new materials cast in a new mould type at a new strain rate, the effect of the size of the mould on changes in results had to be determined because strain rate was already known to be a factor that affects the results[48]. For that purpose, S170 was cast in both Type A (n=4) and Type B (n=10) moulds. The two mould types differed in dimensions (Table 3). The larger moulds (Type B) used for the remainder of the fiber selection testing had nominal width 8 mm and target thickness 6 mm with gauge length 65 mm. Type A moulds were 7 mm wide and 6 mm thick, with gauge length 45 mm.

The stress-stretch responses shown in Fig. 22 showed no visible difference between the averages from the two mould sizes throughout the region of interest (up through 20% strain). This alignment was despite the difference in dimensions. Figure 22 shows overlapping curves as both increased to approximately 220 kPa at 20% strain.

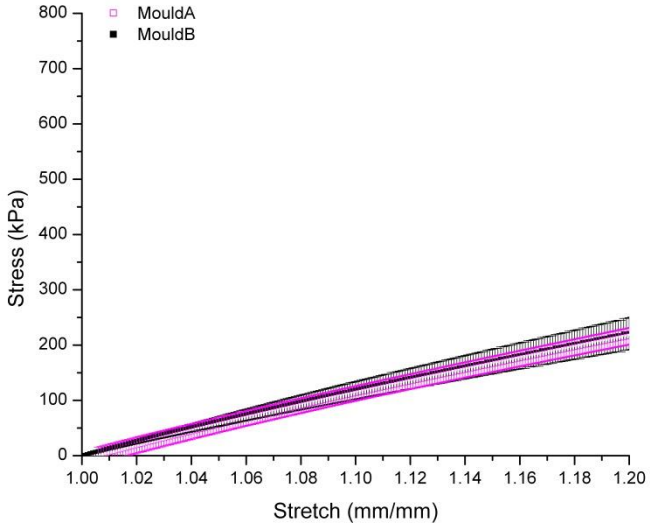

Figure 22. Stress-stretch dependence on mould size for Sylgard 170. Cast in the Type A moulds (n=4) as compared to Sylgard 170 cast in Type B moulds (n=10). The samples were pre-cycled five times to 8.5% strain (Type A) or to 7.5% strain (Type B) before being pulled to failure at 5.00 mm/min.

Quantitatively, as shown in Table 8, stress at the given strains for the two mould types were approximately equivalent for Sylgard 170. At 10% strain, Sylgard 170 cast in Type A moulds experienced 112 kPa and those cast in Type B moulds 118 kPa. At 20%, Type A-cast Sylgard 170 reached 216 kPa and Type B-cast 221 kPa. Comparison of the average instantaneous stress of Sylgard 170 cast in Type A moulds with Sylgard 170 cast in Type B moulds reported insignificant differences at ε=10%, 12.5%, 15%, 17.5%, and 20%. This is indicated in Fig. 23 by the bars over the groups (Student's *t*-test, $p < 0.05$). Differences were not statistically significant up through 20% strain, but appeared to grow larger at 50% strain. Figure 23 shows inconsistencies

at 20% strain. At 60% strain, samples from Type A moulds experienced higher stress on average than Type B samples.

Table 8. Instantaneous stress dependence on mould size for Sylgard 170 in both Type A and Type B moulds. The instantaneous stress is calculated for each sample, and the average is reported with one standard deviation. The two were statistically insignificant at all five strain points (Student's *t*-test, $p < 0.05$).

	Instantaneous Stress (kPa)				
Sylgard 170	**10%**	**12.50%**	**15%**	**17.50%**	**20%**
Mould A (4)	112.53 ± 15.10	139.37 ± 15.33	165.47 ± 15.71	191.03 ± 16.28	216.14 ± 16.93
Mould B (10)	118.22 ± 16.67	144.61 ± 19.99	170.39 ± 23.36	195.66 ± 26.74	220.66 ± 30.27

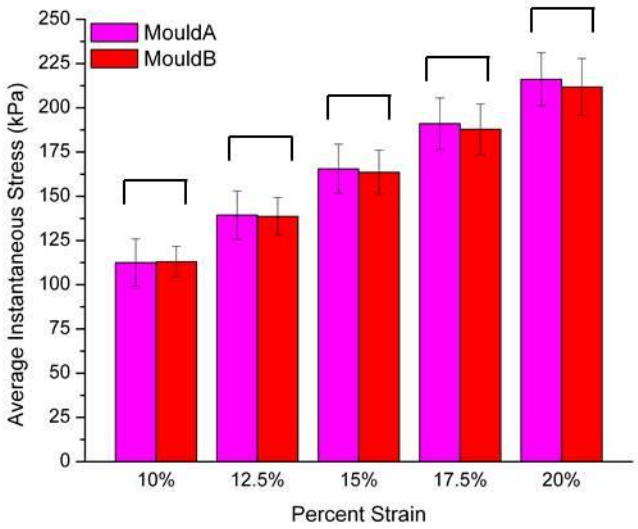

Figure 23. Instantaneous stress dependence on mould size. Samples from Type A moulds (n=4) and Type B moulds (n=10) were evaluated at 10%, 12.5%, 15%, 17.5% and 20% strain and compared to one another. Bars over a strain percent indicate no statistical significance between the sizes (Student's *t*-test, $p < 0.05$).

Furthermore, an analysis of the linear range of samples cast in Type A and Type B moulds for Sylgard 170 showed insignificant differences between the two groups. The tangential modulus, Table 9, decreased for both groups as strain increased. From 0-20% strain, samples cast in Type A moulds had tangential moduli that ranged from 1104-1015 kPa as stretch increased. For the same strain range, samples cast in Mould B had tangential moduli that ranged from 1008-1079 kPa.

Table 9. Tangential modulus dependence on mould size for Sylgard 170. The tangential modulus for each sample is calculated at the specified strain and averaged across the samples (sample size is indicated in parentheses). The two were statistically insignificant at all five strain points (Student's *t*-test, $p < 0.05$).

	Tangential Modulus (kPa)				
Sylgard 170	**10%**	**12.5%**	**15%**	**17.5%**	**20%**
Mould A (4)	1103.70 ± 56.18	1062.64 ± 56.11	1037.06 ± 49.88	1017.66 ± 52.00	1015.48 ± 51.23
Mould B (10)	1079.24 ± 137.08	1045.94 ± 131.34	1028.30 ± 139.59	1010.16 ± 140.21	1007.51 ± 139.36

Based on the tangential modulus analysis, the maximum segmented modulus should not be different for samples cast in different size moulds. The two test groups showed statistically insignificant differences in stress at 10%, 12.5%, 15%, 17.5%, and 20% strain and insignificant differences in the

tangential moduli at those strains. These two stress-strain responses should not show differences, and thus the maximum slope of the curves should show no difference. This modulus for Mould A samples was 1291.80 ± 71.17 kPa, and was found statistically insignificant from Mould B samples (1308.13 ± 211.01 kPa).

As previously noted, the difference in stress between the two moulds was noticeable at 60% strain. It was expected that by the ultimate stretch, a significant different in UTS would be present between Type A and Type B cast Sylgard 170. The ultimate tensile stress was different for those cast in Type A moulds and occurred at a lower strain (75% v. 105%). The UTS experienced by samples from Type A moulds, 631.1 ± 214.0 kPa, was reportedly less than the Type B samples (770.6 ± 139.5 kPa). The UTS occurred on average earlier for Type A samples, 62% strain v. 78% strain. The Type A cast samples produced samples ranging from 358 kPa to 827 kPa over stretches from 1.35 to 1.78 for ultimate values. Type B moulds produced samples ranging in UTS from 528 kPa to 1037 kPa over stretches from 1.44 to 2.09.

Table 10. Ultimate tensile stress and stretch dependence on mould size of Type A and Type B cast Sylgard 170. The average and standard deviation are reported, with the sample size indicated in parentheses.

Sylgard 170	Ultimate Tensile Stress (kPa)	Ultimate Tensile Stretch (mm/mm)
Mould A (4)	631.13 ± 214.03	1.62 ± 0.20
Mould B (10)	770.62 ± 139.45	1.78 ± 0.22

As a result of the protocols calling for different strain rates, the results from the Dragon Skin tests cannot directly be compared to the WWR tests. Changes in strain rate did not permit direct comparisons across tests but correlations can be made. At a strain rate of 1.5 mm/min, S160 was stiffer than S184, which was stiffer than S170. At a strain rate of 5 mm/min, S170 was stiffer than DS20, which was stiffer than DS10. These trends suggest that at a strain rate of 5 mm/min, S160 would remain the stiffest material, and that at a strain rate of 1.5 mm/min, DS10 would be the least stiff. Therefore if the analogue results show too low stress, a stiffer base should alter the response accordingly.

4.3 Dragon Skin Base Comparison

Base material testing of Dragon Skin 20 was conducted with Type B moulds (Table 3) and the Cyclic Preloaded Uniaxial Loading protocol (Section 3.8.2). Dragon Skin 10 and Dragon Skin 20 were chosen to provide softer bases for comparison with Sylgard 170.

Sylgard 170 was compared directly with the Dragon Skin materials as it was the lowest curve of the three Sylgard materials previously tested. From prior knowledge, Dragon Skin is extremely extensible and was thought to provide the lower bounds for the base material summary. Both Dragon Skin 10 and Dragon Skin 20 showed on average a lower stress than that of Sylgard 170 at all strains greater than 3% (Fig. 24A). This was due to the pre-cycling and extreme stretch capacity of the two Dragon Skins. The steepness of the curves indicated both Dragon Skin 10 and Dragon Skin 20 were softer materials than Sylgard 170. The overall lower values of stress for Dragon Skin samples are visually represented in Fig. 24B and quantified in Table 11. The stress of Dragon Skin 20 was greater than Dragon Skin 10 at 10%, 12.5%, 15%, 17.5%, and 20% strain (Fig. 24B). Stress associated with Sylgard 170 was at least twice as great as Dragon Skin 20 at these five strain points. More specifically, at 10% strain, Dragon Skin 10 was 31% of the Sylgard 170 stress (36.66 v. 118.22 kPa). Dragon Skin 20, 55.65 kPa stress at 10% strain, experienced half as much stress as Sylgard 170. By 20% strain, the differences were larger, with Dragon Skin 10 reporting 50.17 kPa and

Dragon Skin 20 recording 82.27 kPa. At this strain, Sylgard 170 reached a stress of 220.66 kPa. At 20% strain, neither Dragon Skin reached the stress of the 10% strained Sylgard 170. Both Dragon Skin materials are less stiff than Sylgard 170.

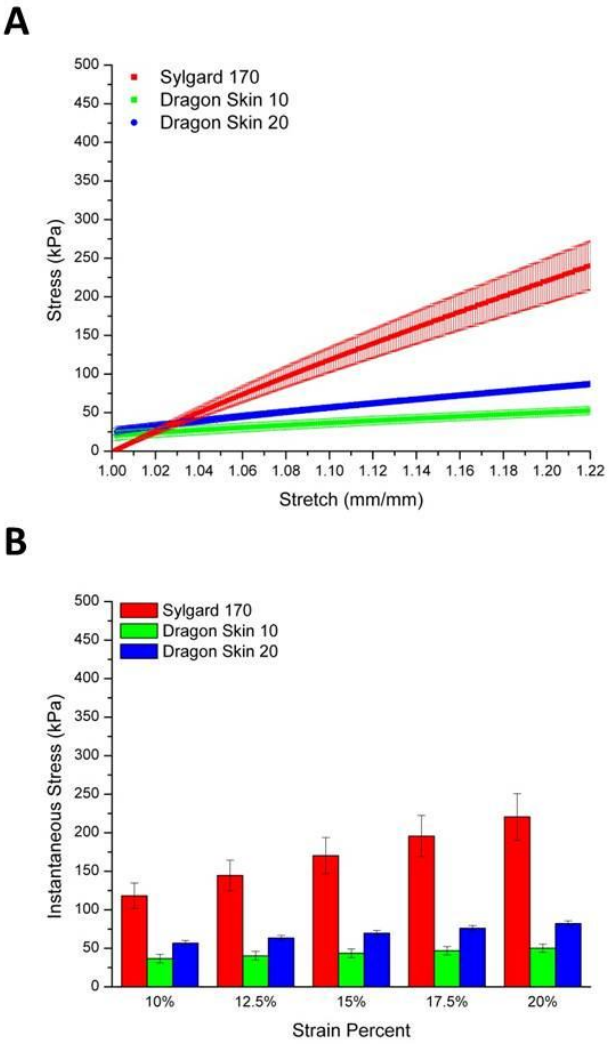

Figure 24. Comparison of Dragon Skins to Sylgard 170 of A) stress-stretch relationship and B) average instantaneous stress at the five strains. Sylgard 170 (n=10) is compared to Dragon Skin 10 (n=3) and Dragon Skin 20 (n=3) resulting in two additional bases that are less stiff than Sylgard 170.

Table 11. Instantaneous stress comparison of more base materials: Sylgard 170 with Dragon Skin 10 and Dragon Skin 20. Average and standard deviation are reported with sample size indicated in parentheses.

	Instantaneous Stress (kPa)				
Mould B Bases	**10%**	**12.50%**	**15%**	**17.50%**	**20%**
Sylgard 170 (10)	118.22 ± 16.67	144.61 ± 19.99	170.39 ± 23.36	195.66 ± 26.74	220.66 ± 30.27
Dragon Skin 10 (3)	36.66 ± 6.81	40.25 ± 6.70	43.65 ± 6.64	46.96 ± 6.54	50.17 ± 6.52
Dragon Skin 20 (3)	56.65 ± 4.10	63.33 ± 3.95	69.79 ± 3.96	76.10 ± 4.01	82.27 ± 4.07

The locations of the stress-strain curves of Dragon Skin 10 and Dragon Skin 20 in relation to Sylgard 170 were expected after analyzing the tangential and maximum segmented moduli (Tables 12 and 13). Dragon Skin 10 had the lowest stress of the three base materials at all five strain points. It was anticipated that its tangential modulus at each of the five points would be the lowest of the three base materials. Dragon Skin 10 was the most easily extensible, and thus would require less force to stretch the material, resulting in a lower tangential modulus. The linear stress-strain curve should be reflected in the tangential modulus comparison at 10%, 12.5%, 15%, 17.5%, and 20% strain and remain consistent at the lowest value for the five base materials. For Dragon Skin 10, the tangential modulus ranged from 131 to 147 kPa, the lowest of all the materials. Dragon Skin 20, which

also was more easily extensible than Sylgard 170, recorded a tangential modulus between Dragon Skin 10 and Sylgard 170 at each of the five strain points. Dragon Skin 10 ranged from 147 to 131 kPa as strain increased.

Table 12. Tangential modulus for Dragon Skin bases compared with Sylgard 170, at five strain points. The average and one standard deviation are reported, with sample size indicated in parentheses.

Tangential Modulus (kPa)					
Mould B Bases	**10%**	**12.5%**	**15%**	**17.5%**	**20%**
Sylgard 170 (10)	1079.24 ± 137.08	1045.94 ± 131.34	1028.30 ± 139.59	1010.16 ± 140.21	1007.51 ± 139.36
Dragon Skin 10 (3)	147.32 ± 13.42	142.88 ± 11.19	135.55 ± 8.61	131.80 ± 14.14	130.83 ± 11.26
Dragon Skin 20 (3)	275.75 ± 24.26	263.71 ± 21.66	256.24 ± 19.21	250.69 ± 17.61	250.93 ± 17.89

Based on the apparent linear nature of the Dragon Skin samples and the reported stress values, Dragon Skin 10 should experience the lowest maximum segmented modulus. Both Dragon Skin 10 and Dragon Skin 20 should also have maximum segmented moduli significantly lower than that of Sylgard 170. Dragon Skin 10 had a maximum segmented modulus equal to 186 kPa and Dragon Skin 20 modulus was higher at 329 kPa. Both were significantly lower than that of Sylgard 170 (1308 kPa). This result matches expectations in that the Dragon Skins were known to be more extensible

materials, and therefore less force per unit area would be necessary to stretch the material, agreeing with the data above.

Table 13. Maximum segmented modulus of Dragon Skin bases compared with Sylgard 170. Each sample is divided into segments, the elastic modulus calculated, and the maximum per sample averaged for a representative modulus. Average and standard deviation are reported with sample size indicated in parentheses.

	Maximum Segmented Modulus (kPa)
Sylgard 170 (10)	1308.13 ± 211.01
Dragon Skin 10 (3)	185.95 ± 20.96
Dragon Skin 20 (3)	328.13 ± 23.05

Ultimate values of stress and stretch were not calculated for Dragon Skin samples. One safety limit for the tensile testing protocol was set to stop testing after 200 mm extension. All Dragon Skin samples would have exceeded this limit if permitted. Since failure was not obtained for the Dragon Skin samples (both DS10 and DS20), no ultimate data is presented.

4.4 Base Material Selection Conclusions

Using the information shown above, Sylgard 170 was selected as the base material to embed fibers in for subsequent tests. Its average stress-stretch curve is located in the middle of the five base materials tested. This decision allowed for immediate shifting of the base materials if the composites proved to be too strong or too weak. If the composites did not reach a high enough stress at a given strain, a different base material was selected to increase the tensile strength of the composite. In regards to viscosity, Sylgard 170 should allow for the smoothest pour in the open-top moulds due to its low viscosity relative to the other base materials. Other than Sylgard 184, Sylgard 170 has the longest pot life of the five materials examined, allowing for a smoother cast and ease of use. Interpolated demould time was also a factor, as having the ability to remove the cast after one hour at 60 °C speeds up the casting process (Table 4). All five bases provided useful information for the development of a base material database but due to the overwhelming benefits of Sylgard 170, it was chosen for the next stage of testing until patient data was readily available. Dragon Skin 20 was also included as a base material for Type C moulds after it became apparent that that reinforced Sylgard 170 had average stresses from 10-20% strain too high for more than one patient.

Chapter 5 – Results and Discussion for Fiber Selection Tests

After the initial round of tests, both the protocol and the mould were updated. After showing successfully that reinforcement increased the tensile strength of the three Sylgards and identifying relationships between the five base materials, the effects of fiber reinforcements were to be tested. The addition of the wires anchored by washers provided a minimum of 5.54 fold increase in stress from the unreinforced samples (base Sylgard 160 at 10% strain), and upwards of tenfold increase by 20% strain (base Sylgard 170). A lesser increase was desired to replicate AAA patient properties. Therefore a new set of fibers were tested: silk sutures, gauze, cotton woven dressing, and 100% pure silk thread.

5.1 Reinforced Sylgard 170 Stress-Stretch Responses

The initial material embedded was silk sutures. It is known that sutures hold edges of wounds and incisions together and therefore should increase the stiffness of Sylgard 170. As shown in Fig. 25, on average, there was a significant increase in stiffness from 6% to 10% strain. The suture-reinforced Sylgard 170 curves show three regions, in each of which the response was essentially linear. At low strain, the initial region was similar to that of the base material. At mid strains, the response was affected by the addition of sutures, and stiffness increased markedly. After mechanical

failure of the sutures, the response did not correspond to that of the purse base material in the third section within the region of interest. The further the suture-reinforced samples were stretched, the more they resembled unreinforced base material. The curves generated by this reinforcement were non-linear as desired, but the middle region did not have the optimal *J*-shape.

After 60% strain, there was no sizeable difference in stress between the Sylgard 170 and suture-reinforced averages, though at that stretch the samples were pulled beyond the region of interest. The maximum difference in stress between Sylgard 170 and suture-reinforced samples occurred at 10.9% strain, 182 kPa. As strain increased, the difference between suture-reinforced and pure Sylgard 170 decreased. At 10% strain, there was a significant difference (178 kPa) in stress between the groups. By 20% strain, the difference decreased to 125 kPa though still significant. By 60% strain, the difference was within 50 kPa suggesting the reinforced samples behaved similarly to the unreinforced Sylgard 170 by this strain.

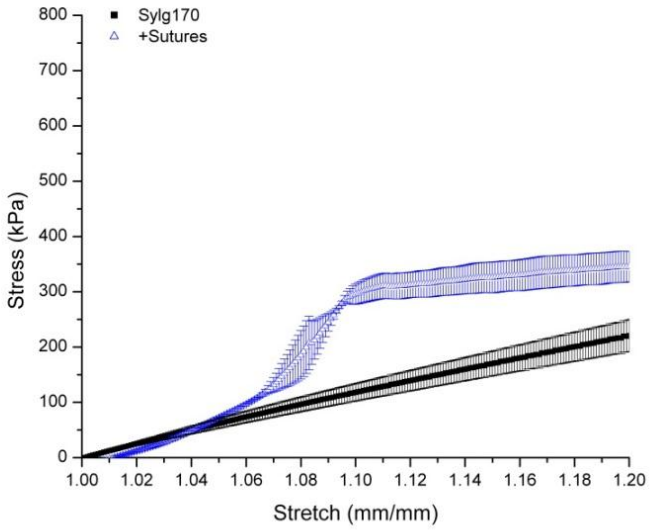

Figure 25. Effect of sutures on stress-stretch relationship of Sylgard 170 up to 1.2 mm/mm stretch. The linear nature of Sylgard 170 (n=10) is reinforced with the embedment of silk sutures (n=3).

To obtain variation to compare to the suture-reinforced Sylgard 170, two different types of gauze were embedded. Utilizing two methods of manipulating gauze prior to embedment with the first type of gauze created three separate test groups. Changes to the stress of unreinforced Sylgard 170 by embedding a single-layer of gauze throughout the sample can be seen in Fig. 26A. The gauze affected the properties even at low strain, unlike the sutures, which engaged at 6% strain.

The same gauze, but a different technique with a different number of layers (+GzGL), altered the base material properties differently (Fig. 26B). Again, the impact was seen almost immediately near zero strain, but the twelve-ply gauze reinforced samples' stress level did not appear to taper in the 20% strain range as the single-ply did. This can be attributed to the difference in layers in gauze and perhaps the change in shape and location of the reinforcement. At 20% strain, the stress experienced by the multiply embedded gauze, 673.40 kPa, was significantly different from the unreinforced Sylgard 170, 220.66 kPa, and the single ply gauze, 515.57 kPa. At 10% strain, the single ply gauze was already three times the unreinforced value. The differences between the unreinforced and single ply mould-shaped gauze decreased as the samples were stretched. The difference due to the embedment of multi-layered gauze when compared to the unreinforced Sylgard 170 remained roughly constant.

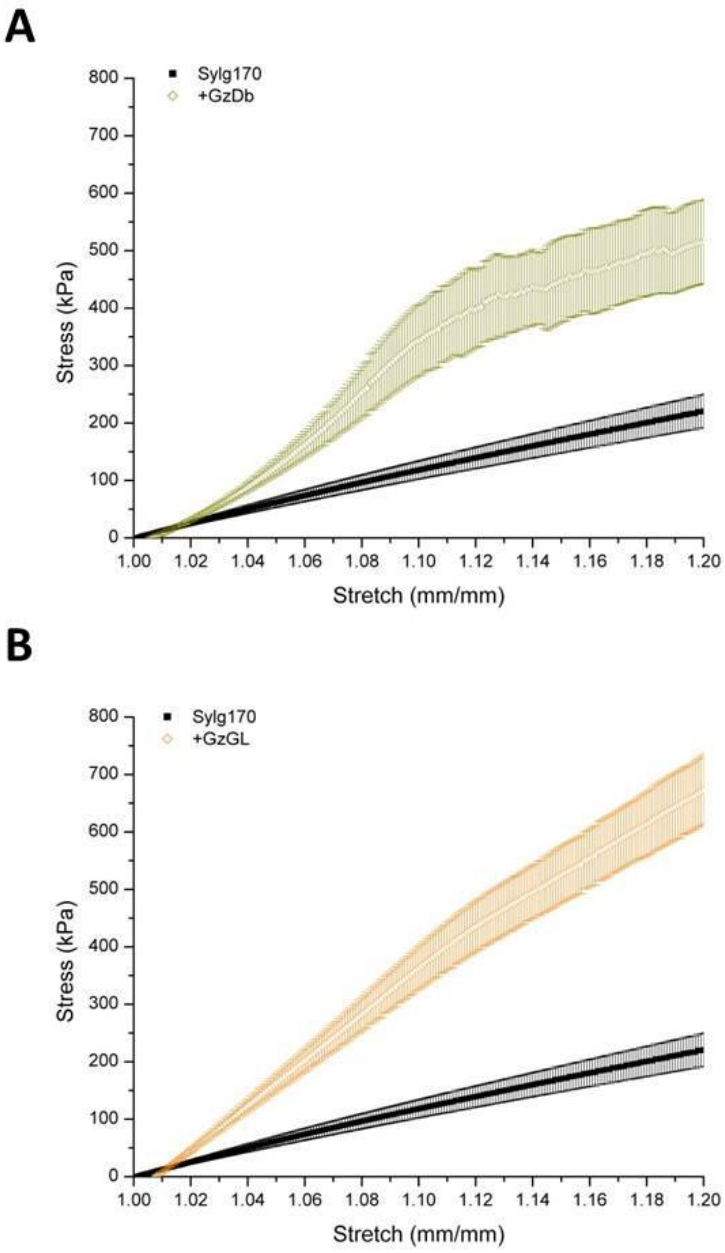

Figure 26. Effect of gauze on average stress-stretch curves of Sylgard 170. Different methods were implemented to achieve different stiffening profiles A) Single layer of gauze cut to Mould B dimensions (n=4) and B) multi-layered gauze cut to replicate the rectangular gauge region of the Type B mould (n=5) both compared to Sylgard 170 (n=10).

Using the same technique as the single layer of gauze cut to match Type B mould dimensions but applying it to woven cotton significantly increased the stress of Sylgard 170. The shape of the stress-stretch curve, Fig. 27, was not markedly altered by the addition of the woven cotton dressing. After 5% strain, both curves appeared linear. The other three fibers drastically altered the curvature of the response. However, the difference between Sylgard 170 and the woven dressing reinforcement increased as strain increased. This suggested a change in the steepness of the curve and larger differences would be present at greater strains.

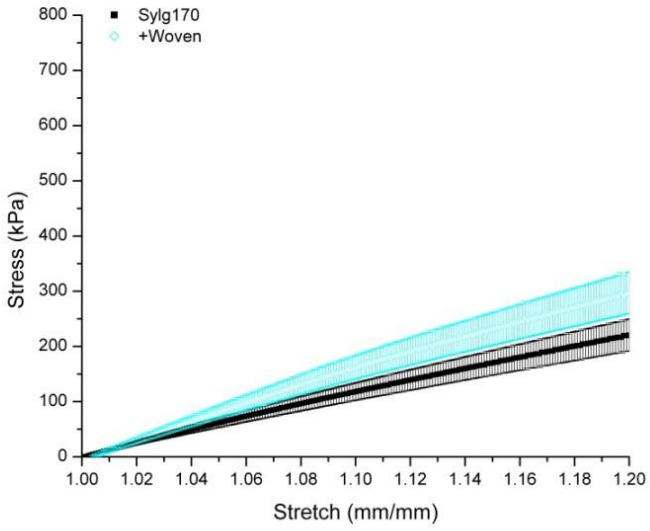

Figure 27. Effect of woven gauze on stress-stretch relationship of Sylgard 170. The average reinforcement of the stress-stretch relationship of Sylgard 170 (n=10) due to the inclusion of cotton woven gauze dressing (n=7).

The inclusion of silk thread was anticipated to solve many of the issues highlighted by failure to embed the vinyl mesh or the inability to predict gauze reinforcement behavior. It was thought that by controllably introducing slacked thread, the stress-stretch curve of embedded thread would shift in a predictable manner. However, this proved not to be true. The slacked thread did not engage as designed, but rather the thread slipped through the base material. However, the taut embedded silk thread, as seen in Fig. 28, produced a non-linear stress-stretch curve. The non-linear results curve was the closest match to desired *J*-shape. The thread broke at repeatedly at approximately 17% strain with an audible snap, drastically changing the stress-stretch response. Through 4% strain, the thread-reinforced samples strongly resembled the unreinforced samples. Beyond 4% strain, there was a sharp increase in stress per increase in strain. At 10% strain, the curve changed steepness yet again implying thread degradation of the thread and ultimately thread failure.

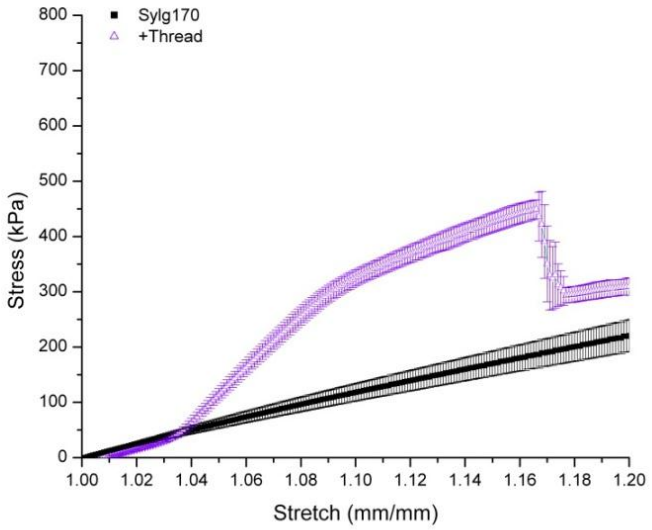

Figure 28. Effect of 100% silk thread on the stress-stretch relationship of Sylgard 170 with embedded silk thread pulled taut throughout (n=6). Unreinforced Sylgard 170 average is based on n=10.

5.2 More Material Properties of Reinforced Sylgard 170

As previously mentioned, comparison of the instantaneous stress at five strains was one way to analyze the effect of the embedded fibers. The five strains analyzed were 10%, 12.5%, 15%, 17.5%, and 20%. At each of these strains, the tangential modulus was calculated to further compare the reinforcement techniques. The tangential modulus does not alone give enough information, so an additional modulus, maximum segmented modulus, was calculated. All reinforcements discussed above were compared to their base, Sylgard 170, using the stress-stretch curves in

Section 5.1. All samples were cast in Type B moulds and subjected to the same protocol.

The overall averages of instantaneous stress, quantified in Table 14, provided a measure of direct comparison among the six sample groups. At none of the five specific strains measured (10%, 12.5%, 15%, 17.5%, and 20% strain) did any reinforcement equal that of the unreinforced Sylgard 170; all fiber-reinforcement significantly altered the stress, as shown in Fig. 29. This figure uses letters to describe reinforcements that are statistically insignificant from one another. Any two reinforcement techniques with identical letters are statistically indeterminable at that particular strain.

Table 14. Instantaneous stress for Type B-cast reinforced Sylgard 170. Sample size is indicated in parentheses for the average stress reported.

	Instantaneous Stress (kPa)				
Type	**10%**	**12.50%**	**15%**	**17.50%**	**20%**
Sylgard 170 (10)	118.22 ± 16.67	144.61 ± 19.99	170.39 ± 23.36	195.66 ± 26.74	220.66 ± 30.27
Sylgard 170 & Silk Sutures (3)	295.85 ± 21.73	314.50 ± 28.97	326.06 ± 33.54	337.66 ± 34.21	345.50 ± 32.95
Sylgard 170 & Cut Gauze Dogbone (4)	343.85 ± 70.93	415.93 ± 80.73	448.43 ± 83.53	485.39 ± 81.02	515.57 ± 82.68
Sylgard 170 & Gauge Length Gauze (5)	363.11 ± 41.84	451.27 ± 50.16	525.66 ± 54.98	599.99 ± 58.75	673.40 ± 66.89
Sylgard 170 & Woven Dressing (7)	162.49 ± 22.89	198.17 ± 27.42	231.66 ± 31.77	264.79 ± 35.99	297.02 ± 40.18
Sylgard 170 & Taut Silk Thread (6)	325.07 ± 15.94	378.31 ± 17.23	425.07 ± 19.19	307.45 ± 33.60	309.50 ± 17.27

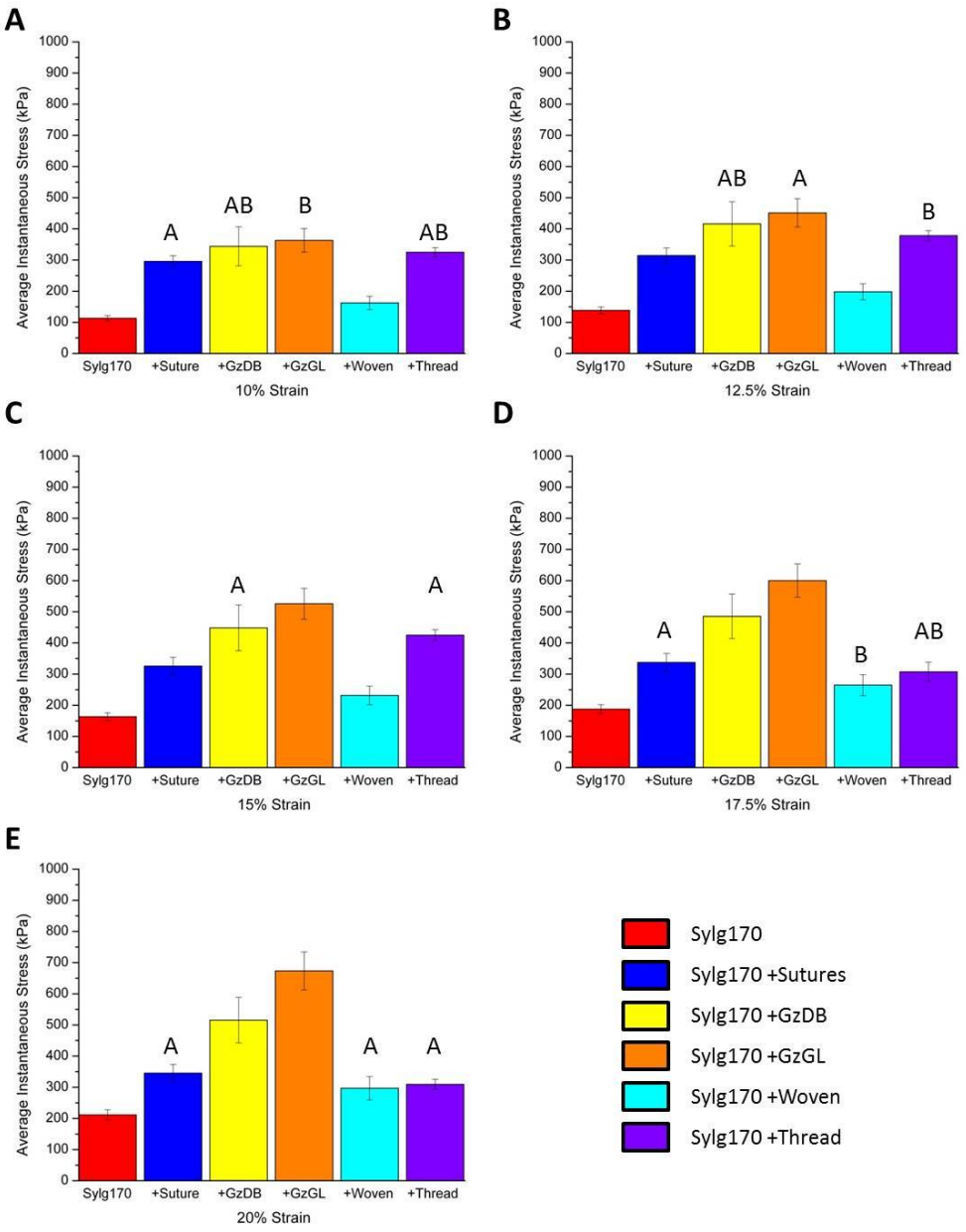

Figure 29. The effects on stress of various reinforcement techniques to Sylgard 170. The average instantaneous stress (kPa) of Sylgard 170 at A) 10% strain, B) 12.5% strain, C) 15% strain, D) 17.5% strain, and E) 20% strain. All samples have cross-sectional area 52.19 ± 5.61 mm^2 and gauge length 60 mm, except Type A Sylgard 170 with cross-sectional area 42 mm^2 and gauge length 45 mm. Means labeled with same letters are not statistically significantly different (ANOVA, Fisher's PLSD, $p < 0.05$).

Reinforcing Sylgard 170 showed increases in stress at 10% strain ranging from 44.27 kPa with the addition of woven cotton dressing to 244.89 kPa with the addition of twelve-ply gauze in the gauge region of the samples. As strain increased, reinforcements developed distinguishable effects on the intrinsic properties of Sylgard 170. By 12.5% strain, the embedded silk sutures developed a response unlike others (Fig. 29B), and at 15% strain, the difference in stress for the gauze techniques was evident (Fig. 29C). At 20% strain, reinforcement by silk sutures, woven cotton dressing, and silk thread were not statistically distinguishable from one another. They were however, as shown in Fig. 29E, still significantly different from unreinforced Sylgard 170 (ANOVA, Fisher's PLSD, $p < 0.05$).

At most, these reinforcements increased the stress level of Sylgard 170 3.12 times (+GzGL at 12.5% strain). At 20% strain, the impact on Sylgard 170 was less strong for both sutures and threads than it was at earlier strains. At low strains, both more than doubled the stress of unreinforced Sylgard 170, but after physical failure of the reinforcement, the increase in stress was approximately 50%.

A second material property analyzed was the tangential modulus at each point the stress was analyzed. Changes in tangential modulus as strain increased indicated the consistency of the stress-stretch curves. For example, at 10% strain, Sylgard 170 had a tangential modulus of 1079 kPa, and by 20% strain, it was 1008 kPa (Table 15). Comparatively, Sylgard 170

remained constant as strain increased, suggesting a linear response. In contrast, silk suture-reinforced Sylgard 170 had a tangential modulus of 6000 kPa at 10% strain. The increase in tangential modulus was expected as the suture was mechanically intact and absorbing stress. The tangential modulus of silk-suture reinforced Sylgard 170 at 12.5% strain, however, was significantly lower at 444 kPa. Between 10% and 12.5% strain, the sutures mechanically failed. As strain increased, the sutures failed, and the steepness of the response curve changed drastically.

Table 15. Tangential modulus results for reinforced Sylgard 170 cast in Type B moulds as calculated for each of the five particular strains. Sample size is indicated in parentheses, and stress (kPa) is reported as the average with one standard deviation.

Tangential Modulus (kPa)					
Type	**10%**	**12.5%**	**15%**	**17.5%**	**20%**
Sylgard 170 (10)	1079.24 ± 137.08	1045.94 ± 131.34	1028.30 ± 139.59	1010.16 ± 140.21	1007.51 ± 139.36
Sylgard 170 & Silk Sutures (3)	5988.02 ± 4392.14	443.74 ± 218.42	408.71 ± 244.20	478.76 ± 225.80	339.77 ± 399.70
Sylgard 170 & Cut Gauze Dogbone (4)	4350.88 ± 882.89	1266.99 ± 1370.02	2657.51 ± 699.35	1266.99 ± 1370.02	1777.04 ± 562.00
Sylgard 170 & Gauge Length Gauze (5)	3989.34 ± 495.10	3287.49 ± 312.69	2984.81 ± 490.06	2989.51 ± 359.85	2908.16 ± 331.45
Sygard 170 & Woven Dressing (7)	1519.44 ± 191.66	1401.25 ± 176.74	1331.86 ± 174.93	1320.47 ± 174.61	1297.67 ± 173.68
Sylgard 170 & Taut Silk Thread (6)	3061.28 ± 314.30	2023.99 ± 91.94	1828.90 ± 116.22	-14933.97 ± 8423.08	-10067.85 ± 6306.86

For most of the reinforced samples, the tangential modulus at 10% strain was significantly different from Sylgard 170. This 10% strain tangential modulus was increased to 3061 kPa by silk thread, 4350 kPa by gauze, and 6000 kPa by sutures. Negative values were found for this modulus from the addition of silk thread because the threads mechanically failed between 17.5% and 20% strain, with one sample failing earlier. The amount of stress to deform was drastically different once the reinforcements failed.

Based on visual analysis of the stress-strain responses, the maximum segmented modulus for all reinforcement types besides the addition of woven dressing should be significantly different from unreinforced Sylgard 170. All other reinforcement types displayed a non-linear response curve, suggesting the slope for at least one segment will be much higher than unreinforced Sylgard 170. Data given in Table 16 shows maximum segmented moduli varied from 1308 kPa for unreinforced Sylgard 170 up to 8188 kPa for the addition of silk sutures. The maximum tangential modulus for reinforcement by woven cotton dressing was 1826 kPa, a 518 kPa significant increase to the unreinforced sample. Statistical analysis revealed that all reinforcement methods increased the maximum segmented modulus of unreinforced Sylgard 170, suggesting that no two curves were the same. The two gauze reinforcement types did not have statistically significant moduli but had visually different curves. Similarly, the maximum segmented

modulus of the single ply gauze was not statistically significant from the silk thread-reinforced samples, but the response curves were not the same.

Table 16. Maximum segmented modulus for reinforced Sylgard 170 cast in Type B moulds. Each individual sample was divided into three segments for the strain ranges listed, and the maximum of the three moduli were then averaged across the samples (kPa).

	Maximum Segmented Modulus (kPa)
Sylgard 170 (10)	1308.13 ± 211.01
Sylgard 170 & Silk Sutures (3)	8187.64 ± 405.05
Sylgard 170 & Cut Gauze Dogbone (4)	4693.97 ± 1170.97
Sylgard 170 & Gauge Length Gauze (5)	4059.10 ± 504.35
Sygard 170 & Woven Dressing (7)	1825.75 ± 266.65
Sylgard 170 & Taut Silk Thread (6)	5038.07 ± 383.08

To compare changes to the base material as a result of fiber reinforcement, the ultimate tensile strength was also recorded. The pre-cycled uniaxial loading samples were tested to failure. For unreinforced Sylgard 170, the

maximum stress before failure, 770.62 kPa was only statistically significant from the inclusion of woven cotton dressing (1083.18 kPa). The additional of twelve-ply gauze reported an UTS of 936.05 kPa, the second highest as shown in Fig. 30A. The inclusion of taut silk thread had UTS 855.40 kPa with the single ply gauze reaching a maximum of 657.49 kPa. The samples with silk sutures failed after a maximum a stress of 682.14 kPa. Sample to sample variation of UTS was large within test groups. The differences in UTS, Fig. 30A, show less of an effect at higher strain than previously noted at lower strains. For example, the addition of twelve-ply gauze increased stress by 450 kPa at 20% strain. But at failure, the difference from unreinforced Sylgard 170 was less than 200 kPa. For the woven dressing, the opposite occurred. The difference in stress for this technique from unreinforced Sylgard 170 at 20% was 100 kPa. This difference increased to 300 kPa by failure at 80% strain.

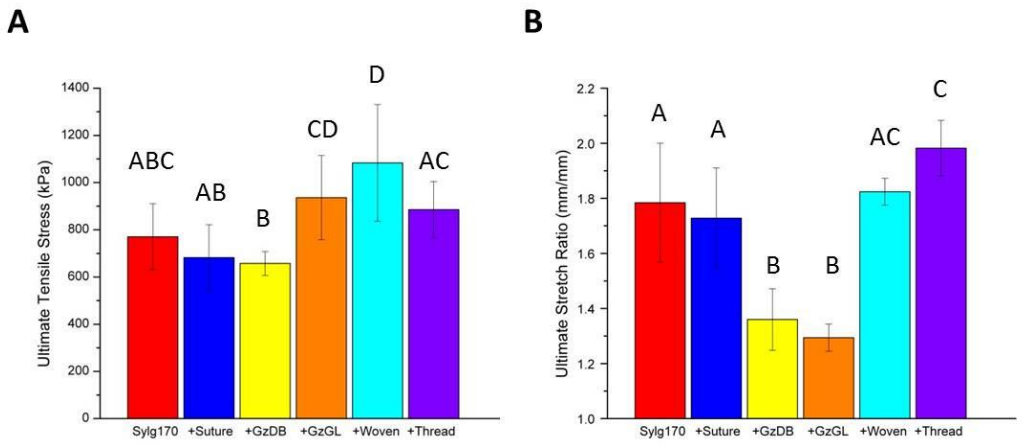

Figure 30. Ultimate tensile stress and stretch for Type B samples pre-cycled uniaxial tested samples. A) The UTS (kPa) is plotted for the average of each group and B) the stretch ratio (mm/mm) at this stress is reported. Averages with similar letters represent statistically indeterminable averages.

Although only the woven cotton dressing reinforcement significantly altered the ultimate tensile stress of unreinforced Sylgard 170, all but the sutures and woven cotton dressing increased the ultimate stretch. Figure 30B highlights the changes in extensibility before failure. As with the UTS comparison, common letters designate statistically insignificant differences in the ultimate stretch ratio. Silk sutures did not increase the UTS or the λ_{ULT}. This behavior was anticipated based on the stress-stretch response at low strains. The sutures mechanically failed early and as strain increased the stress level of the suture-reinforced Sylgard 170 matched that of unreinforced Sylgard 170. The rate at which stress increased as strain increased for suture-reinforced Sylgard 170 slowed to 8 kPa per 2.5% strain at 20% strain. Unreinforced Sylgard 170, on the other hand, increased

steadily at 25 kPa/2.5% strain. At higher strains, it can be hypothesized that the suture-reinforced Sylgard 170 would show similar responses to unreinforced Sylgard 170 as the difference in stress between the two decreased rapidly. The absence of an effect of this reinforcement on the ultimate values is therefore expected.

For example, the inclusion of single ply gauze in the Type B shape did not affect the UTS of unreinforced Sylgard 170. It did, however, significantly alter the ultimate stretch. The ultimate tensile stress for single ply gauze occurred at λ_{ULT} =1.36, or 36% strain, whereas unreinforced Sylgard 170 did not reach its λ_{ULT} until 1.78, or 78% strain. The twelve ply gauze (+GzGL) significantly increased the UTS of unreinforced Sylgard 170 while simultaneously significantly decreasing the ultimate stretch (Fig. 30). The addition of silk thread, though not affecting the UTS, significantly increased the ultimate stretch to nearly 100% elongation (λ_{ULT}=1.98). The embedment of woven cotton dressing significantly altered the UTS without making substantial changes to λ_{ULT}.

5.3 Reinforced Sylgard 170 Conclusions

Different stress-stretch curve shapes were obtained by embedding various materials. Additionally, several levels of stress were achieved as a result of the material properties of the reinforcements. Though significantly altering the stress, the addition of woven dressing did not alter the shape of the

stress-stretch response of Sylgard 170. Before using woven dressing with a softer base, further testing would be necessary. The strength difference between fibers and base would increase, and thereby load could be engaged by the reinforced fibers differently. The inclusion of silk thread did not alter the UTS, but did increase the $\lambda_{ULT.}$ By not losing any strength of extensibility, thread was a suitable reinforcement to progress with. The significant increase in stress at low strains within the region of interest would not affect the overall integrity of the sample.

Chapter 6 – Results and Discussion for Synthetic Analogues

Results reported in this chapter focus on samples cast with Type C moulds. Although successful, mould-cast were too thick for comparison to patient tissue. The average thickness of six patient samples was 2.09 ± 0.8 mm, with the thinnest 1.35 mm. Synthetic test samples of 6 mm were therefore too thick. New moulds were therefore prepared to offer better comparisons to patient data. Additionally, a new protocol was adopted: the Cyclic Uniaxial Loading protocol. Samples were uniaxially stretched five times each to five target stretches. The first target (equivalent to 10% strain) was λ=1.1, followed by λ=1.125, 1.15, 1.175 and finally λ=1.2. However, use of a cyclic protocol led to material softening, with repeat strain cycles differing in their stress-stretch paths. Nevertheless, this protocol was better matched to the protocol by which patient tissue samples were tested, and as such, these results were used to compare directly to patients in Chapter 7.

6.1 Repeatability of Mould C-Cast samples

With this casting technique and test protocol, it was desired to test the repeatability of Mould C-cast unreinforced samples. To ensure the samples were made consistently regardless of the time between casts (up to one month), two sets of Sylgard 170 were cast using one Type C mould per set. The average stress-stretch for each set is plotted in Fig. 31 with nineteen

total useable samples fabricated. There was a high sample usability rate because the nineteen samples did not show severe edge effects from open-air casting. Minimal differences in the average response per sample were found, with the maximum variation of stress, 17.71 kPa. This variation occurred during the first cycle to 20% strain. Ignoring which set they belonged to, the largest sample-to-sample variation in stress was 33.67 kPa. This difference occurred during the initial cycle of testing (first cycle to 10% strain). As the protocol continued to higher strains, the sample-to-sample variation remained constant. By the fifth cycle to 20% strain, the maximum sample-to-sample was 32 kPa. This data confirmed the repeatability of Mould C-cast samples from set to set sans reinforcement. Samples should also be repeatable when reinforcements were introduced.

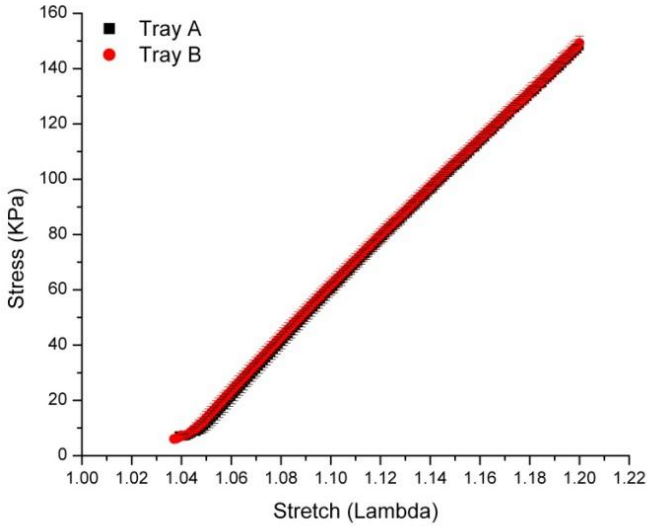

Figure 31. Stretch-stress variability across Mould C-cast Sylgard 170. The average stress-stretch relationship for two unreinforced Sylgard 170 sets from the fifth cycle to 20% strain. Tray A (n=10) and Tray B (n=9) showed little variability from one another.

6.2 Reinforcement Effects on Mould C-Cast Sylgard 170

6.2.1 Damage Assessment

It was well known that during testing, soft materials accumulate some damage at each incremental stretch level[59–61]. Therefore, it was important to examine the path of the fifth and final cycle to one stretch λ, and the initial curve to the subsequent stretch ($\lambda + 0.025$). This suggested there would have been no difference between the fifth cycle and a subsequent sixth cycle to that same stretch. Figure 32 compares five cycles to one strain for unreinforced Sylgard 170 (Figs. 32A, 32C, 32E) and internally reinforced Sylgard 170 (Figs. 32B, 32D, 32F) at three stretches (complete data is given

in Appendix A). As would be expected for unreinforced Sylg170, the change in stress was linearly correlated to the change in strain at low strains. As shown by the lack of variation from the five loading cycles to each λ=1.1, 1.15, and 1.2, no damage was accumulated by repeating cycles to the same stretch for unreinforced samples. In contrast, the introduction of fibers internally (Figs. 32B, 32D, 32F), showed damage accumulating as new strains were reached. The initial loading cycle to 10% strain experienced higher stresses than subsequent cycles to the same strain. As strain increased, the difference in stress between initial and final load to the same stretch decreased but was still apparent by the gaps shown in Fig. 32.

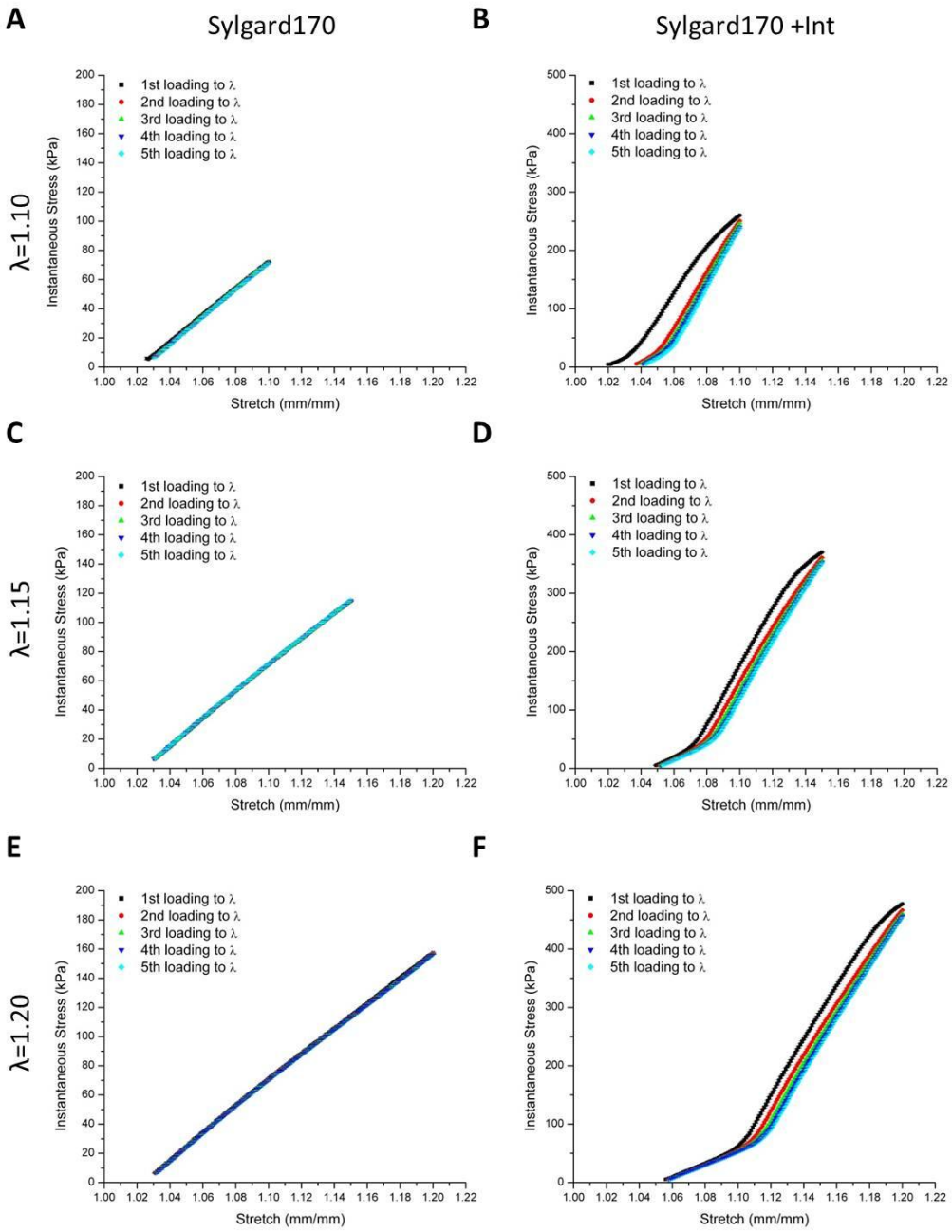

Figure 32. Comparison of stress during the five loading cycles for unreinforced Sylgard 170 (the left column) and internally reinforced Sylgard 170 (the right column) with one fiber parallel to the direction of test. The individual loading cycles are shown to λ=1.1, 1.15, and 1.2. Additional stretches and test groups are shown in Appendix A.

6.2.2 Longevity Testing

The human aorta is unique in its ability to withstand continuous loading and unloading as blood flow changes for many years, even decades. This is attributed to its content of both collagen and elastin, which withstand the pressure changes associated with the cardiac cycle. To test both the longevity of the composites and the best representative cycle of the data, one sample each of unreinforced Sylgard 170, Sylgard 170 with internal reinforcement (+Int), and Sylgard 170 with external reinforcement (+Ext) were used. To analyze the degradation of the reinforcement and to determine whether the location of the fiber altered properties, 500 loading-unloading cycles were compared.

By comparing the final load to a target stretch and the initial load to the successive target stretch, the responses of unreinforced Sylgard 170 correlate well with one another (Fig. 33A). This linear relationship for the die-cut samples shown in Fig. 33A was also observed for the single-cast specimens (cast in Types A and B moulds). The integrity of the sample remained intact throughout testing, with no sign of softening or weakening from testing. This was further exemplified by the samples with reinforcements in the perpendicular direction for both internally reinforced Sylgard 170 (+Int $\perp$) and externally reinforced Sylgard 170 (+Ext $\perp$), Figs. 33C and 33E, respectively. Although the samples were reinforced, they were cut such that the fibers were perpendicular to the axis of testing. Since the

samples were not being tested to engage the fibers, it was not expected to observe damage in these samples.

In contrast, the nature of this relationship deviated from its linearity with the addition of fibers orientated parallel to the test direction, and two distinct cycles are shown for each target strain, suggesting damage accumulation at new strains. The internally reinforced Sylgard 170 samples (Fig. 33B) reached 477.36 ± 0.15 kPa at the first cycle to 20% strain. By the fifth cycle to 20%, the stress of internally reinforced Sylgard 170 decreased to 455 kPa, a difference of 22 kPa. The internal, external, and double-stranded reinforced samples, Figs. 33B, 33D, 33F, followed the loading path of the fifth cycle to 10% strain as the initial cycle to 12.5% strain begins. This pattern was observed for all three reinforced groups, and as such, the fifth cycle was further seen as a representative of the material. Additionally, five cycles matched the testing protocol for patient AAA tissue.

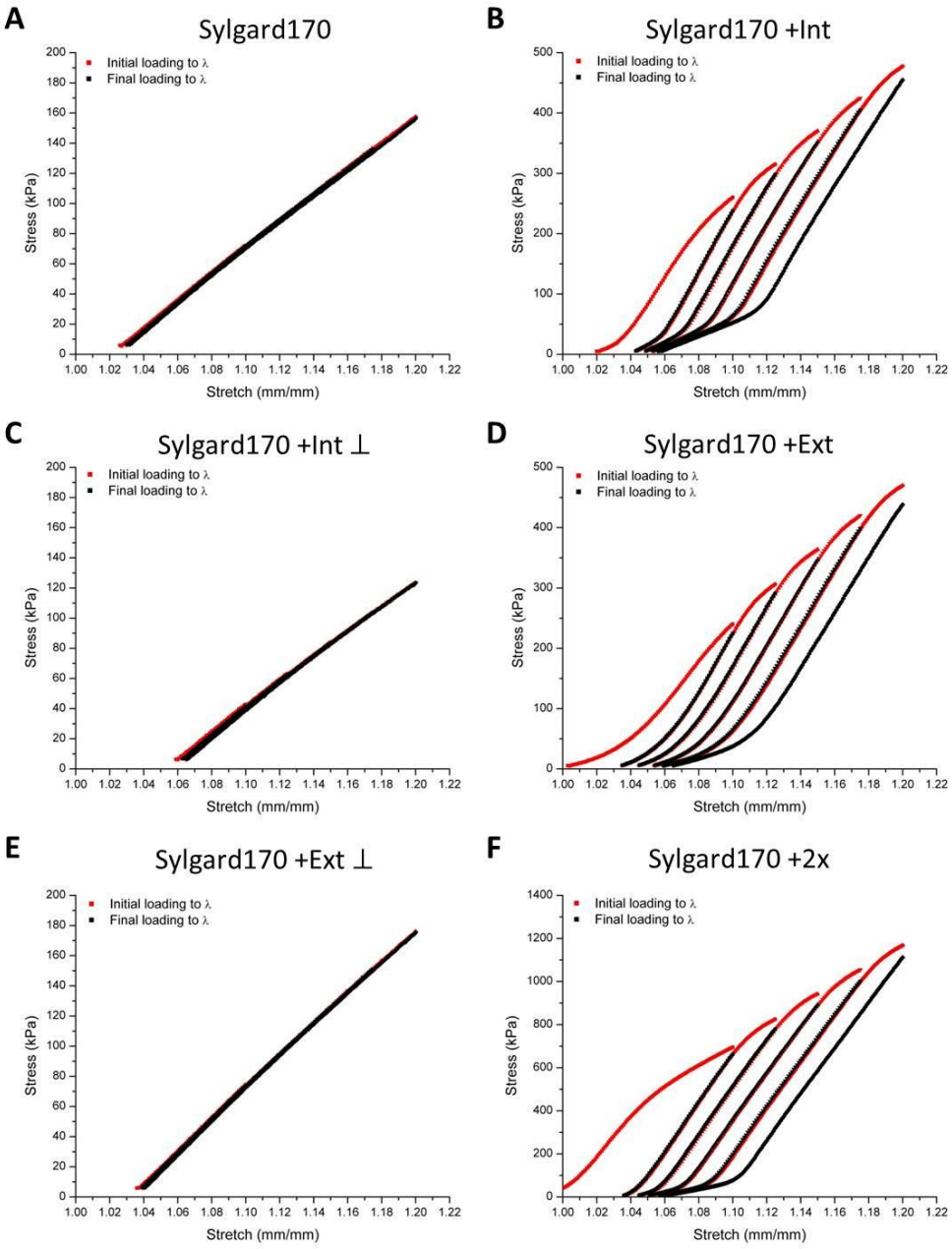

Figure 33. Initial and final loading cycle comparison of single Mould C-cast samples. One sample each for (A) unreinforced Sylgard 170, (B) internally reinforced Sylgard 170, (C) the perpendicular-cut internally-reinforced Sylgard 170, (D) externally reinforced Sylgard 170, (E) the perpendicular-cut externally-reinforced Sylgard 170, and (F) double-stranded externally-reinforced Sylgard 170 displaying the initial and final loading cycles to λ=1.1, 1.125, 1.15, 1.175, and 1.2.

Figure 34 shows a representative set of data for 500 loading cycles from 10-15% strain for the Type C-cast samples. Data points were pulled from the stress-stretch curves at 0.5% strain intervals. As cycle number increased, the maximum cycle to subsequent cycle difference was 1.6 kPa for unreinforced Sylgard 170. The maximum difference in instantaneous stress of 500 cycles occurred between the initial and final cycle at 10.5% strain. This maximum difference was 10.3 kPa. Over the course of 500 testing cycles, the unreinforced Sylgard 170 experienced a lower stress of no more than 10.3 kPa. However, it was not anticipated that this behavior would hold for reinforced samples, as due to expected fiber degradation.

With the external fiber-reinforced sample, the maximum cycle to subsequent cycle variation occurred between the initial and second cycle at 10% strain, which differed by 100 kPa. This difference was also seen for the internally-reinforced sample between the first and second cycle, at 10% strain. Both reinforced types and the unreinforced Sylgard 170 showed the most change in stress from the initial cycle to the second cycle. For reinforced samples, this was expected due to the strain softening shown in stress-strain analysis.

As cycle number increased towards 500, the differences in stress decreased. This was seen for all points as strain increased. Between the first and five hundredth cycle, there was a difference of 100 kPa at for the externally reinforced sample (occurred at 10% strain). By the penultimate and final cycles, the largest difference in stress between the two cycles 10.9 kPa. This

occurred at 15% strain. For the internally reinforced sample, the difference between initial and final cycles at 10% strain was 102.4 kPa. Similarly, by the 499th and 500th cycles, the largest difference in stress was 10.2 kPa, occurring at 15% strain. By the fifth cycle for both the reinforced samples, the change cycle to cycle in stress had substantially minimized. Differentials as large as 100 kPa were down to 3 kPa and continued to decrease thereafter. The data reported in this chapter refers to the fifth cycle to each strain level.

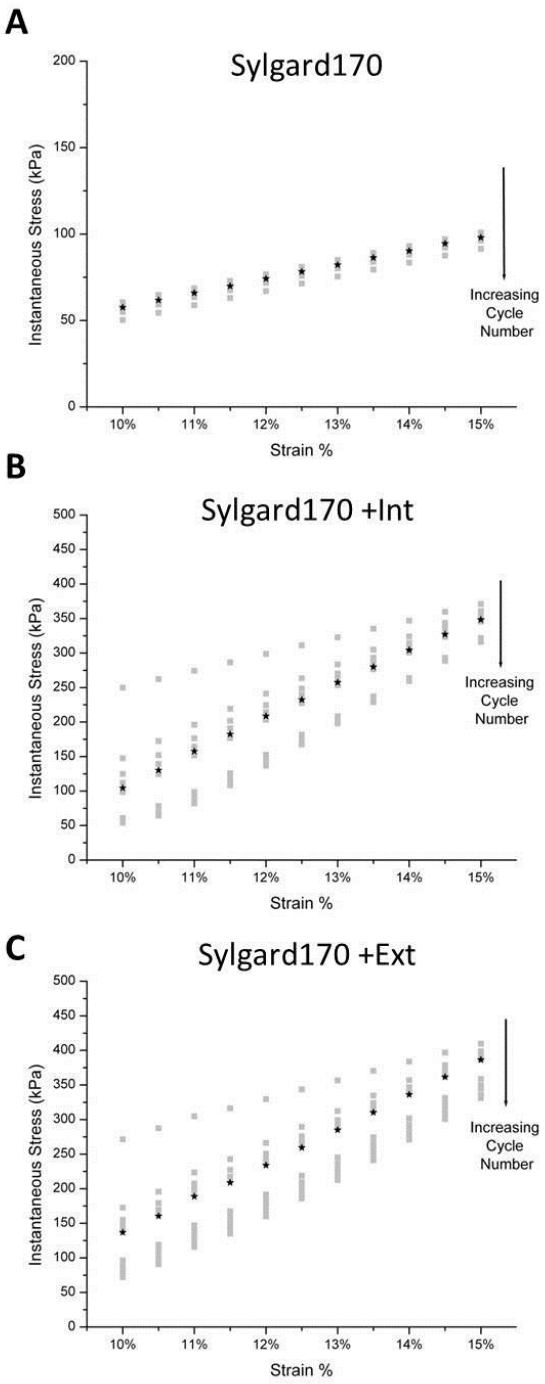

Figure 34. Longevity tests for Type C-cast Sylgard 170: for (A) Sylgard 170, (B) Internally Reinforced Sylgard 170 (+Int) and (C) Externally Reinforced Sylgard 170 (+Ext). 500 cycles from 10-15% strain were tested, and a select number of cycles plotted. The representative data set for all tests is depicted with (*) marking the fifth and final cycle in typical testing.

6.2.3 Stress-Stretch Responses

Using Sylgard 170 as a base, fibers either were embedded in the material (Sylgard 170 & Internal Thread Reinforcement) or were attached to the outer face of the pure cast (Sylgard 170 & External Thread Reinforcement and Sylgard 170 & Double-stranded External Thread Reinforcement). Unreinforced Sylgard 170 cast in Type C moulds produced linear stress-stretch curves on average across cycles to the five target stretches, shown in Fig. 35A. These samples were undamaged even after pulling to larger strains. As strain increased, softening was apparent in the three reinforced groups with the fibers aligned parallel to the test direction (Figs. 35B, 35D, 35F). These figures illustrate the importance of comparing specific strain cycles and not an overall average combining the final cycles to each strain.

One sample each for internally and externally reinforced Sylgard 170 was cut with fibers perpendicular to the axis of testing to illustrate the impact, or lack thereof, of the fibers when oriented in the non-axial direction. The stress-stretch relationships for these two samples were also plotted for visual comparison in Figs. 35C and 35E, respectively. Both the internally reinforced perpendicular sample (+Int $\perp$) and the externally reinforced perpendicular sample (+Ext $\perp$) displayed the same linear, non-softened nature shown by the unreinforced Sylgard 170 samples.

Internally reinforced Sylgard 170 (Fig. 35B) showed data affected by strain softening. The final cycles to each 10%, 12.5%, 15%, 17.5%, and 20% strain have their own stress-stretch paths.

Large variability was seen in the external reinforced samples (Fig. 35D) because some threads did not complete all twenty-five test cycles (five to each target strain) with mechanical integrity. Even greater variability was seen with the double-stranded reinforced samples (Fig. 35F), because one of the two attached threads broke during the first four cycles to 20% strain. The breaking of the threads did not occur during the same strain cycle. This data was kept to show the variability because the sample showed a relationship closer to a single external fiber sample after breakage.

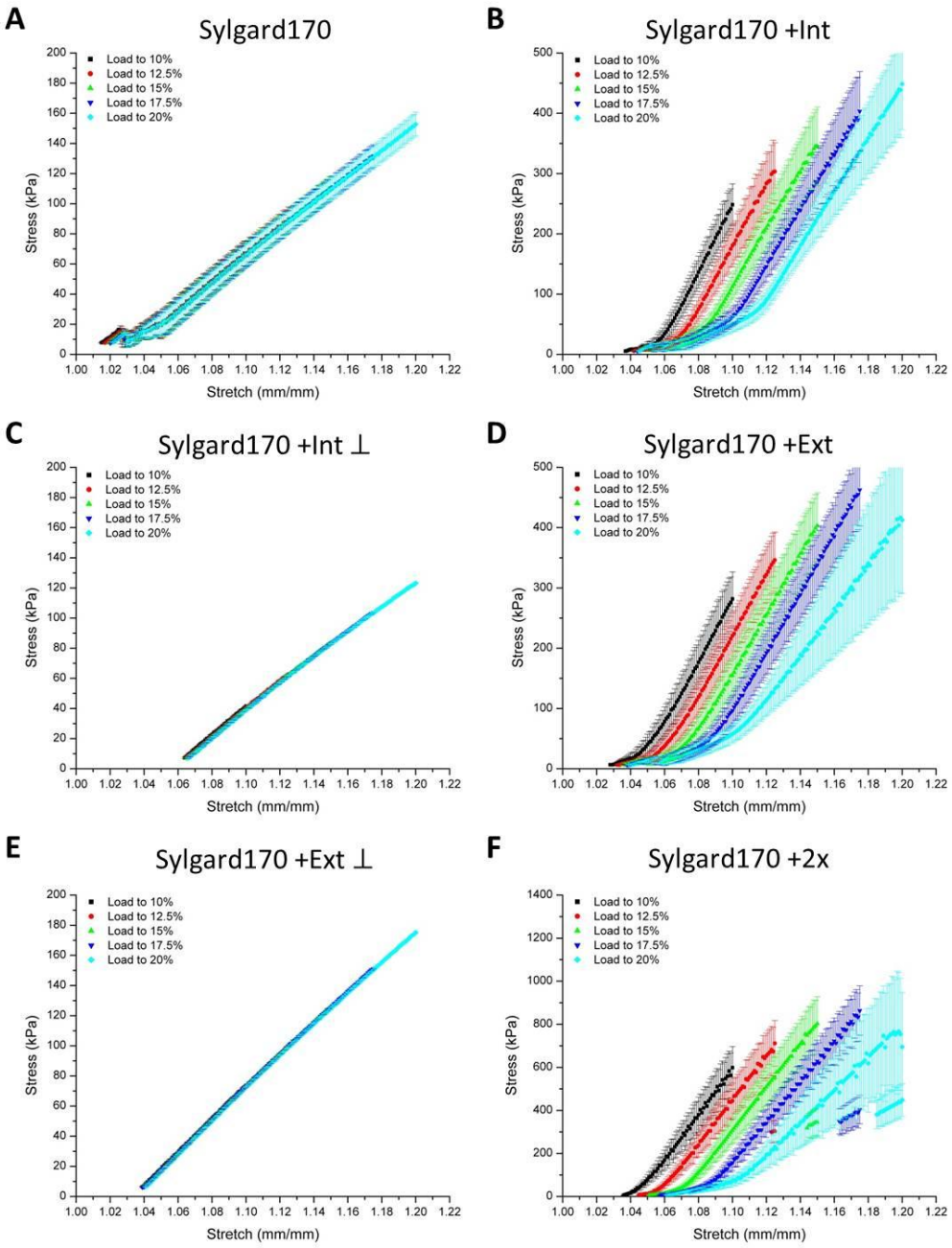

Figure 35. Stress-stretch for Sylgard 170 composites, reporting the mean and standard deviation (where applicable) of the fifth loading cycle of Mould C-cast (A) Sylgard 170 (n=19), (B) internally reinforced S170 (n=19), (C) perpendicular cut (⊥) of internally reinforced S170 (n=1) (D) externally reinforced S170 (n=18), (E) perpendicular cut (⊥) of externally reinforced S170 (n=1), and (F) double-stranded externally reinforced S170 (n=4) at each of the following strain levels: ε=10%, 12.5%, 15%, 17.5%, and 20%.

Each reinforcement technique altered the stress-stretch relationship of Sylgard 170 significantly, provided the reinforcements engaged in the longitudinal direction. Average stress at 10% strain was shifted upward for the internally reinforced, externally reinforced, and double stranded externally reinforced from the unreinforced Sylgard 170. This pattern continued as strain was increased to each 12.5%, 15%, 17.5%, and 20%.

To quantify the effect of the reinforcements on Sylgard 170, the average instantaneous stress was calculated at the endpoints of the fifth cycle to each target stretch (λ=1.1, 1.125, 1.15, 1.175 or 1.2). Peak stress at the fifth cycle to 10% strain showed values for reinforced samples at least 3.7 times greater than the 67.34 ± 8.43 kPa recorded for unreinforced samples (Table 17, Fig. 36A). At 20% strain, Fig. 36E, the internally and externally reinforced Sylgard 170 were about 2.8 times the unreinforced stress.

It was anticipated that the double-stranded externally reinforced samples were produce larger stress than single-stranded reinforced samples because both strands need to be stretched. At 10% strain, this proved to be true with the double-stranded reinforced Sylgard 170 approximately 4.8 times as great as the unreinforced stress. At 10% strain, the double-stranded reinforced samples had been 8.8 times the unreinforced value, increasing stress to 586.75 ± 113.00 kPa.

Both perpendicular samples (with fibers perpendicular to testing axis) were included for visual comparison of the change in stress shown in Fig. 36, but were not included in statistical analysis. One sample with fibers in the perpendicular direction was considered valid to visually represent its data set due to the repeatable nature of samples cast in Type C. These perpendicular samples were not included in statistical testing as there was only one sample each. At the five specifically examined strains, all four test groups were significantly different from one another, with the exception of the single-fiber reinforcements at 20% strain (Fig. 36).

Table 17. Instantaneous stress for Mould C-cast reinforced Sylgard 170. Sample size is indicated in parentheses for the average stress (kPa).

	Instantaneous Stress (kPa)				
Type	**10%**	**12.50%**	**15%**	**17.50%**	**20%**
Sylgard 170 (19)	67.34 ± 8.43	89.32 ± 8.32	110.64 ± 7.96	131.72 ± 7.63	152.63 ± 7.97
Sylgard 170 & Internal Thread (19)	247.39 ± 34.69	304.72 ± 51.49	348.37 ± 63.13	398.68 ± 70.20	445.16 ± 79.11
Sylgard 170 & External Thread (18)	281.12 ± 44.83	346.45 ± 48.37	403.38 ± 56.51	461.96 ± 60.51	417.06 ± 125.99
Sylgard 170 & Double-stranded External Thread (4)	586.75 ± 113.00	698.81 ± 121.76	801.98 ± 135.05	854.46 ± 129.20	713.86 ± 281.48

From Fig. 36, the impact on stress of the reinforcements was evident. At ε=10%, 12.5%, 15%, 17.5% and 20%, the reinforcements at least doubled the stress level of unreinforced Sylgard 170. Although statistically significantly different at 20% strain, the single-fiber reinforced samples closely resemble one another through all points tested. Both single-fiber reinforcements resulted in stress between the unreinforced and double-stranded reinforced samples at all strains.

The double-stranded samples reached double the stress of the single external reinforcements at 10%, 12.5%, and 15% strain (Table 17). At 17.5% strain, it was only an 85% increase and by 20% strain even less. Degradation of one fiber led to the decrease in the difference between the double-stranded and single-stranded external reinforcements at these high strains.

The stress of Sylgard 170 increased by approximately 22 kPa each 2.5% strain step. Similarly, the internal perpendicular single sample increased by a range of 19-21 kPa each step and the external perpendicular sample increased by 24-26 kPa. All three were linear, unlike the reinforced samples. Sylgard 170 internally reinforced samples' stress continued to increase with further increase to strain.

As with previous protocols, the maximum stress at the end of the fifth cycle to each target stretch (quantified in Table 17 and shown in Fig. 38) illustrated the importance of fiber alignment. Additionally, at 20% strain, the

maximum stress of internal and external reinforcements was not significant (445.16 ± 79.11 and 417.06 ± 125.99 kPa, respectively). By internally reinforcing the sample, the maximum stress experienced at 10% strain of the unreinforced Sylgard 170 was increased 3.5 times. Though significantly different at 20% strain, the internal and external reinforcements were similar enough to proceed with just external reinforcements for the reinforced tubular composites because patient samples often did not exceed 15% strain with mechanical integrity.

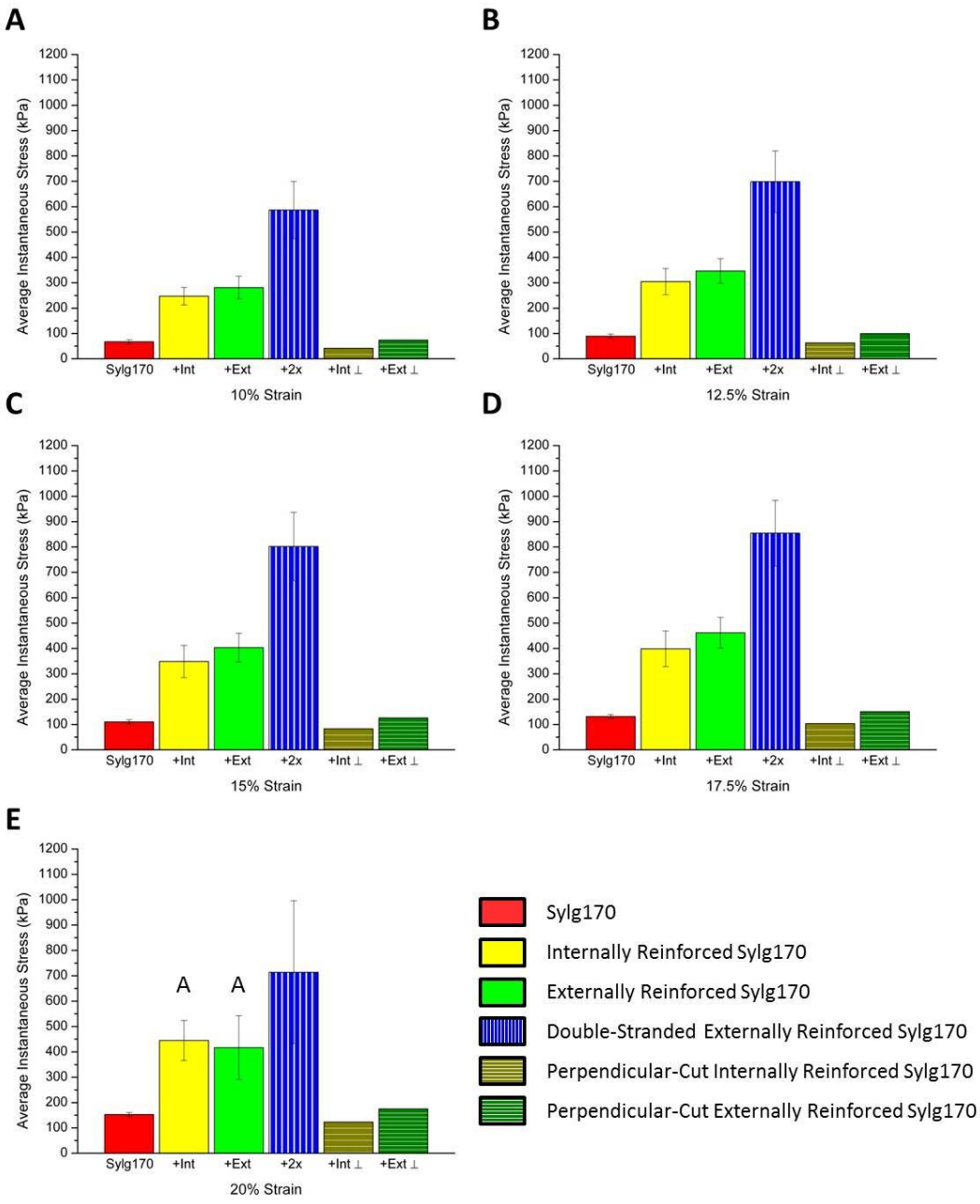

Figure 36. Average stress comparison for Sylgard 170 composites. Comparison of the effects of various reinforcement techniques to the average instantaneous stress (kPa) of Sylgard 170 at (A) 10% strain, (B) 12.5% strain, (C) 15% strain, (D) 17.5% strain, and (E) 20% strain. All samples have cross-sectional area 15.67 ± 0.98 mm and gauge length 35 mm. Means with different letters are significantly different (ANOVA, Fisher's PLSD, $p < 0.05$). Perpendicular samples, cut with fibers aligned ⊥ to the test direction, are included for visual comparison purposes.

Differences in stress at each of the five target strains implied differences in tangential moduli as well. In general, the tangential modulus was calculated as the slope of the best fit line of the twelve surrounding data points inclusive of the target strain. However, due to the test protocol for uniaxial cyclic testing, it was not feasible to measure a modulus surrounding the point of interest. Therefore, for the Type C-cast data, the tangential modulus is taken as the slope of the best fit line of the twelve data points leading up to the target strain, with the target included.

During the final loading cycle to 10% strain, all reinforcements significantly altered the tangential modulus of the unreinforced Sylgard 170 (ANOVA, Fisher's PLSD $p < 0.05$), reported in Table 17. Statistically indeterminable from one another, the internal and external single-fiber reinforcements increased the tangential modulus up to six times the unreinforced value. This occurred at 10% strain. Though the tangential modulus was always greater for the single-fiber reinforcements, the differential from the unreinforced modulus decreased as the test progressed. By 20% strain, the tangential modulus for single-reinforced samples was at least four times as great as the unreinforced samples. The change in tangential modulus was amplified by doubling the quantity of fibers. At 10% strain, the double-stranded reinforcement increased the tangential modulus from 920 kPa for unreinforced samples up to 10287 kPa. At 20% strain, the average tangential modulus for the double-stranded externally modified samples was

statistically insignificant from the unreinforced control group. After stretched to 1.175, only one sample remained intact to complete five cycles to λ=1.2. This significantly affected the reported tangential modulus, with individual sample results ranging from -7201 kPa to 10262 kPa. All samples remained included because the stress levels were not equivalent to the unreinforced samples and thus deemed relevant. Over the course of the testing protocol (as strain increased), the tangential modulus of the reinforced Sylgard 170 decreased, as evidenced in Table 18. The stiffness of the fibers weakened as the composites were continuously strained and thus required less force per unit area to stretch the composite.

Table 18. Tangential modulus for Mould C-cast reinforced Sylgard 170. The tangential modulus was calculated for each reinforcement type using the twelve points leading up to the target strain.

Tangential Modulus (kPa)					
Type	**10%**	**12.5%**	**15%**	**17.5%**	**20%**
Sylgard 170 (19)	920.76 ± 31.68	888.11 ± 21.93	875.50 ± 20.93	875.28 ± 31.95	880.34 ± 45.88
Sylgard 170 & Internal Thread (19)	5528.96 ± 569.02	4837.35 ± 723.87	4438.17 ± 822.81	4389.92 ± 865.26	4281.39 ± 855.76
Sylgard 170 & External Thread (19)	5245.69 ± 558.37	4925.64 ± 483.99	4797.68 ± 512.94	4820.22 ± 505.78	3857.42 ± 1235.99
Sylgard 170 & Double-stranded External Thread (4)	10287.78 ± 1336.86	9678.15 ± 1253.49	9433.04 ± 1284.34	9064.25 ± 1163.84	1053.82 ± 7844.45

To further compare the linearity of the stress responses, the maximum segmented modulus was calculated. The maximum segmented modulus for Sylgard 170 did not significantly change as strain increased. The modulus was greater than the tangential modulus, indicating a change in the steepness of the curve. The five maximum segmented moduli average to 1000 kPa for unreinforced Sylgard 170. There was not a specific range for which the maximum occurred, other than before 7.5% strain. This held true even when strained up through 20% strain. The maximum steepness occurred by 7.5% strain for unreinforced Sylgard 170.

Table 19. Maximum segmented modulus for reinforced Sylgard 170 Mould C-cast samples. Each individual sample for the given target stretch had its final loading cycle segmented into 0-1.2% strain ranges. The elastic modulus of each range was calculated, and the largest modulus averaged across the samples (kPa).

Maximum Segmented Modulus (kPa)					
Type	**λ = 1.1**	**λ = 1.125**	**λ = 1.15**	**λ = 1.175**	**λ = 1.2**
Sylgard 170 (19)	996.43 ± 29.81	996.85 ± 29.92	1002.34 ± 29.29	1000.20 ± 33.24	1003.97 ± 32.31
Sylgard 170 & Internal Thread (19)	5688.87 ± 566.21	5341.23 ± 834.55	5043.50 ± 1004.60	4963.94 ± 1021.89	4857.34 ± 1080.74
Sylgard 170 & External Thread (19)	5374.35 ± 576.16	5228.87 ± 564.07	5107.70 ± 544.35	5050.92 ± 542.53	4048.33 ± 1363.84
Sylgard 170 & Double-stranded External Thread (4)	10779.73 ± 1641.70	10520.14 ± 1509.51	10281.67 ± 1544.47	9585.25 ± 1327.01	8132.89 ± 2934.29

The maximum segmented modulus ranged from 4857 to 5688 kPa for internally reinforced Sylgard 170. Unlike the unreinforced samples, the maximum segmented modulus location occurred closer to the target strain. For loading up to 10% strain, the maximum occurred from 7.5 to 8.8% strain. For loading up through 12.5% strain, the maximum occurred from 8.8 to 10% strain, with one exception. One sample had a maximum segmented modulus significantly lower than the others did. The exception occurred preceding the target strain. The particular sample also dropped to 2000 kPa by 20% strain for a maximum and was always at the target stretch. A second

sample at 15% strain began to drop in maximum segmented modulus. These two samples experienced fiber degradation earlier than the rest of the samples. Both individual fibers mechanically failed prior to the test completion.

The maximum segmented modulus for externally reinforced samples ranged from 4048 to 5374 kPa. Similar to the internally reinforced group, the highest maximum reported occurred during the 10% strain cycle. As the protocol continued and the samples were stretched to higher strains, the fibers wore down, and less stiff responses were seen. Lower maximum moduli also occurred. For loading up through 10% strain, the maximum segmented modulus occurred between 7.5 and 10% strain. For the other four cycles, maximum segmented modulus occurrence was less predictable.

The double-stranded maximum segmented modulus was approximately twice that of the single external fiber moduli for four of the five cycles. Loading up to 17.5% strain, the modulus decreased to 1.9 times the value as fibers were deteriorating.

6.3 Reinforcement Effects on Mould C-Cast Dragon Skin 20

Although reinforcement of Sylgard 170 was successful and promising, a softer base material was needed to mimic several of the patients (Table 23). Dragon Skin 20 was selected as the appropriate base material and was externally reinforced with 100% silk thread. In addition, two perpendicular samples, DS20 +Ext ⊥, were tested. The perpendicular samples were included for visual comparative purposes only. The unreinforced Dragon Skin 20 average stress-stretch, Fig. 37A, showed similar properties to Sylgard 170 (Fig. 35A) in that the linear nature was undisturbed as higher strains were reached, and there was no sign of damage occurring up through 20% strain. Similarly, the externally reinforced Dragon Skin 20, Fig. 37B, was comparable to the external reinforcement of Sylgard 170 (Fig. 35D) in that the shape of the curves was the desired *J*-shape.

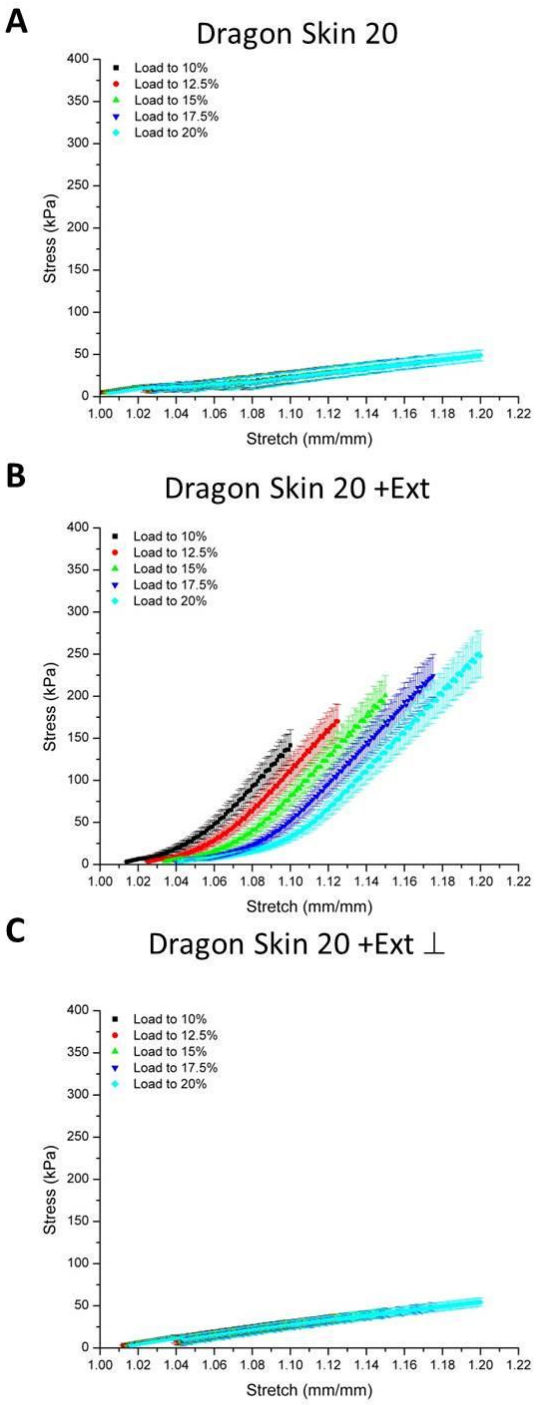

Figure 37. Average stress-stretch for Dragon Skin 20 (A) unreinforced samples (n=6), (B) externally reinforced samples (n=4), and (C) perpendicular cut of externally reinforced samples (n=2) to target strains: 10%, 12.5%, 15%, 17.5%, and 20%.

Additionally, higher stresses were registered for each strain when compared to unreinforced samples, and softening was noticeable as new strains were reached for the first time. The changes to instant stress are quantified in Table 17. As predicted from previous tests, both the Dragon Skin 20 and the Dragon Skin 20 Reinforced samples had lower stresses than their Sylgard 170 counterparts did. At 10% strain, Dragon Skin 20, with a stress of 23.54 kPa was lower than Sylgard 170's 67.34 kPa and Dragon Skin 20 external reinforcement's stress, 140.67 kPa, was less than Sylgard 170 reinforced by the same technique, 281.12 kPa. The increased strength is illustrated in Fig. 38 alongside the perpendicular samples to show the benefit of aligning the fibers with the direction of testing. Reinforcement of Dragon Skin 20 increased stress sixfold at 10% strain, and this pace was near maintained at the other four points of interest, as there was at least a fivefold difference.

Table 20. Instantaneous stress for Mould C-cast Dragon Skin 20 for unreinforced and externally reinforced samples at 10%, 12.5%, 15%, 17.5%, and 20% strain. The average and one standard deviation are reported with sample size indicated in parentheses. The reinforced samples were statistically significantly different from the unreinforced samples at all five strains (Student's *t*-test, $p < 0.05$).

Instantaneous Stress (kPa)					
Type	**10%**	**12.50%**	**15%**	**17.50%**	**20%**
Dragon Skin 20 (6)	23.54 ± 7.65	30.16 ± 7.43	36.70 ± 7.28	42.62 ± 6.91	48.79 ± 6.75
Dragon Skin 20 & External Thread (4)	140.67 ± 20.43	171.08 ± 22.69	197.97 ± 24.87	224.18 ± 27.35	250.55 ± 29.73

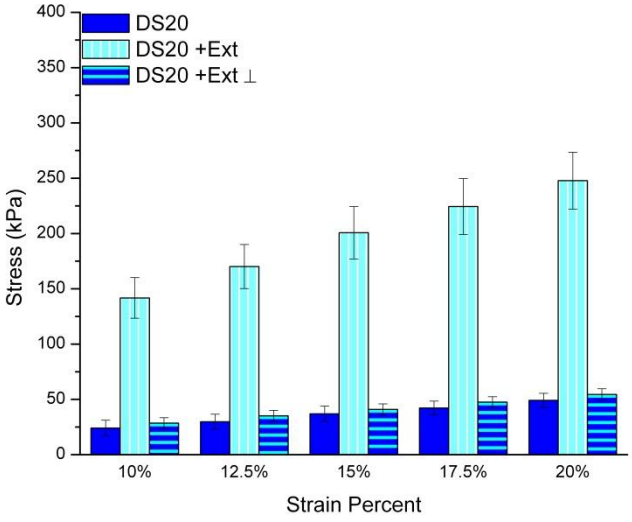

Figure 38. Average instantaneous stress comparison of Dragon Skin 20 die-cut samples. The stress (kPa) for the unreinforced samples (n=6) is significantly different from the reinforced (n=4) samples (Student's *t*-test, p <0.05). The externally-reinforced, perpendicular-cut samples (blue-striped columns), are included for visual comparison purposes only.

Dragon Skin 20 had similar tangential moduli at the five strains examined (Table 21). As strain increased, the tangential modulus slightly decreased indicating a less stiff response. The Dragon Skin 20 tangential modulus was much lower than Sylgard 170 at 10% strain, 295 kPa as compared to 921 kPa. This was expected based on the differences in stress-strain response observed in Fig. 24A with Type B Moulds. At 20% strain, the tangential modulus was still significantly different from Sylgard 170 (880 kPa for S170 as compared to 254 kPa for DS20).

By externally reinforcing Dragon Skin 20, the tangential modulus increased by more than eight times the unreinforced Dragon Skin 20. At 10% strain, the tangential modulus for reinforced Dragon Skin 20 was 2428 kPa, as compared to 295 kPa for unreinforced Dragon Skin 20. At 15% strain, the difference was 2005 kPa, but at 20% strain, the difference between the unreinforced and reinforced Dragon Skin 20 was 2061 kPa. The order of materials based on stiffness was Dragon Skin 20, Sylgard 170, Dragon Skin 20 & single-fiber reinforcement, Sylgard 170 & single-fiber reinforcement, Sylgard 170 & double-stranded external reinforcement, with double-stranded external reinforcement of Dragon Skin 20 not tested.

Table 21. Tangential modulus of reinforced Mould C-cast Dragon Skin 20. Sample size is indicated in parentheses with the average and standard deviation reported for the modulus at each strain calculated.

Tangential Modulus (kPa)					
Type	**10%**	**12.5%**	**15%**	**17.5%**	**20%**
Dragon Skin 20 (6)	294.61 ± 16.48	274.53 ± 22.16	271.49 ± 8.37	257.87 ± 21.68	253.88 ± 13.35
Dragon Skin 20 & External Thread (4)	2427.68 ± 252.20	2324.33 ± 226.27	2277.52 ± 227.45	2269.63 ± 243.61	2314.52 ± 237.37

Maximum segmented moduli were also evaluated (Table 22). These values were similar to the tangential moduli. For all five strains, the maximum moduli centered about 350 kPa for unreinforced Dragon Skin 20. Although not consistently in one segment, the maximum occurred by 7.5% strain in all samples at all five points. The reinforced Dragon Skin 20, as anticipated, had an increase in maximum segmented modulus of 2127 kPa at 10% strain. The response was less steep as strain increased. Although unreinforced maximum occurred at earlier strains, reinforced maximum moduli occurred closer to the endpoints of the cycle.

Table 22. Maximum segmented modulus for Dragon Skin 20 composites cast in Type C moulds. Sample size is indicated in parentheses, with the average and one standard deviation reported.

Maximum Segmented Modulus (kPa)					
Type	**λ = 1.1**	**λ = 1.125**	**λ = 1.15**	**λ = 1.175**	**λ = 1.2**
Dragon Skin 20 (6)	335.30 ± 13.24	340.59 ± 8.87	335.58 ± 12.47	339.70 ± 13.79	338.00 ± 9.46
Dragon Skin 20 & External Thread (4)	2462.47 ± 298.76	2444.03 ± 246.96	2403.77 ± 250.33	2377.34 ± 245.49	2364.43 ± 228.44

6.4 Conclusions

Although successful, Type A- and Type B-cast samples were too thick for comparison to patient tissue. The average thickness of the patient samples (n=6) was 2.09 ± 0.8 mm, ranging as low as 1.35 mm. Thinner test samples were therefore desired, and Mould C-cast samples fabricated. Based on available patient data, both reinforced Sylgard 170 and reinforced Dragon Skin 20 would be suitable analogues based on stress values and curvature analysis. Specific details related to the comparison for individual patients are discussed in Chapter 7.

Chapter 7 – Patient Comparison to Analogues

The ability to mimic patient material properties was the motivation behind this thesis. Keeping variability between patients in mind, several base materials were reinforced with a variety of fibers that differed in strength or embedment technique to achieve this goal. One set of target properties was the instantaneous stress of the individual patient samples at 10%, 12.5%, 15%, 17.5%, and 20% strain. A second goal was to match the *J*-shape non-linearity of the patient stress-stretch curves. This goal was discussed in terms of the tangential modulus and the maximum segmented modulus.

One measure to evaluate the nature of the analogue was to examine the stress-strain relationship and to quantify small linear portions with a modulus. Due to the non-linear relationship, the tangential modulus at specific strains and a representative maximum segmented modulus over a strain range were both reported. The maximum moduli for patient samples were the maximum of segmented pieces of twelve data points per sample for the fifth cycle to the reported stretch. For example, each patient's response to 10% strain was divided into sections of 12 or 13 data points. The elastic modulus for each section was calculated, and the maximum reported as the 10% Maximum Segmented Modulus. The same was done for 12.5% and 15% strain. For non-patient samples, the same method of separation and calculation were performed for each individual sample. The average of the

maximum values was then calculated and reported as the representative maximum segmented modulus. This process was repeated for the strain ranges 0-10%, 0-12.5%, and 0-15% strain.

Dragon Skin 20 reinforced samples were the best match for the maximum segmented modulus for multiple patients, consistent through 0-10%, 0-12.5%, and 0-15% strain ranges. Dragon Skin 20 reinforced samples have an average maximum segmented modulus of approximately 2450 kPa in 0-10% strain range (Table 19). Patients 2, 5, 6, and 7 record a similar maximum segmented modulus (approximately 3000 kPa) in the same range.

As expected, Dragon Skin 20 samples have a lower average maximum segmented modulus than Sylgard 170. It should be noted that as the externally reinforced Sylgard 170 samples were tested, the difference in stiffening slightly decreased. On the contrary, reinforced Dragon Skin 20 samples fluctuated about the 2400 kPa mark. Up through 17.5% strain, external reinforcement of Sylgard 170 was approximately 5000 kPa, closer to that exhibited by Patient 3 (Fig. 41).

Patient 7 (Fig. 42) has an upwards trend in maximum segmented modulus showing an increase in stiffness as the strain increased, as does Patient 3. Other patients were not able to be tested over as many cycles, so the pattern was indeterminable.

7.1 Stress Analysis of Patient AAA Tissue

Every aorta is unique in its properties, and a benefit of this system is the ability to match multiple patients to different analogues and adjust the properties as needed. Over the timeline of this project, eight patient samples were acquired. Priority testing of the patient tissue was given to the biaxial protocols, but in the event of the acquired tissue being too small to cut a useable cruciform or early failure in one of the four branches, a uniaxial protocol was used. Patients 2, 3, 5, 6, and 7 all underwent uniaxial testing with some benefiting from early failure in one arm of the preferred biaxial cruciform shape. Patient 1 was excluded as only biaxial testing was performed and Patient 4 was excluded from all measurements except dimensional analysis because the protocol was shortened in an attempt to extend the test life of the specimen. All synthetic samples were tested at a rate of 0.1295 mm/s for the composite samples with gauge length 35 mm, as called for in the cyclic uniaxial protocol. Resultant stress-stretch responses, such as Patient 5 and Patient 6 (Fig. 39), are separated by target stretch so as not to combine cycles. Patients 2 and 3 were oriented such that the longitudinal axis was tested, and the remaining three patients were tested such that the circumferential direction was stretched. These designations were recorded in each table of data for which patient data is reported for clarity.

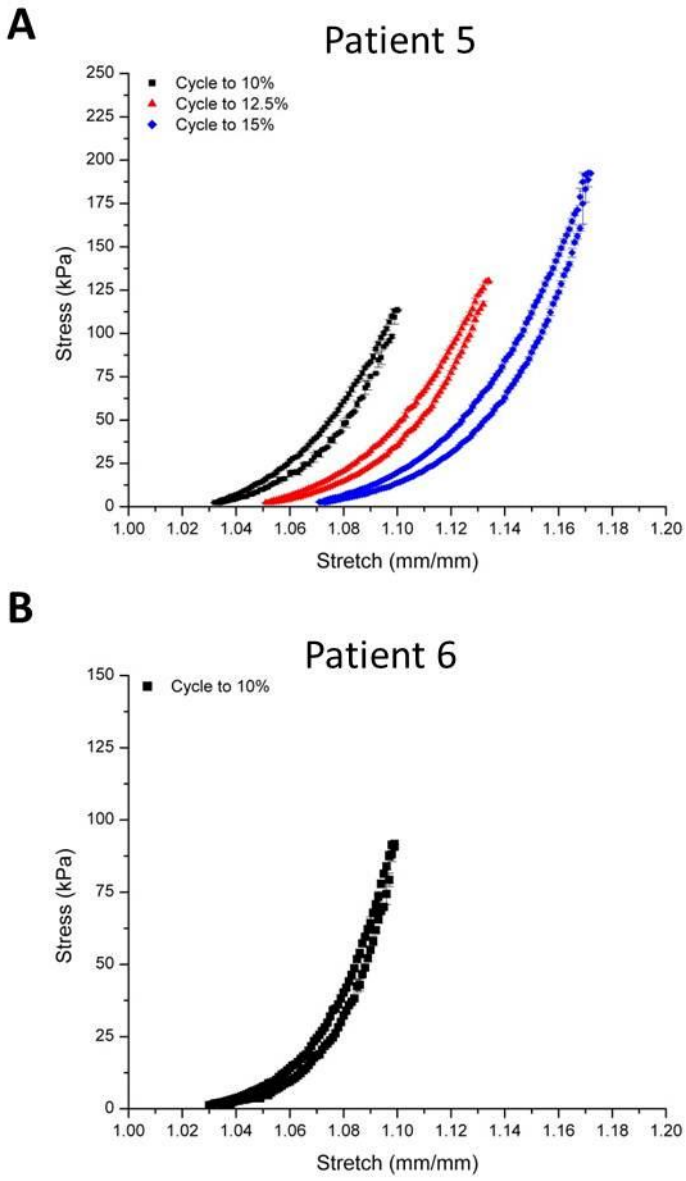

Figure 39. Resultant stress-stretch response for Patient 5 (A) and Patient 6 (B). Five loading cycles to each target stretch were run, with the final cycle plotted for comparison to synthetic analogues. Patient 6 did not successfully complete five cycles to λ=1.125, and as such, only the data to λ=1.1 is shown. Data collected by Mr. Francesco Pancheri, and analyzed by the author.

To further the description as to each aorta being different, the instantaneous stress, reported in Table 23, compare Patients 2 and 3. Patient 2 experienced 113.5 kPa stress, whereas Patient 3 was closer to 300 kPa at 10% strain. Both of these samples failed to reach five cycles to 17.5% strain without questions of damage accruing. Patient 2 did not reach the 17.5% target at all, and although Patient 3 completed testing through the fifth cycle to 20% strain, the stress level decreased suggesting weakening. At the five target strains of the protocol, Patients 2 and 3 did not converge to a similar stress. The rate at which Patient 2 increased was nearly half that of Patient 3 for strain steps equal to 2.5%.

Table 23. Instantaneous stress for patient AAA samples tested uniaxially. Data was collected by Mr. Francesco Pancheri, but analyzed by the author.

Date Tested	Patient	Direction*	Average Instantaneous Stress (kPa)				
			10%	12.50%	15%	17.50%	20%
3/2/2011	2	Long.	113.48	151.15	192.59		
3/29/2011	3	Long.	289.76	362.37	446.45		
11/10/2011	5	Circ.	113.71	106.07	111.87		
11/11/2011	6	Circ.	91.70				
3/7/2012	7	Circ.	136.11	144.03	237.42	171.55	266.09

*Direction refers to the orientation of the specimen in the aorta: longitudinal (Long.) or circumferential (Circ.)

Patients 5, 6, and 7 were tested circumferentially, so they should not be directly compared to the longitudinal patients. At 10%, these patients center around 100 kPa (114, 92, and 136 kPa respectively) and were more similar to Patient 2 at this strain. Patient 6 was not strong enough to continue testing through 12.5% strain and could only be considered in comparisons to 10% strain.

More specifically, patient to patient differences were highlighted by the variation in results of the two samples tested in the longitudinal direction. At 10% strain, Patient 2 reached approximately 113 kPa, but Patient 3 experienced more than twice that (289 kPa). By 15% strain, Patient 2 reached almost 200 kPa. This value was only a fraction of the stress experienced by Patient 3 at a lower strain (10%). The differences between these two patients were further exemplified by the tangential and maximum segmented moduli tables (Table 24 and Table 25, respectively). Tangentially, Patient 2 increased steadily around 1000-1200 kPa as strain increased from 10%-15%, but Patient 3's modulus was closer to 3000 kPa. Both, however, were fairly constant.

Table 24. Tangential modulus for patient AAA samples tested uniaxially (kPa). Gaps in data are due to slight changes to the end points of the patient testing protocol. Data was collected by Mr. Francesco Pancheri and analyzed by the author.

Tangential Modulus (kPa)					
Patient	**10%**	**12.5%**	**15%**	**17.5%**	**20%**
Patient 2	2995.94	4153.09	3423.97		
Patient 3	7149.83	7805.52	9455.13		
Patient 5	3096.75	2732.97		4887.51	
Patient 6	3133.43				
Patient 7	2831.13		3882.96		4174.76

Samples tested in the circumferential direction showed lower stresses than Patient 3 and were closer to Patient 2 despite the directionality. At 10% strain, the circumferential specimens reported similar stresses. Patient 5's stress did not increase with strain as others did (Fig. 39A). Patient 6, Fig. 39B, did not have the mechanical integrity to complete five cycles to 12.5% strain after the five cycles to 10%. Patient 7 (Fig. 42A), on the other hand, successfully completed the entire uniaxial testing protocol to 20% strain (to five strains over twenty-five total loading-unloading cycles). Looking at the tangential modulus for these patients, it can be seen that Patient 5 was losing

strength as the stretch increased to 1.125 (Fig. 39A). The lack of increase in stress translates to a decrease in tangential modulus, as expected. Patient 7 increased in tangential modulus from 10% to 12.5% strain, and had its steepest slope at 15% strain (Fig. 42A). Though not as high as any of the previous slopes, the modulus dips at 17.5% strain and increased beyond that at 20%. The maximum segmented modulus showed a consistent modulus around 3000 kPa. Not including Patient 3, all other patients center their maximum segmented modulus between 2000 and 4000 kPa, whereas Patient 3 was closer to 8000 kPa.

With only one data point per patient, statistical tests could not be achieved. However, of the five representative patients, four show similar tangential moduli, approximately 3000 kPa. One patient, who also exhibited higher stresses at each strain, showed a higher tangential modulus (7000 kPa) at this strain. During subsequent loading cycles, patients either saw an increase or decrease in the modulus indicating the wellness of the sample. By 15% strain (15 cycles of load), the patients were roughly around 3000 kPa with Patient 3 now up to 9455 kPa, much higher than the others.

A second modulus was calculated to compare the effects of the reinforcement techniques implemented in cyclic testing. The fifth cycle of data to each target stretch was used and divided into segments of thirteen to fourteen data points each. A modulus is calculated for each segment as the slope of

the best-fit line through those points, and the maximum of those is recorded as the maximum segmented modulus and reported in Table 25.

Table 25. Maximum segmented modulus for patient AAA samples tested uniaxially. Each data set to a particular stretch was further divided into multiple equal segments. The elastic modulus was calculated, and the largest of those segments reported. Gaps in data are due to slight changes to the patient testing protocol. Data was collected by Mr. Francesco Pancheri and analyzed by the author.

Maximum Segmented Modulus (kPa)					
Patient	**λ = 1.1**	**λ = 1.125**	**λ = 1.15**	**λ = 1.175**	**λ = 1.2**
Patient 2	2967.24	4144.31	3369.74		
Patient 3	7149.83	7840.30	9384.13		
Patient 5	3028.38	2703.53		4726.92	
Patient 6	3133.43				
Patient 7	2855.09		3870.95		3929.08

The maximum segmented modulus shows clear increases due to the reinforcements for all five target cycles implying a significant variation to the stress-strain relationship of both Sylgard 170 and Dragon Skin 20. During the stretch to λ=1.15, for example, the maximum slope for Sylgard 170 is on average 1002 kPa, but with externally modified samples, the maximum is

5107 kPa. The externally modified sample has at least one portion of the curve that is much stiffer than any segment of the unreinforced Sylgard170 curve. The same is seen for Dragon Skin 20 and its externally modified sample at 15% strain, 335.6 v. 2403.8 kPa. At 20% strain, although the average tangential modulus was not significantly different from unreinforced samples, the maximum segmented modulus provides more information. During the loading-unloading cycle to λ=1.2, the maximum segmented modulus for double is significantly greater than unreinforced samples, eight times greater suggesting on average failure occurred during this test cycle.

As we would expect from stress analysis, the maximum segmented modulus for Patient 3 is higher than other patients. During the same stretch range, Patient 3 has higher stress, so the curvature of the stress-strain curve must be different. The other patients fall in similar stress ranges exemplified by similar maximum segmented modulus to λ=1.1 at approximately 3000 kPa.

Examining stress-stretch curves and the instantaneous stress data, potential matches for analogues become apparent. The differences in stress seen in Table 23 underscore the importance of having more than one analogue, as was anticipated, and the reason for also including Dragon Skin 20 composites. The large difference between Patient 3 and the remainders in the pool of patients demanded at minimum a second analogue.

7.2 Patient 2 and Externally Reinforced Dragon Skin 20

The stress table suggests Sylgard 170 with thread was too stiff to represent Patient 2, and it was best replicated by the externally reinforced Dragon Skin 20. Early on it was apparent that Sylgard 170 would be too stiff a base if reinforcements were to be included to alter the shape of the stress-stretch curve. Dragon Skin 20 was used as a less stiff based and reinforced in the same manner as the Sylgard 170 external samples. It was chosen that external reinforcement would be the only one included, as opposed to also including internal reinforcements. This decision was due to the inability to internally reinforce three-dimensional, hollow samples. Using a lost-wax casting method it would be near impossible to reinforce the middle of the samples as done here with the open air casts. Thus the external method, most similar to grafts used in surgery, was used. The stress-stretch relationship for Patient 2 is plotted with the Dragon Skin 20 Reinforcement Averages for direct comparison in Fig. 40A. The *J*-shape curve of the composite mimicked the patient tissue well to the approximate locations of stresses examined. The inconsistencies were highlighted by modulus comparison, Fig. 40B. Tangentially, the synthetic matches best by 15% strain, but the maximum segmented modulus showed the patient to have a much higher slope at all three strains than the composite.

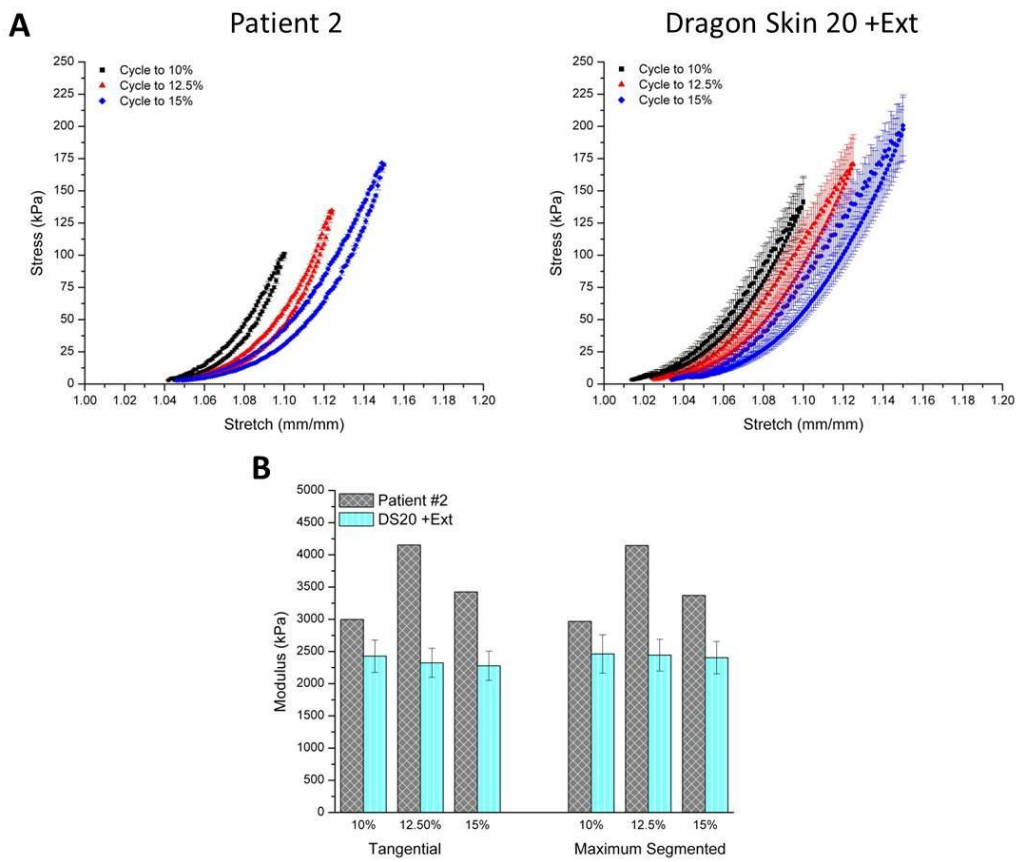

Figure 40. Patient 2 and externally reinforced Dragon Skin 20 comparison of A) stress-stretch loading and unloading curves and B) tangential and maximum segmented moduli.

7.3 Patient 3 and Externally Reinforced Sylgard 170

Patient 3 was an early analyzed sample, and as such, was the basis for the Mould C reinforcement experiments. The stress-stretch relationships for this patient and the externally reinforced Sylgard 170 (+Ext) were plotted side-by-side for direct comparison in Fig. 41A, as was done with Patient 2 above. Instantaneous stress at 10% strain for Patient 3 was determined to be 289 kPa, very close to the external reinforcement stress of 281 kPa. Though the

patient sample has a higher stress at each 10%, 12.5%, and 15% strain than the external reinforcement, the maximum difference was less than 50 kPa. When compared with the standard deviation for at times 56 kPa (Table 17), the difference was minimal. The two remain closed (within 300 kPa) for both 12.5% and 15% strain, important because there was approximately 400 kPa standard deviation with the moduli calculations for external reinforcement. The closeness of the tangential moduli was depicted in Fig. 41B as the Patient was within one standard deviation of the external reinforced composite. Similar to Patient 2, its closed analogue, the maximum segmented modulus (also Fig. 41B) was higher for the patient than the reinforced silicone.

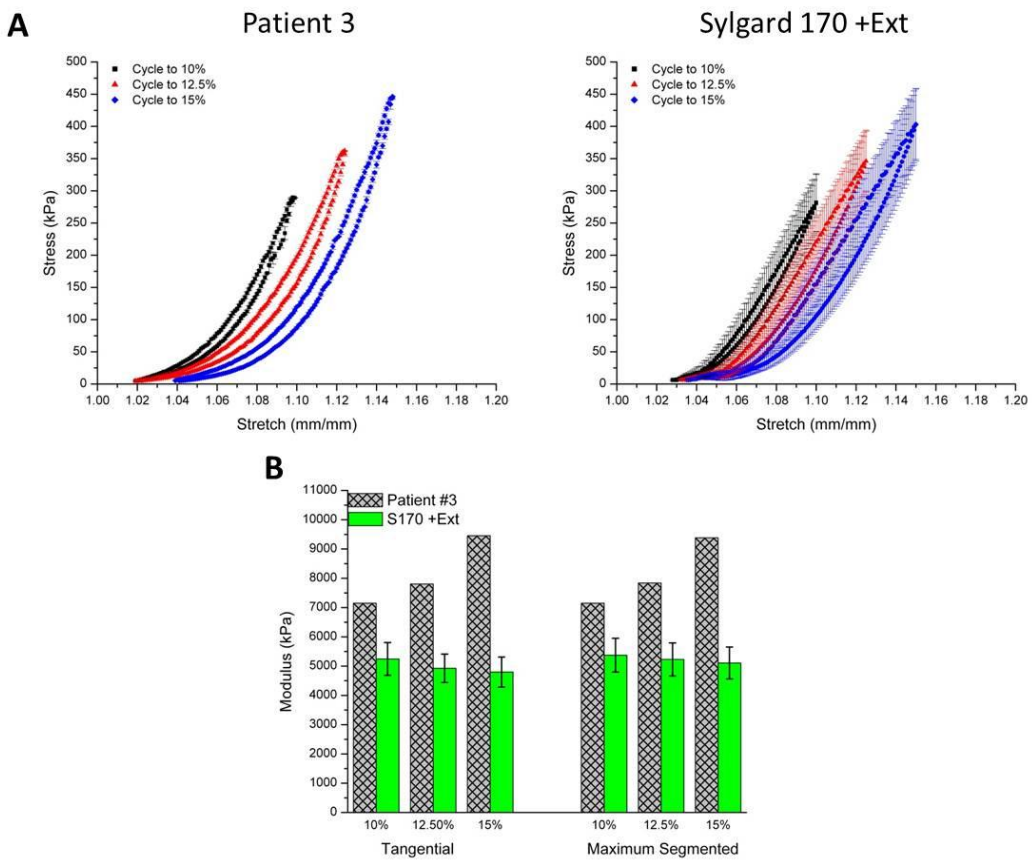

Figure 41. Patient 3 and externally reinforced Sylgard 170 comparison of A) stress-stretch loading and unloading curves and B) tangential and maximum segmented moduli.

7.4 Patient 7 and Externally Reinforced Dragon Skin 20

The high stresses registered by Patient 3 were not seen with Patient 7's testing. On the contrary, this patient appeared to behave most similar to Patient 2 and reinforced Dragon Skin 20. In this case, the composite overshoots the target stresses for Patient 7 by 30 kPa at 10% strain, but the composite was within 5 kPa of target at 15% strain. The comparison to Patient 7 was treated differently because the biaxial machine overshot the

target stretch at all points. The curves in Fig. 42 show the best match to this patient as possible, given the error by the machine.

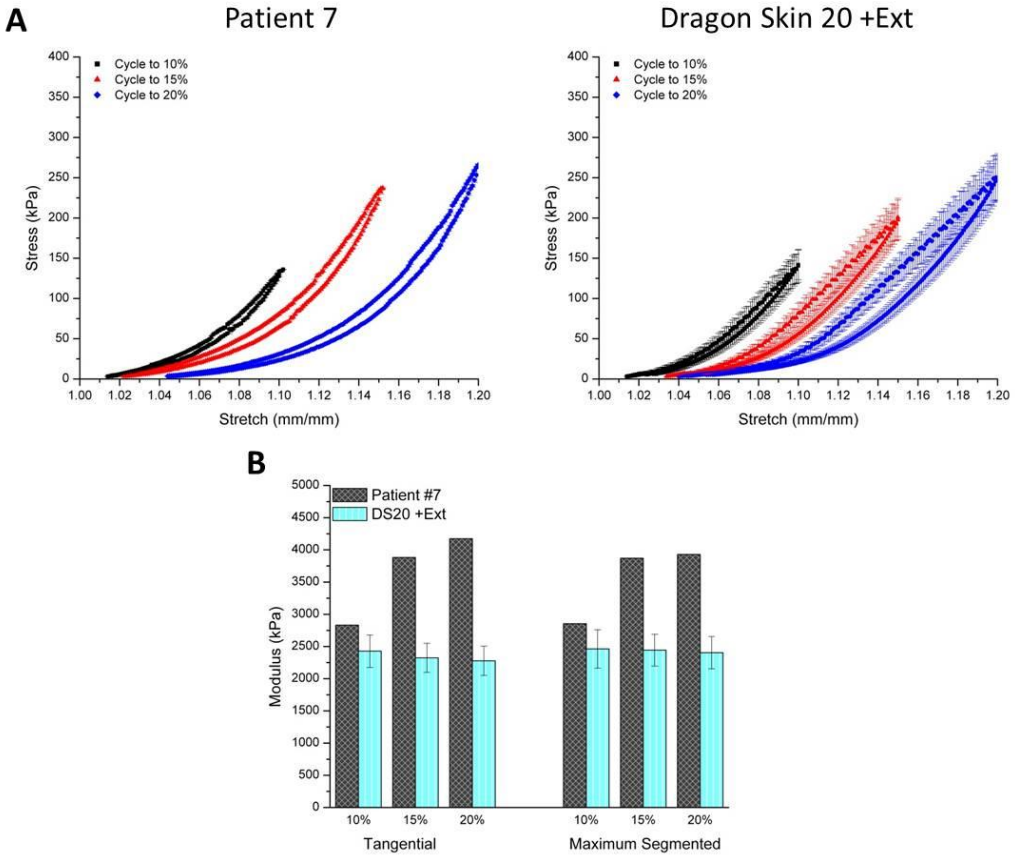

Figure 42. Patient 7 and externally reinforced Dragon Skin 20 comparison of A) stress-stretch loading and unloading curves and B) tangential and maximum segmented moduli.

7.5 Conclusions

A suitable analogue for Patient 5 was not recommended at this time due to the weakened state of the tissue during testing. At 10% strain, Patient 5 was identical to Patient 2, and the suggestion of Reinforced Dragon Skin 20 would be made. However, at larger strains, Patient 5 exhibits weakening responses with lower stress and higher strains without causing rupture. For this reason, only 10% data was examined as valid. Patient 6, as mentioned, failed after the five cycles to 10% strain and the stress at the first target stretch was lower than any composite tested. Unfortunately, there was no other data to compare at this time to this material, but externally reinforced Dragon Skin 10, or a material that stretched more easily than Dragon Skin 20, would be used to emulate this patient.

Chapter 8 – Results and Discussion for 2-D Pressure Testing

The synthetic analogues were being developed to create thin-walled replicates of patient models for analysis in the laboratory. In addition to comparing the one-dimensional stress-strain data, the two-dimensional expansion of the synthetic under pressure was analyzed (Fig. 18).

8.1 Wall Strength Analysis

The strength of the samples were evaluated and compared to the value shown for average patient wall strength by Vorp et al., 650 kPa[35]. The changes in diameter were evaluated for one thick-walled unreinforced sample and one reinforced sample through video analysis. By using the law of Laplace, wall strength was estimated for these samples at various pressure points. At a pressure of 14 psi, the unreinforced Sylgard 170 tube had approximated tension 323 kPa with the reinforced tube at 289 kPa (Table 26). By a pressure of 27 psi, the unreinforced Sylgard 170 sample had an increase in diameter equal to approximately 7 mm. At this dilation, the wall strength was 727 kPa, as shown in Fig. 43C, and shortly after the tube burst (Fig. 43E). For the unreinforced sample, by a pressure of 30 psi, the wall strength was approximated at 610 kPa with a roughly no change in diameter. The reinforced tubes, as shown in Fig. 43D, attempted to expand in between the fibers but were held in place. At 34 psi, and a wall strength equivalent to

the unreinforced Sylgard 170 tubular sample, the reinforced tubular sample burst in the longitudinal direction (Fig. 43F) as would be expected.

One thin-walled reinforced sample saw an increase in diameter of 2 mm in response to an internal pressure of 23 psi. Approximate wall strength for this sample prior to burst was calculated at 1120 kPa, but the wall strength of the thin-walled unreinforced samples were not available for comparison.

The wall strength of the Sylgard 170 material, 730 kPa, is comparable to the average patient wall strength, 650 kPa.

Table 26. Pressure tension relations for thick-walled samples. Changes in pressure and diameter were measured and converted to wall tension of the sample using Laplace's Law. The bold values indicate the burst pressure of the samples.

Thick-walled 3-D sample			Reinforced thick-walled 3-D sample		
Pressure (psi)	**Diameter (mm)**	**Tension (kPa)**	**Pressure (psi)**	**Diameter (mm)**	**Tension (kPa)**
7.02	20.6	139	7.10	22.1	140
9.73	21.3	199	9.91	21.6	191
12.06	22.8	264	12.54	22.3	249
14.15	23.7	323	14.54	22.3	289
24.59	26.3	622	22.01	22.5	442
25.33	29.1	708	30.09	22.7	610
27.06	**27.9**	**727**	**34.39**	**23.9**	**731**

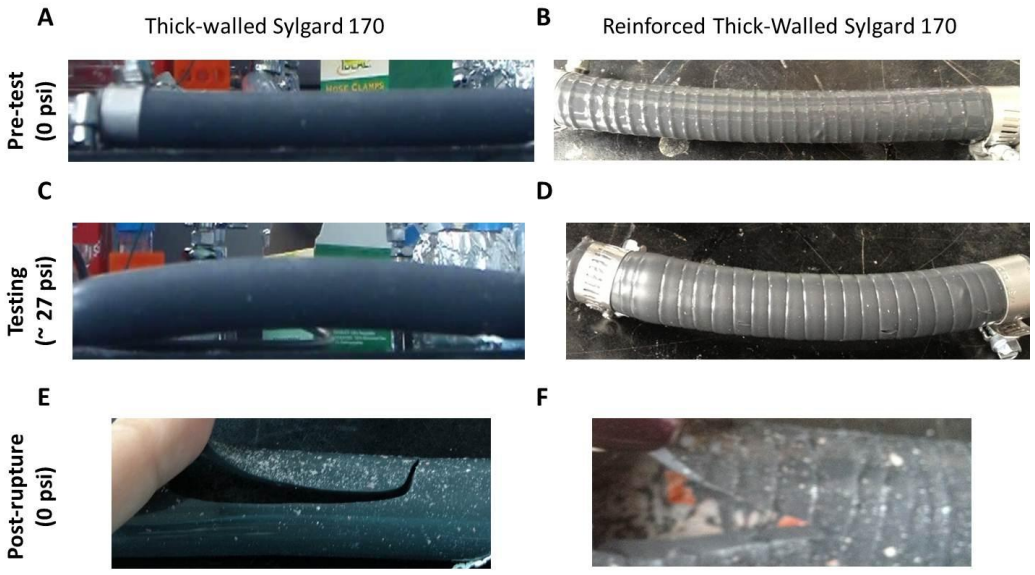

Figure 43. Reinforcement changes to diameter pre-test, during testing, and post-rupture. Three different pressure states are depicted for one thick-walled unreinforced tubular sample and one thick-walled reinforced tubular sample made of Sylgard 170.

8.2 Burst Pressure Analysis

The maximum pressure before burst was recorded for each sample tested. Samples that failed at the clamps were not included in analysis because they failed due to setup error and were tested without being mechanically sound. The target length for tubes was set to 200 mm, but the average length of the tubes tested was 172.83 ± 27.63 mm. The large variability was a result of multiple factors. Such factors included the shrinkage of the wax, especially the brown wax, as it cooled and the trimming of certain samples if defects were noticed under the clamps.

The thick-walled samples were intended to have wall thickness equal to 3.302 mm. These samples (both control and reinforced) had an average wall thickness 3.79 ± 0.18 mm, averaged over at least eight measurements. The intended thickness did not take into account the shrinkage as the wax solidified. The thin-walled samples were intended to have wall thickness 1.143 mm and on average were 1.59 ± 0.16 mm.

The average burst pressure for thick-walled controls, 28.23 ± 3.89 psi, was significantly different from the thin-walled samples, 6.95 ± 2.59 psi (Student's *t*-test, $p < 0.05$). The thickness of the samples affected the maximum pressure before failure as would be expected with a doubling of the thickness. The significant difference due to thickness was also seen in the reinforced thick and thin samples, 35.33 ± 3.64 versus 21.10 ± 4.59 psi, respectively.

The effect of the reinforcements, as seen in Fig. 44, significantly increased the burst pressure experienced within the thickness groups (Student's *t*-test, $p < 0.05$). By reinforcing the thick-walled samples, the burst pressure was significantly increased from 28.23 ± 3.85 psi to 35.33 ± 3.64 psi. The same reinforcement technique applied to thin-walled samples increased the burst pressure experienced by 14.15 ± 3.36 psi (6.95 ± 2.59 to 21.10 ± 2.14 psi).

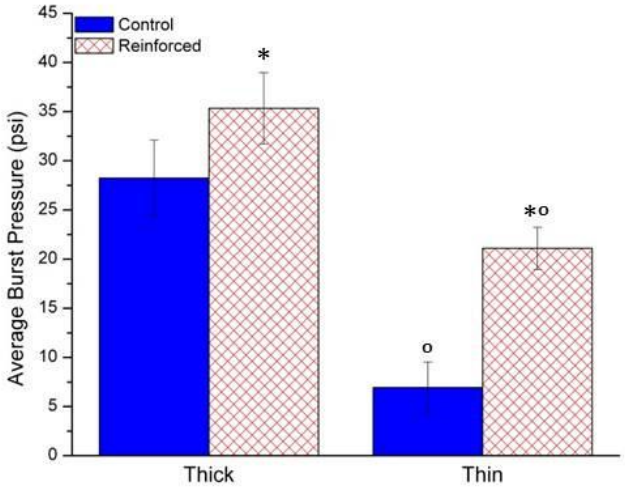

Figure 44. Average burst pressure comparison for control and reinforced tubes compared by the tube thickness. Thick controls (n=4), Thick reinforced tubes (n=6), thin controls (n=3) and thin reinforcements (n=3) were tested. * signifies statistical significance between tube type (Student's *t*-test, $p < 0.05$) and º signifies statistical significance between the thickness of the tubes.

The increase in burst pressure was evidenced in the physical swelling of the tubes while pressure increased. Both thickness control tubes had visible swelling early that gradually increased until failure. On the contrary, visible swelling was reduced in reinforced samples. As pressure increased, the tubes began to swell in the 5 mm gaps between threads, as shown in Fig. 43. As pressure continued to increase, the threads weakened and began to break one by one (there was an audible cascade of snapping) and the tube then swelled immediately and burst.

Chapter 9 – Conclusions and Future Directions

9.1 Conclusions

In this project, synthetic materials intended to mimic Patient AAA material properties were fabricated using multiple base materials and fibers for reinforcement. The following conclusions were drawn.

- Base material stiffness varied from 185.95 kPa to 2124.69 kPa, while the strength varied from 780.15 kPa to 1406.37 kPa for the three Sylgard materials (Dragon Skins unable to be tested). Base tangential moduli varied from 130.83 kPa (DS20 at 20% strain) to 2089.07 kPa (S160 at 20% strain).
- Wire-washer reinforced samples varied from 17243.79 kPa to 20568.38 kPa in stiffness, and from 7064.97 kPa to 18923.02 kPa in tangential modulus.
- Reinforcement of Sylgard 170 with different fiber types varied in stiffness from 1825.75 kPa to 8187.64 kPa, in strength from 631.12 kPa (+Suture) to 1083.18 kPa (+Woven), and in tangential modulus from 1519.44 kPa to 5988.02 kPa.
- Reinforcement of Sylgard 170 with different quantity of fibers varied the stiffness from 4048.33 kPa to 10779.73 kPa, and varied the tangential modulus from 5528.96 kPa to 10287.78 kPa at 10% strain and from 1053.82 kPa to 4281.39 kPa at 20% strain.

- Reinforcement of Dragon Skin 20 varied the stiffness to 2462.47 kPa and the tangential modulus to 2427.68 kPa.
- *J*-shape curves were obtained from thread and suture reinforced materials but not gauze reinforced materials.
- Relative locations of the base materials translated to the relative locations of reinforced materials. For example, unreinforced Dragon Skin 20 experienced lower stress than unreinforced Sylgard 170 throughout the region of interest, and as expected reinforced Dragon Skin 20 experienced lower stress than reinforced Sylgard 170.
- Silk thread reinforced Dragon Skin 20 proved to be a suitable analogue for Patients 2 and 7 based on stress analysis and curvature.
- Silk thread reinforced Sylgard 170 proved to be a suitable analogue for Patient 3 based on stress analysis and curvature.
- The thickness of synthetic models significantly altered the burst pressure from 6.95 psi to 28.32 psi with a change in thickness of 2.2 mm.
- Reinforcement of synthetic models significantly altered the burst pressure for thin-walled samples from 6.95 psi to 21.10 psi, as well as for thick-walled samples (28.23 psi to 35.33 psi).
- Wall strength analysis showed that the reinforcements did not alter the absolute wall strength of the material, but did so without largely

changing the diameter allowing the material to withstand more pressure.

- The wall strength of the externally reinforced Sylgard 170, 730 kPa, was comparable to that of the average patient wall strength, 650 kPa, reported by Vorp et al.[35]

Using three variations of PDMS, the silicone showed an increase in stress more than five times its natural value. Sylgard 170 actually increased its capacity for stress 9.8 times its inherent capabilities. Several other base materials, including Dragon Skins 10 and 20, were tested to provide a range of samples to compare with available patient data. By testing this particular group, adjustments were easily made when the first composite, though a great match for its target (externally-reinforced Sylgard 170 and Patient 3), was much too stiff for the remaining patient pool.

Additionally a catalogue of embedded fibers was generated varying in curvature. This directory provides another layer of modularity in the emulation process. As testing went along the benefits of silk thread were highlighted. The ability to approximate stress increased to the base relying on the number of threads in the gauge region allowed for accurate predictions of results.

Of the available seven patients, one was excluded for not undergoing uniaxial testing and another for a change in test procedure. Two of the five other

patients either failed early in testing or showed signs of degradation. The remaining patients' properties were well matched with one of two composites. Patients 2 and 7 were best emulated with the use of reinforced Dragon Skin 20, whereas Patient 3 required a much stiffer base and the externally reinforced Sylgard 170 corresponded well.

9.2 Future Directions

One important feature of this work was the ability to pick a reference point and adapt the material to reach those goals. As shown, each patient AAA had different mechanical properties, and one silicone analogue would not represent the individual patients as best possible. With patient testing, it was noted that the stiffness of the tissue varied greatly. It was evident with Patient 3 that a stiffer material would be necessary then Patient 2 and this was achieved using Sylgard 170 as a base material and reinforcing with silk thread. Therefore, with Patient 7, it was an obvious adjustment to switch the base material to a less stiff option. Future work would include expanding the pool of base materials at the lab's disposal and better utilizing available internet databases. Additionally, more fibers of different materials for even more options could be categorized to make an appropriate AAA replica keeping in mind the external reinforcements were greatly appreciated during 3-D replications.

Additional future work would include the development of a 3-D replicate of patient AAAs with the material. This project ended with trying to create a hollow aneurysm with Sylgard 170 but failure to remove the sample from the exterior mould. Dragon Skin 20 however was used to create a successful hollow patient-replicate but two had not yet been made. In addition, no reinforcements to the patient-replicates had been added. Most future work would focus on the addition of patients and the materials with which to replicate those properties.

Appendix A: Mould C-cast Reinforced Sylgard 170

Stress-Stretch

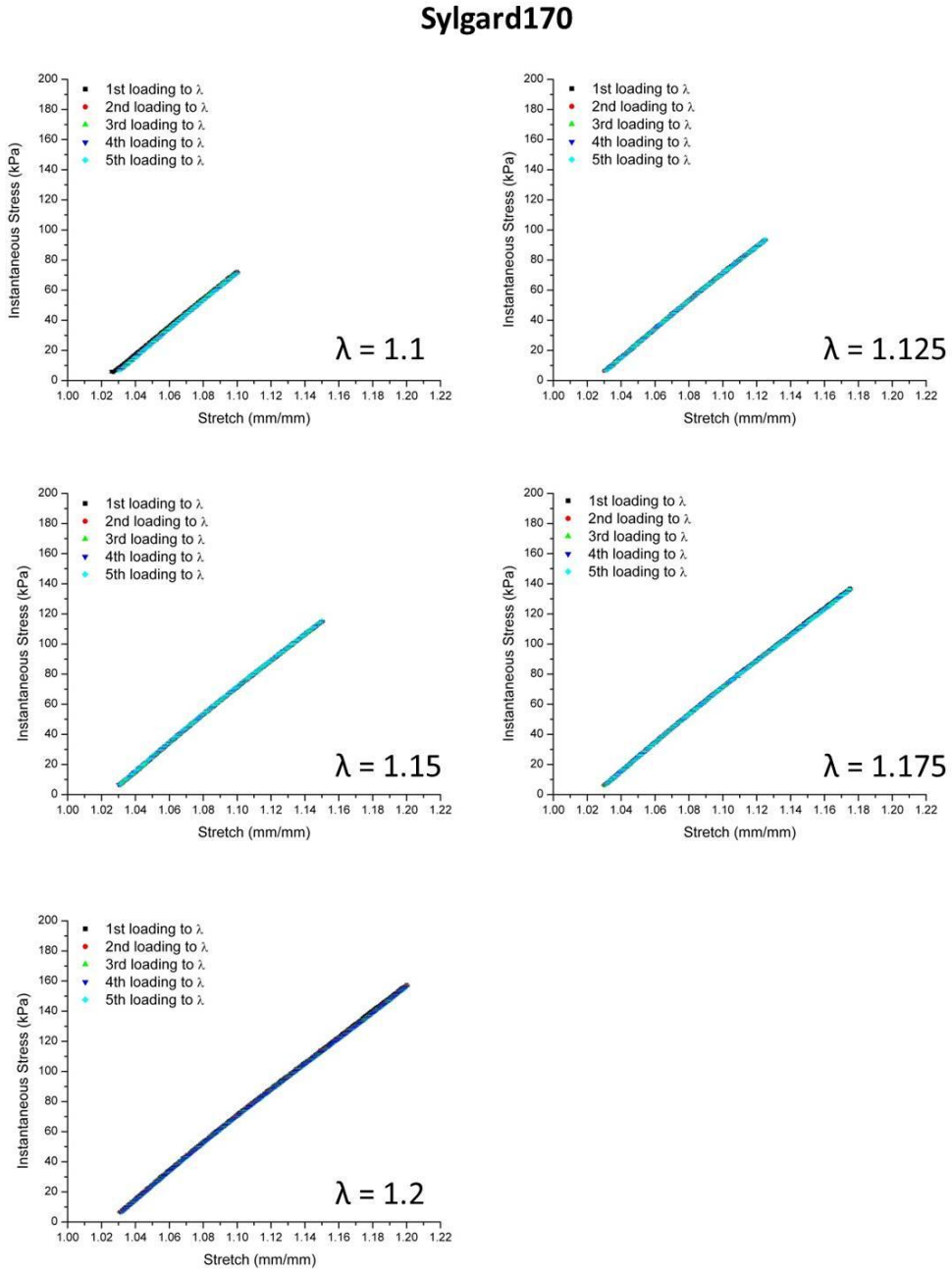

Internally-reinforced Sylgard170 (S170 +Int)

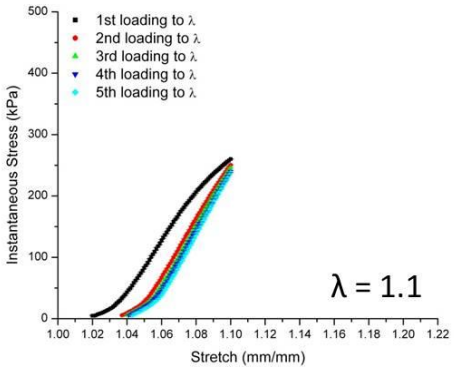

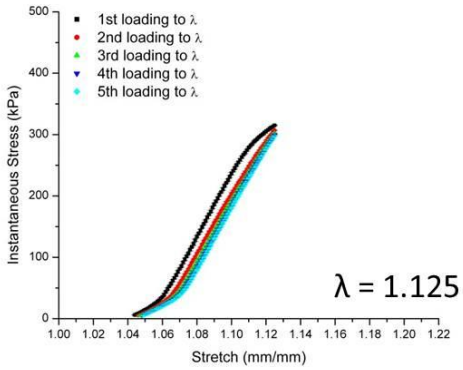

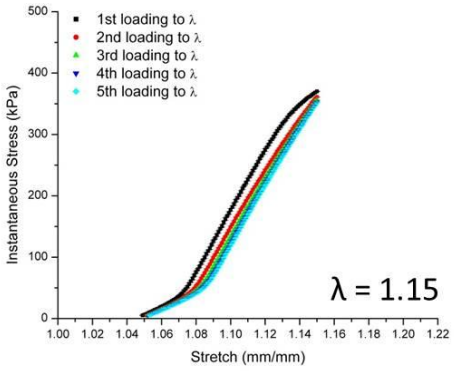

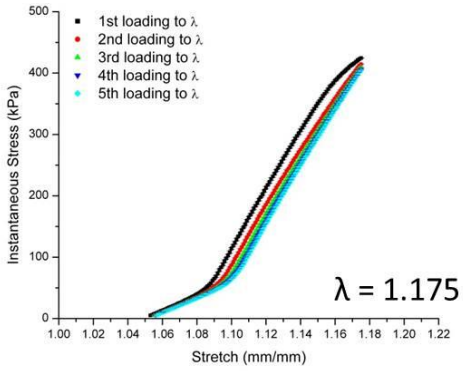

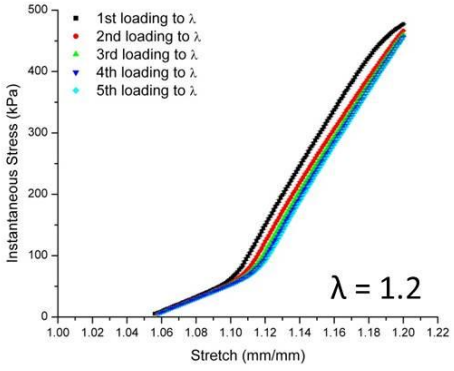

Externally-reinforced Sylgard170 (S170 +Ext)

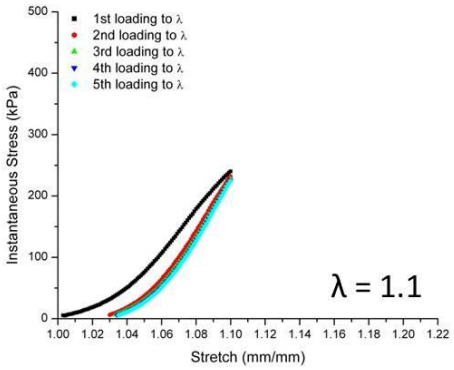

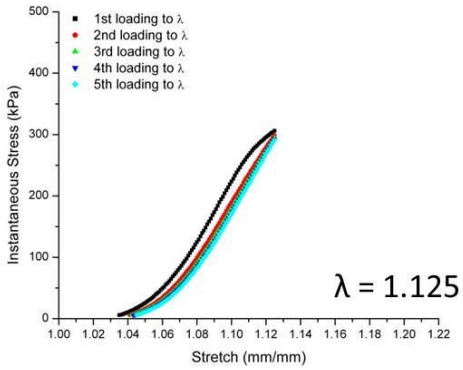

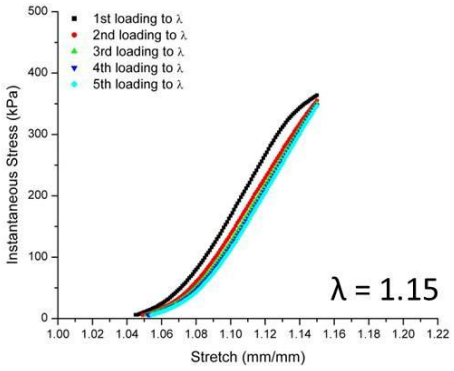

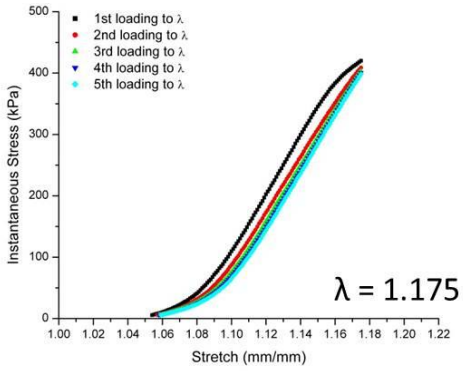

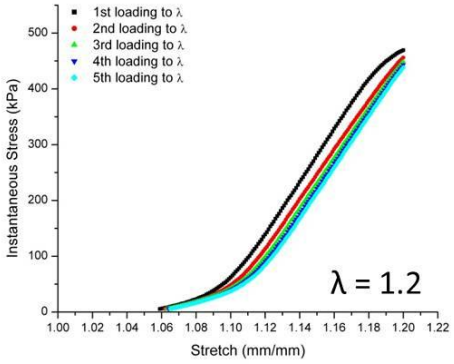

Double-stranded externally reinforced Sylgard170 (S170 +2x)

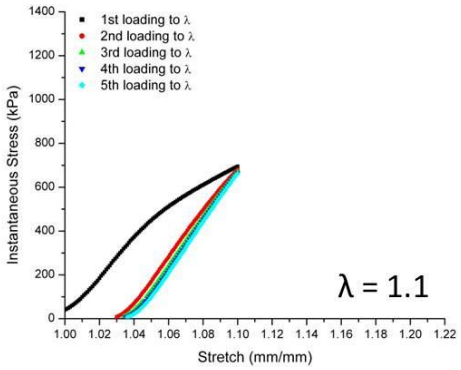

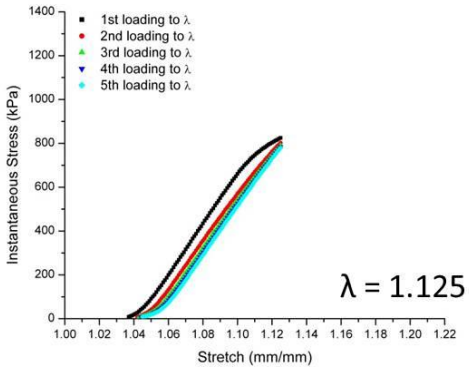

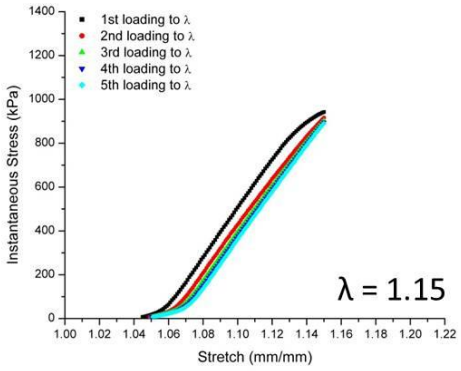

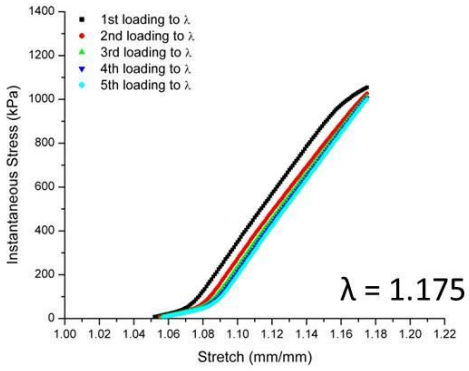

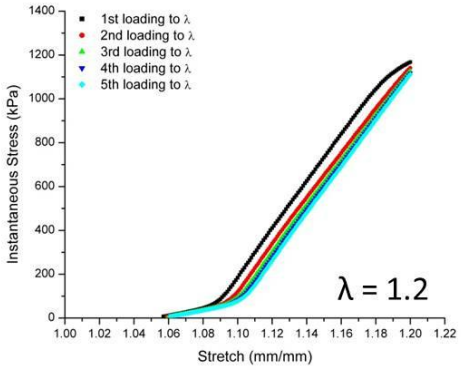

References

1. Centers for Disease Control and Prevention, N. C. for H. S. Compressed Mortality File 1999-2009. *CDC WONDER Online Database, compiled from Compressed Mortality File 1999-2009 Series 20 No. 2O, 2012* at <http://wonder.cdc.gov/cmf-icd10.html>

2. Hirsch, A. T. *et al.* ACC/AHA 2005 guidelines for the management of patients with peripheral arterial disease (lower extremity, renal, mesenteric, and abdominal aortic): executive summary a collaborative report from the American Association for Vascular Surgery/Society for Vas. *Journal of the American College of Cardiology* **47**, 1239–312 (2006).

3. Baas, A. F. & Kranendonk, S. E. Abdominal Aortic Aneurysm. *Clinical Cardiogenetics* 423–435 (2011).doi:10.1007/978-1-84996-471-5

4. Sakalihasan, N., Limet, R. & Defawe, O. D. Abdominal aortic aneurysm. *Lancet* **365**, 1577–89 (2005).

5. Estrera, A. L., Miller, C. C., Azizzadeh, A. & Safi, H. J. Thoracic aortic aneurysms. *Acta chirurgica Belgica* **106**, 307–16

6. Lindsay, J. Diagnosis and treatment of diseases of the aorta. *Current problems in cardiology* **22**, 485–542 (1997).

7. Baxter, B. T. *et al.* Elastin content, cross-links, and mRNA in normal and aneurysmal human aorta. *Journal of vascular surgery : official publication, the Society for Vascular Surgery [and] International Society for Cardiovascular Surgery, North American Chapter* **16**, 192–200 (1992).

8. Genovese, K., Collins, M. J., Lee, Y. U. & Humphrey, J. D. Regional Finite Strains in an Angiotensin-II Induced Mouse Model of Dissecting Abdominal Aortic Aneurysms. *Cardiovascular Engineering and Technology* **3**, 194–202 (2012).

9. MedlinePlus: Bethesda(MD): National Library of Medicine (US) Aortic Aneurysm. *updated 2012* at <http://www.nlm.nih.gov/medlineplus/ency/imagepages/18072.htm>

10. Derubertis, B. G. *et al.* Abdominal aortic aneurysm in women: prevalence, risk factors, and implications for screening. *Journal of vascular surgery : official publication, the Society for Vascular Surgery [and] International Society for Cardiovascular Surgery, North American Chapter* **46**, 630–635 (2007).

11. National Center for Advancing Translational Sciences, O. of R. D. R. Abdominal Aortic Aneurysm. *Genetic and Rare Diseases Information Center (GARD)* at <http://rarediseases.info.nih.gov/GARD/Condition/9181/Abdominal_aortic_aneurysm.aspx>

12. Centers for Disease Control and Prevention, N. C. for H. S. Compressed Mortality File 1968-1978. *CDC WONDER Online Database, compiled from Compressed Mortality File CMF 1968-1988, Series 20, No. 2A, 2000* at <http://wonder.cdc.gov/cmf-icd8.html>

13. Centers for Disease Control and Prevention, N. C. for H. S. Compressed Mortality File 1979-1998. *CDC WONDER Online Database, compiled from Compressed Mortality File CMF 1968-1988, Series 20, No. 2A, 2000 and CMF 1989-1998, Series 20, No. 2E, 2003.* at <http://wonder.cdc.gov/cmf-icd9.html>

14. Lederle, F. a The rise and fall of abdominal aortic aneurysm. *Circulation* **124**, 1097–9 (2011).

15. Heller, J. a *et al.* Two decades of abdominal aortic aneurysm repair: have we made any progress? *Journal of vascular surgery : official publication, the Society for Vascular Surgery [and] International Society for Cardiovascular Surgery, North American Chapter* **32**, 1091–100 (2000).

16. Dillavou, E. D., Muluk, S. C. & Makaroun, M. S. A decade of change in abdominal aortic aneurysm repair in the United States: Have we improved outcomes equally between men and women? *Journal of vascular surgery : official publication, the Society for Vascular Surgery [and] International Society for Cardiovascular Surgery, North American Chapter* **43**, 230–8; discussion 238 (2006).

17. Uk, T., Aneurysm, S. & Participants, T. Mortality results for randomised controlled trial of early elective surgery or ultrasonographic surveillance for small abdominal aortic aneurysms. The UK Small Aneurysm Trial Participants. *Lancet* **352**, 1649–55 (1998).

18. Hannawa, K. K., Eliason, J. L. & Upchurch, G. R. Gender differences in abdominal aortic aneurysms. *Vascular* **17 Suppl 1**, S30–9 (2009).

19. Golledge, J., Muller, J., Daugherty, A. & Norman, P. Abdominal aortic aneurysm: pathogenesis and implications for management. *Arteriosclerosis, thrombosis, and vascular biology* **26**, 2605–13 (2006).

20. Kuivaniemi, H. & Elmore, J. R. Opportunities in abdominal aortic aneurysm research: epidemiology, genetics, and pathophysiology. *Annals of vascular surgery* **26**, 862–70 (2012).

21. Blanchard, J. F., Armenian, H. K. & Friesen, P. P. Risk factors for abdominal aortic aneurysm: results of a case-control study. *American journal of epidemiology* **151**, 575–83 (2000).

22. Annambhotla, S. *et al.* Recent advances in molecular mechanisms of abdominal aortic aneurysm formation. *World journal of surgery* **32**, 976–86 (2008).

23. Brady, A. R., Thompson, S. G., Fowkes, F. G. R., Greenhalgh, R. M. & Powell, J. T. Abdominal aortic aneurysm expansion: risk factors and time intervals for surveillance. *Circulation* **110**, 16–21 (2004).

24. Ogata, T. *et al.* The lifetime prevalence of abdominal aortic aneurysms among siblings of aneurysm patients is eightfold higher than among siblings of spouses: an analysis of 187 aneurysm families in Nova Scotia, Canada. *Journal of vascular surgery : official publication, the Society for Vascular Surgery [and] International Society for Cardiovascular Surgery, North American Chapter* **42**, 891–7 (2005).

25. Majumder, P. P., St Jean, P. L., Ferrell, R. E., Webster, M. W. & Steed, D. L. On the inheritance of abdominal aortic aneurysm. *American journal of human genetics* **48**, 164–70 (1991).

26. Kuivaniemi, H. *et al.* Familial abdominal aortic aneurysms: collection of 233 multiplex families. *Journal of vascular surgery : official publication, the Society for Vascular Surgery [and] International Society for Cardiovascular Surgery, North American Chapter* **37**, 340–5 (2003).

27. Verloes, A., Sakalihasan, N., Koulischer, L. & Limet, R. Aneurysms of the abdominal aorta: familial and genetic aspects in three hundred thirteen pedigrees. *Journal of vascular surgery : official publication, the Society for Vascular Surgery [and] International Society for Cardiovascular Surgery, North American Chapter* **21**, 646–55 (1995).

28. Johansen, K. Aneurysms. *Scientific American* **247**, 110–1, 114–5, 118 passim (1982).

29. Sakalihasan, N., Heyeres, A., Nusgens, B. V, Limet, R. & Lapière, C. M. Modifications of the extracellular matrix of aneurysmal abdominal aortas as a function of their size. *European journal of vascular surgery* **7**, 633–7 (1993).

30. Lederle, F. A. In the clinic. Abdominal aortic aneurysm. *Annals of internal medicine* **150**, ITC5–1–15; quiz ITC5–16 (2009).

31. Edgar, E. Computational and experimental investigation of steady flow fields, turbulence and hemodynamic wall stresses in patient-specific abdominal aortic aneurysm models. (2008).

32. Dorfmann, a, Wilson, C., Edgar, E. S. & Peattie, R. a Evaluating patient-specific abdominal aortic aneurysm wall stress based on flow-induced loading. *Biomechanics and Modeling in Mechanobiology* **9**, 127–39 (2010).

33. Kahraman, H. *et al.* The diameters of the aorta and its major branches in patients with isolated coronary artery ectasia. *Texas Heart Institute journal / from the Texas Heart Institute of St. Luke's Episcopal Hospital, Texas Children's Hospital* **33**, 463–8 (2006).

34. Van 't Veer, M. *et al.* Biomechanical properties of abdominal aortic aneurysms assessed by simultaneously measured pressure and volume changes in humans. *Journal of vascular surgery* **48**, 1401–7 (2008).

35. Vorp, D. a *et al.* Wall strength and stiffness of aneurysmal and nonaneurysmal abdominal aorta. *Annals of the New York Academy of Sciences* **800**, 274–6 (1996).

36. Di Martino, E. S. *et al.* Biomechanical properties of ruptured versus electively repaired abdominal aortic aneurysm wall tissue. *Journal of vascular surgery : official publication, the Society for Vascular Surgery [and] International Society for Cardiovascular Surgery, North American Chapter* **43**, 570–6; discussion 576 (2006).

37. Raghavan, M. L., Webster, M. W. & Vorp, D. a Ex vivo biomechanical behavior of abdominal aortic aneurysm: assessment using a new mathematical model. *Annals of biomedical engineering* **24**, 573–82 (1996).

38. Vande Geest, J. P., Sacks, M. S. & Vorp, D. a The effects of aneurysm on the biaxial mechanical behavior of human abdominal aorta. *Journal of biomechanics* **39**, 1324–34 (2006).

39. Vande Geest, J. P., Schmidt, D. E., Sacks, M. S. & Vorp, D. a The effects of anisotropy on the stress analyses of patient-specific abdominal aortic aneurysms. *Annals of biomedical engineering* **36**, 921–32 (2008).

40. Doyle, B. J. *et al.* Experimental modelling of aortic aneurysms: novel applications of silicone rubbers. *Medical engineering & physics* **31**, 1002–12 (2009).

41. Shergold, O. a., Fleck, N. a. & Radford, D. The uniaxial stress versus strain response of pig skin and silicone rubber at low and high strain rates. *International Journal of Impact Engineering* **32**, 1384–1402 (2006).

42. Corning, D. Silicones : Overview II Sophisticated Chemical Building Block. (2004).

43. Colas, A. Silicones : Preparation , Properties and Performance.

44. Kim, T. K., Kim, J. K. & Jeong, O. C. Measurement of nonlinear mechanical properties of PDMS elastomer. *Microelectronic Engineering* **88**, 1982–1985 (2011).

45. Schneider, F., Fellner, T., Wilde, J. & Wallrabe, U. Mechanical properties of silicones for MEMS. *Journal of Micromechanics and Microengineering* **18**, 065008 (2008).

46. Whitesides, G. M. The origins and the future of microfluidics. *Nature* **442**, 368–73 (2006).

47. Gordan, O. D. *et al.* On pattern transfer in replica molding. *Langmuir : the ACS journal of surfaces and colloids* **24**, 6636–9 (2008).

48. Khanafer, K., Duprey, A., Schlicht, M. & Berguer, R. Effects of strain rate, mixing ratio, and stress-strain definition on the mechanical behavior of the polydimethylsiloxane (PDMS) material as related to its biological applications. *Biomedical microdevices* **11**, 503–8 (2009).

49. Viale-Bouroncle, S. *et al.* Soft matrix supports osteogenic differentiation of human dental follicle cells. *Biochemical and biophysical research communications* **410**, 587–92 (2011).

50. Begum, Z., Kola, M. Z. & Joshi, P. Analysis of the properties of commercially available silicone elastomers for maxillofacial prostheses. **2**, 1–5 (2011).

51. Aziz, T., Waters, M. & Jagger, R. Analysis of the properties of silicone rubber maxillofacial prosthetic materials. *Journal of dentistry* **31**, 67–74 (2003).

52. Vable, M. (M *Mechanics of Materials Online Book*. 83–148 (2012).

53. Smooth-On Inc. Dragon Skin ® Series Technical Bulletin. at <http://www.smooth-on.com/tb/files/DRAGON_SKIN_SERIES_TB.pdf>

54. Doyle, B. J. *et al.* An experimental and numerical comparison of the rupture locations of an abdominal aortic aneurysm. *Journal of endovascular therapy : an official journal of the International Society of Endovascular Specialists* **16**, 322–35 (2009).

55. Doyle, B. J., Cloonan, A. J., Walsh, M. T., Vorp, D. a & McGloughlin, T. M. Identification of rupture locations in patient-specific abdominal aortic aneurysms using experimental and computational techniques. *Journal of biomechanics* **43**, 1408–16 (2010).

56. Dow Corning Product Information: Sylgard(R) 170 Silicone Elastomer. (1999).

57. Dow Corning Information about Dow Corning ® Brand Silicone Encapsulants Silicones and Electronics. *2008*

58. Dow Corning Product Information: Sylgard(R) 184 Silicone Elastomer. 1–4 (1999).

59. Corbett, T. J., Doyle, B. J., Callanan, a, Walsh, M. T. & McGloughlin, T. M. Engineering silicone rubbers for in vitro studies: creating AAA models and ILT analogues with physiological properties. *Journal of biomechanical engineering* **132**, 011008 (2010).

60. Horny, L. *et al.* Mullins effect in human aorta described with limiting extensibility evolution. 768–771 (2010).

61. Xiong, J., Wang, S. M., Zhou, W. & Wu, J. G. Measurement and analysis of ultimate mechanical properties, stress-strain curve fit, and elastic modulus formula of human abdominal aortic aneurysm and

nonaneurysmal abdominal aorta. *Journal of vascular surgery : official publication, the Society for Vascular Surgery [and] International Society for Cardiovascular Surgery, North American Chapter* **48**, 189–95 (2008).